PARTICLE PATH DETERMINATION

IN LARGE ICE MASSES

USING THE FINITE ELEMENT METHOD

PARTICLE PATH DETERMINATION IN LARGE ICE MASSES USING THE FINITE ELEMENT METHOD

by

Michael Stephan Killeavy

A Thesis

Submitted to the School of Graduate Studies

in Partial Fulfillment of the Requirements

for the Degree

Master of Engineering

McMaster University

May 1985

MASTER OF ENGINEERING (1985)
(Civil Engineering)

McMASTER UNIVERSITY
Hamilton, Ontario

TITLE: Particle Path Determination In Large Ice Masses Using the Finite Element Method

AUTHOR: Michael Stephan Killeavy, B.A.Sc., University of Toronto

SUPERVISOR: Dr. D.F.E. Stolle

NUMBER OF PAGES: ix, 87

ABSTRACT

A stream function finite element model is developed to solve for particle paths within a large ice mass. A steady-state primitive variable finite element model, treating ice as an incompressible non-Newtonian fluid, is used to furnish the necessary input velocities and rotations for the stream function finite element model. Time-integration along the particle paths is used to determine the age of the ice within the ice mass.

Two ice masses are studied: the Barnes Ice Cap, Baffin Island, N.W.T., and Mount Logan, Yukon Teritory. It is shown that if a realistic approximation of the velocity field of an ice mass can be established, the age of ice determined by time-integration along particle paths corresponds to the age determined by standard methods. Results of simulations using a transient model suggest that the elastic response of large ice masses is negligible.

ACKNOWLEDGEMENTS

I would like to thank the following individuals and organization for the assistance given to me during the research and preparation of this thesis:

- My supervisor, Dr. D.F.E. Stolle, for his valuable help and criticism.
- G. Holdsworth, of Environment Canada, for providing data on Mount Logan, Yukon Territory.
- To my family, for their support and understanding.
- The Natural Sciences and Engineering Research Council, grant number A-5795, for supporting research for this thesis is deeply appreciated.

TABLE OF CONTENTS

TABLE OF CONTENTS (continued)

LIST OF FIGURES

LIST OF FIGURES (continued)

LIST OF FIGURES (continued)

LIST OF TABLES

CHAPTER 1
INTRODUCTION

1.1 Introduction

Glacier ice covers 10 per cent of the earth's land surface and during the past ice ages it has covered as much as three times this amount [25]. Since the end of the World War II much interest has been paid to the study of glacier dynamics. Paterson [26] gives a good summary of the reasons for the increased interest in glacier dynamics.

One of the most important reasons for studying the behaviour of glaciers is that they provide a detailed and continuous record of past climate and atmospheric chemistry over a period of approximately 100 000 years. This record is primarily due to the fact that the ratio of O^{16} to O^{18} atoms depends on temperature [6]. Air bubbles entrained in glacier ice contain samples of the air at the time the bubble was formed [26]. The glacier ice is sampled by drilling into the glacier and extracting an ice core.The age of the ice must be determined for this information to be useful. Many methods have been advanced for the determination of the age of ice cores. It is the purpose of this thesis to develop a method for determining the age of the ice based on the finite element method.

The finite element method offers distinct advantages over the standard methods of determining particle paths and calculating the age of glacier ice. Firstly, the complex nature of the glacier velocity field does not have to be simplified. Secondly , the finite element method can accomodate the variation in material properties in the glacier. Thirdly, the finite element method can accomodate the irregular geometry of the glacier surface and the bed.

In Chapter Two a brief review of ice deformation is given. Several of the standard methods for determining the age of ice cores are discussed in Chapter Three. The finite

element models used to establish the age of the ice cores are developed in Chapter Four. In Chapter Five the method developed in Chapter Four is used to study two real ice masses: the Barnes Ice Cap, N.W.T.; and Mount Logan, Yukon Territory. Also, a study of the deformation in the vicinity of the glacier divide is undertaken. To verify the results of the primitive variable finite element model and to investigate the transient behaviour of glacier ice, another finite element model is developed in Appendix A. The results of this thesis are summarized and conclusions are drawn in Chapter Seven.

CHAPTER 2

DEFORMATION OF GLACIER ICE

2.1 Glacier Ice

Glaciers are composed of ice crystals, air, water, and rock debris; of these ice crystals are the most important component [32]. Glacier ice is formed from the precipitation and subsequent densification of snow or directly from the freezing of glacier surface runoff. By far, the most important source of glacier ice is snow [26].

Snow that is not removed through melting will accumulate and gradually undergo a transformation to glacier ice. Snow is a term restricted to surface material that has not been transformed since it fell [25]. Snow that has survived the summer melt season and has started the transformation to glacier ice is called firn. The firn becomes glacier ice when the interconnecting air passages have been sealed off between grains (a grain may be considered to be a single crystal or an aggregate of several crystals) [25]. This gradual transformation of snow to glacier ice results from changes in crystal and intervening pore spaces due to [30] :

(i) mutual displacement of crystals;

(ii) changes in the size and shape of the crystals; and

(iii) internal deformation of the ice crystal.

The relative importance of these mechanisms changes as the density of the material increases. The net result is that the crystals grow and become joined together while air pockets are eliminated . For a comprehensive treatment of snow-ice transformation, the reader is refered to [25].

2.2 Deformation of Ice

Glaciers creep in response to gravity loading. For many years ice was treated as a viscous Newtonian fluid, that is, strain-rate was assumed to be directly proportional to the deviator stress. However, actual glacier velocities turned out to be more sensitive to small changes in velocity than this theory predicted [25]. During the late 1940's it was realized that ice deforms like other polycrystalline solids such as metals, rather than like fluids. The treatment of glacier deformation as a non- Newtonian viscous fluid has been successful in explaining many features of glacier flow [25].

Creep is most pronounced at higher temperatures, suggesting that creep is a thermally activated process. Higher temperatures increase the mobility of atoms which contribute to the energy requirements for various creep mechanisms [30].

The variation of strain with time, known as the creep curve is normally divided into three regions (Figure 2.1). These three divisions are normally arbitrary, and often a material will not exhibit all phases [21] :

(i) First stage - primary or transient creep where strain- rate diminishes with time due to the predominant strain hardening process.

(ii) Second stage - secondary creep, the material exhibits an apparent linear increase in strain with time due to a balance between strain hardening and strain softening processes. During this stage the strain-rate is at a minimum value; this is apparent steady-state creep.

(iii) Third stage - also refered to as tertiary creep. The existance of this stage depends on the stress level and temperatures. Increasing strain-rate is characteristic of this stage.

In glacier dynamics attention is confined to the deformation of ice during secondary creep because of the stable flow characteristics and negligible transient behaviour at stress and temperature levels common in glaciers.

2.3 Deformation of Polycrstalline Ice

Polycrystalline ice consists of randomly oriented grains of ice. Depending on the stress levels involved after initial elastic deformation, polycrystalline ice will exhibit the three stages of creep [30] . During transient creep, polycrystalline ice exhibits an initial decrease in deformation rate, unlike single crystals of ice which exhibit an initial increase in deformation rate. This reduction in strain-rate is attributed to the interference between crystals that are randomly oriented. During secondary creep there is a balance between the effect of dislocations piling-up at grain boundaries (strain hardening) and recrystallization and sliding at grain boundaries producing more favourably oriented crystals for deformation in the direction of the applied stress (strain softening). This balance between the strain hardening process due to randomly oriented crystals and the softening process creates apparent steady-state creep. The single most important stage of creep curve is the secondary creep. It is generally assumed that the deformation of large ice masses undergoes steady-state creep which can be approximated by minimum strain-rate.

Numerous experiments have shown that the relation relating strain-rate to stress, for secondary creep of polycrystalline ice over the range of stresses important in normal glacier flow (50 to 299 KPa) is of the form [25]

$$\dot{\varepsilon} = A\,\sigma^{n} \tag{2.1}$$

where $\dot{\varepsilon}$ is strain-rate, σ is the stress, n is a constant and A is a scalar function that depends on ice temperature, crystal size and orientation. This law, in terms of normal stress, is often

referred to in glaciological literature as Glen's law in honour of his pioneering research in the study of ice deformation.

Values of n vary from 1.5 to 4.2, with the mean being 3 [25]. The constant A is usually given by the Arrhenius relation [24]

$$A = A_o \exp(-Q/RT) \tag{2.2}$$

where A_o is a particular value of A at a given temperature, T is temperature in degrees Kelvin, R is the gas constant, and Q is the activation energy for creep. Other relations have been proposed but many of these can be derived from Equation 2.2 .

In glaciers several stresses act simultaneously, accordingly, the flow law that was established for simple uniaxial stress conditions must be generalized to the multiaxial state of stress. Dorn defines the quantities effective stress and strain-rate which preserve the uniaxial form of the flow law for a multiaxial state of stress, [31]

$$\dot{\varepsilon}_e = \left(\frac{2}{3} \dot{\varepsilon}_{ij} \dot{\varepsilon}_{ij} \right)^{1/2} \tag{2.3}$$

$$\sigma_e = \left(\frac{3}{2} S_{ij} S_{ij} \right)^{1/2} \tag{2.4}$$

where $S_{ij} = \sigma_{ij} - \delta_{ij} \sigma_m$

and $\sigma_m = (\sigma_1 + \sigma_2 + \sigma_3)/3$

These are second invariants of strain-rate and stress. The multiaxial flow law is of the form

$$\dot{\varepsilon}_{ij} = \frac{3}{2} \left(\frac{\dot{\varepsilon}_e}{\sigma_e} \right) S_{ij} \tag{2.5}$$

and the effective strain-rate is given by

$$\dot{\varepsilon}_e = A \sigma_e^n \tag{2.6}$$

The effective stress and strains do not represent the actual states of stress and strain-rates occuring in the glacier, they are merely functions which preserve the form of the uniaxial

creep law when generalized to the multiaxial state. Use of effective strain-rate and effective stress implies that [10]

(i) ice creep is independant of the first stress invariant;

(ii) ice is incompressible;

(iii) the ice is isotropic; and

(iv) the principal axes of the stress and creep strain rate coincide.

The flow law given by Equation 2.6 is used in this thesis. Other workers [34], [20], [21] have formulated other flow laws in somewhat different forms to account for the various behaviour of glacier ice. Van Egmond [32] gives an extensive review of creep literature.

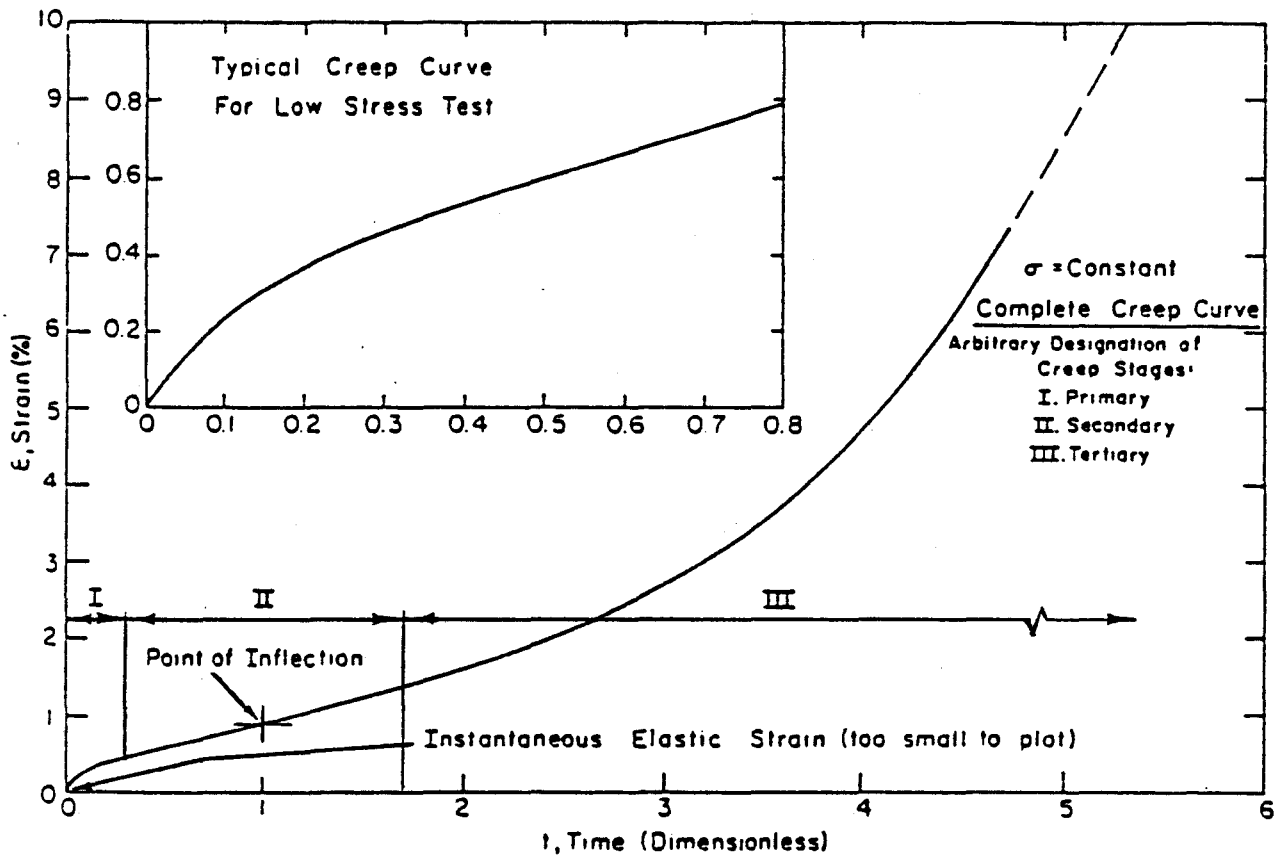

Figure 2-1 Creep Curve for Glacier Ice [21]

CHAPTER 3

STANDARD METHODS OF OBTAINING PARTICLE PATHS AND DATING ICE

3.1 Introduction

Ice cores are often used to extrapolate forward and backward in time in attempts to establish climatic history, or to obtain data about atmospheric chemistry. There are four basic methods for determining the age of ice cores:

(i) radioisotope dating;

(ii) dating by reference horizons;

(iii) dating by counting annual layers; and

(iv) flow models.

Radioisotopes ^{210}Pb, ^{32}Si, and ^{14}C are most commonly used to date ice cores [24]. By knowing the half-life of the radioisotope and the relative concentrations of the radioisotope and its daughter elements, the approximate age of the ice can be established. The accuracy of this method varies, with ^{210}Pb accurate up to 100 years and ^{32}Si accurate up to 1000 years. To properly use this technique large quantities of ice must be collected and melted. This technique is sensitive to contamination by materials not originally present in the ice, which may cause gross errors in determining the age of the ice [25].

Dating the ice by reference horizons involves correlating some aspect of the core to a known event [25]. Usually this involves correlating some particulate matter in the ice to some physical event for which a time scale already exists. For example,dating has been accomplished by correlating radioactive fallout in glacier ice to known nuclear bomb tests. Volcanic debris from major eruptions can also be used to date a reference horizon of ice containing this debris. The major drawback of this method is that a reference horizon is not

always present, nor is it always possible to correlate the particulate matter with a known event such as a volcanic eruption.

Oxygen and hydrogen isotope ratios in glacier ice show seasonal variations [25]. This variation can be used to identify annual layers in glacier ice which can be counted to date the ice core. This method is an accurate method of dating ice cores. Inaccuracies, however may result from uncertainty in correctly identifying the annual layers. This method is labour intensive because of the large number of samples that must be analyzed to give reasonable results [25].

Dating ice by using flow models involves determining the particle paths and integrating velocity along the particle path to obtain the age of the ice at various locations in the glacier;

$$T = \int_s \frac{ds}{v} \tag{3.1}$$

where s is the distance travelled by the ice particle along its path, v is the velocity of the ice particle, and T is the time taken to cover the distance travelled (Figure 3.1).

Owing to the rather complex velocity field within a glacier, the determination of particle paths is very difficult. Surface flow patterns can be determined from field studies by using surveying methods to record the displacement of markers placed on the glacier surface. Field determination of particle paths, however, is time consuming and expensive. Field studies do not render data about particle paths at depth. In general, on a large scale, glaciers can be expected to flow downhill, with horizontal velocity perpendicular to elevation contours. Flow vectors for the Wilkes Local Ice Cap confirm this relation between steepest elevation gradient and flow direction [2].

Many analytical methods have been advanced to determine the particle paths, and hence, the age of the ice. These methods are based, however, on simplifying assumptions which often ignore significant features of glacier flow. These methods generally involve

deriving expressions for horizontal and vertical velocity, based on very simple idealized models. The velocity vector is used to define the instantaneous direction of flow. Solving for the velocity vectors at several points in the glacier will yield the general pattern of flow; flowlines are then drawn based on this general pattern.

3.2 Budd Method

Budd and others [2] studied the Antarctic Ice Cap, and developed a model for obtaining particle paths within the ice sheet. Their model assumes that the ice flows downslope as a column of ice, with the majority of shear at the base (Figure 3.2); that is, constant horizontal velocity is implicit in this assumption. The horizontal and vertical velocities are determined by considering, ice mass geometry, continuity of flow, balance of the glacier and geometry of the glacier, and by assuming that vertical strain-rate is constant with depth. The age of the ice is obtained by integration of velocity along flowlines. Typically, the glacier is divided into several small segments, the velocity vectors for each segment are obtained and once the general pattern is obtained, flowlines are drawn. Irregularities of the bed are ignored in this type of analysis, as are the variations in horizontal velocity along the depth of the glacier. Ice cores dated using this model have corresponded well to the radioisotope dating.

3.3 Nye Method

Nye [22] has advanced a model that assumes a uniform vertical strain-rate along any vertical line in a glacier. The horizontal velocity is assumed to be very small, and basal melting is taken as being negligible. This method is only applicable in regions near the divide of the glacier where horizontal velocity is negligible. If the vertical strain-rate is uniform, the thickness of a layer of ice can be related to the previous thickness of the layer by

considering its distance from the bed, assuming that there is no horizontal movement. The age of the ice can be obtained by relating the initial and reduced thicknesses to the distances above the bed (Figure 3.3) . Dating of cores by using Nye's method does not correlate well with the dating of cores by other methods [5]. For a glacier frozen to its bed the assumption of uniform vertical strain-rate is not applicable. At a frozen bed vertical strain-rate is zero, thus the strain-rate when using Nye's model, should be zero throughout a section that is frozen to the glacier bed [27].

3.4 Dansgaard and Johnsen Method

Dansgaard and Johnsen [5] proposed a model similar to that of Nye, except non-uniform vertical strain-rate is assumed. This method considers vertical strain-rate to be constant with depth to a certain point, then the vertical strain-rate decreases linearly to zero at the frozen bed. The age of cores obtained using this model correspond well with that obtained by using radioisotope methods. This method does not, however, yield favourable results in the vicinity of the glacier bed due to the simplifying assumptions of the model.

3.5 Philberth and Federer Method

Philberth and Federer [28] integrated Glen's law for the case of simple shear to derive a relationship for vertical strain-rate as a function of depth. In their model the ice is assumed to be incompressible, and temperature is assumed to increase linearly with depth. By assuming the case of simple shear they ignore the often significant effect of longitudinal strains on the flow field. The ages of ice obtained from this model for the upper half of the ice cores do not correlate well with the ages obtained with other models or with radioisotope dating.

3.6 Hooke Method

In his study on the foliation of the Barnes Ice Cap , Hooke [14],[15],[16] developed relations for particle paths. He assumes that the ice is perfectly plastic, the mass budget is balanced, the ice is incompressible, and that the bed of the glacier is horizontal with no irregularities. Expressions for the components of the velocity vector are derived from continuity of the ice flow and mass balance. The particle paths are determined from the calculated velocity field. Hooke has made no attempt to date ice cores; rather the derived expressions are used to plot the foliation pattern in the glacier.

3.7 Haefeli Method

Haefeli [8] plotted flowlines for two highly idealized ice sheets, a circular ice sheet and a strip shaped ice sheet. The ice sheet is assumed to be in steady-state, and frozen to its bed, which is horizontal. The variation of horizontal velocity with depth is replaced with a mean horizontal velocity, and the vertical velocity is completely ignored. The simplified model has been used to date ice cores from the Greenland Ice Sheet, however, without much success.

3.8 Summary

The flow models presented above are simple to implement and depending on the velocity field, use of these methods have generated reasonable predictions. These models, however, rely on highly idealized velocity fields which are often unrealistic and simplified glacier and bed geometries. In the following chapter a more general technique is presented, which limits simplifying assumptions inherent in other models.

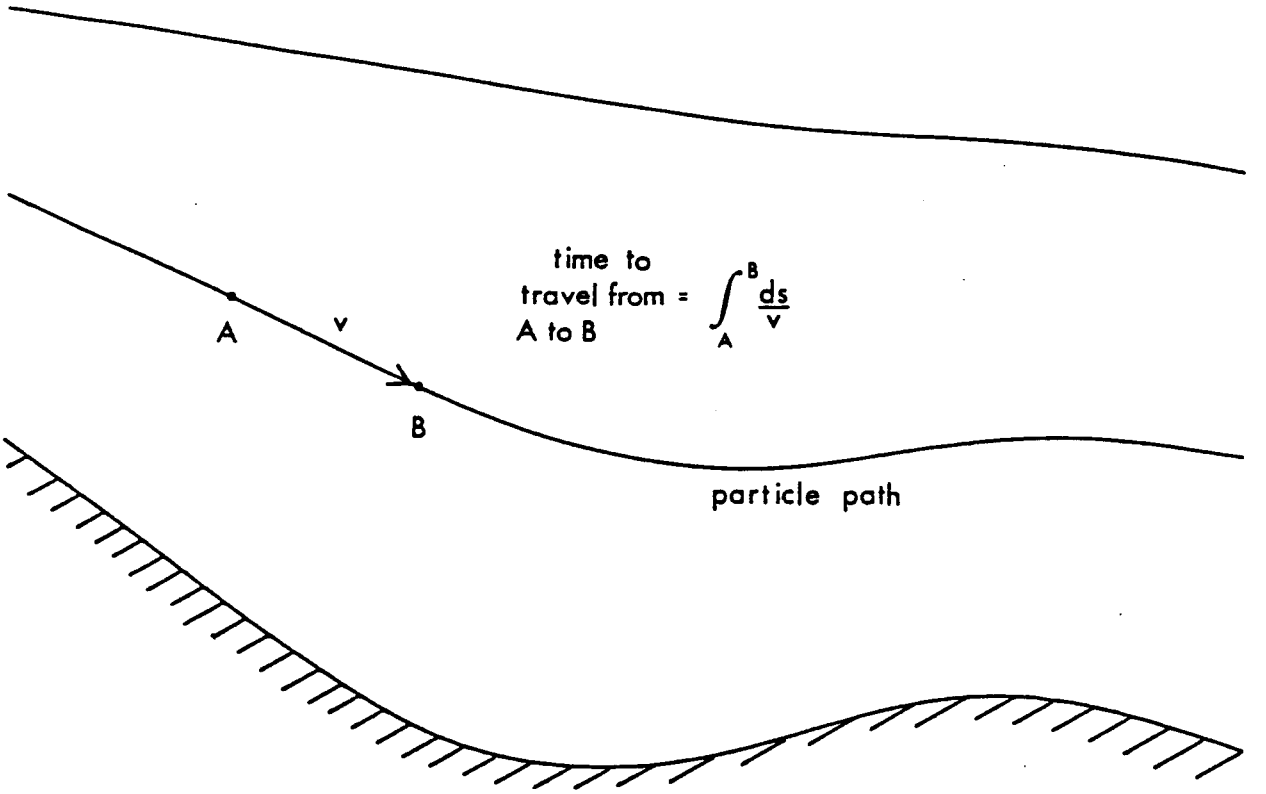

Figure 3-1 Particle Path for a Typical Glacier

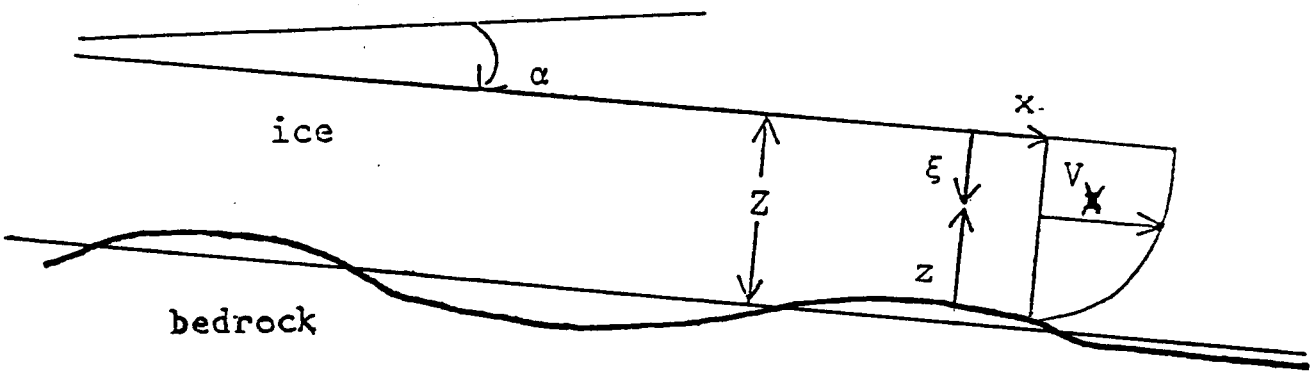

Figure 3-2 Budd Column Model [2]

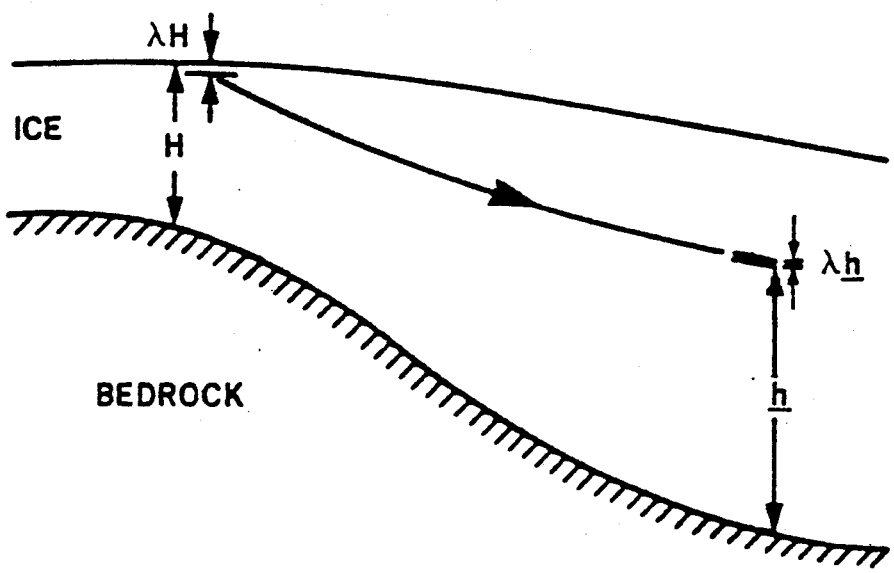

Figure 3-3 Nye Model [12]

CHAPTER 4
FINITE ELEMENT MODEL

4.1 Introduction

Owing to the advent of the finite element method in the late 1950's, many complex boundary-valued engineering problems, for which closed form analytic solutions do not exist, have been solved. The finite element method has been applied successfully to many fields of endeavour, and recently it has been applied to the problem of glacier dynamics [16], [29], [31]. In this thesis, the finite element method is used to solve for particle paths in glaciers. From these particle paths the age of the ice can be determined at various points. The application of the finite element method offers many distinct advantages over standard methods of determining particles paths and the age of ice:

(i) the irregular geometry of the glacier and bed can be accomodated ;

(ii) a more realistic velocity field is accounted for;

(iii) non-uniform material properties can be accounted for in this analysis; and

(iv) particle paths are determinated analytically from the velocity field.

To solve for particle paths, it is possible to formulate the problem of glacier flow directly in terms of a stream function formulation as outlined by Zienkiewicz and Godbole [35]; this approach has been used by Stolle [31]. This type of formulation, however, requires use of plate-bending type elements with C_1 continuity. Further, this formulation demands significant computational resources and, it is difficult to satisfy stress-dependant sliding boundary conditions and compressible flow fields.

In the approach adopted for this study velocities are first computed using a primitive variable formulation, and then particle paths are determined through a

formulation that makes use of the kinematic relationship [18]

$$\nabla^2 \psi + \omega = 0 \tag{4.1}$$

where ψ is stream function and ω is vorticity in the flow field. The vorticity is calculated in the primitive variable formulation by using the relationship [18]

$$\omega = \frac{\partial v_2}{\partial x_1} - \frac{\partial v_1}{\partial x_2} \tag{4.2}$$

where v_1 is the velocity in the x_1 direction and v_2 is the velocity in the x_2 direction. Equation 4.1 is obtained by substituting the stream function gradients for velocities $v_1 = \partial\psi/\partial x_2$ and $v_2 = -\partial\psi/\partial x_1$. This relationship has been used previously to locate free surfaces in polymer extrusion problems [22].

4.2 Primitive Variable Formulation

Stolle [31] developed a finite element model for the problem of steady-state glacier flow subject to gravity loading which uses flow parameters expressed in terms of non-Newtonian fluid rheology. Elastic strains are considered to be negligible and the flow field is assumed to be incompressible. As indicated previously, this model is used to establish the velocity field within the ice mass.

The primitive variable approach adopted for this model is based on the principle of virtual velocities which is used to reduce the equilibrium equations to a suitable integral form

$$\int_V \sigma_{ij} \delta\dot{\varepsilon}_{ij} \, dV - \int_V b_i \delta v_i \, dV - \int_\Gamma T_i \delta v_i \, d\Gamma = 0 \tag{4.3}$$

where δv_i and $\delta\dot{\varepsilon}_{ij}$ are virtual velocities and compatible strain-rates, respectively, b_i are the body forces, V is the volume and T_i are boundary tractions applied to part of the boundary Γ. The primitive variables are the mean normal stress σ_m, and the velocity v_i.

A second virtual work rate equation is necessary to enforce incompressibility

$$\int_V \sigma_m v_{i,i} \, dV = 0 \tag{4.4}$$

This equation states that the internal work rate due to a virtual mean normal stress, σ_m, acting on an incompressible flow field is zero.

Stresses σ_{ij} are related to strain-rates and mean normal stress by

$$\sigma_{ij} = \sigma_m \delta_{ij} + 2\mu \dot{\varepsilon}_{ij} \tag{4.5}$$

with

$$\dot{\varepsilon}_{ij} = \frac{1}{2} (v_{i,j} + v_{j,i}) \tag{4.6}$$

where μ is the strain-rate and temperature dependent viscosity and δ_{ij} is the Kronecker delta. The viscosity μ, is given by

$$\mu = \frac{1}{3} \frac{\sigma_e}{\dot{\varepsilon}_e} \tag{4.7}$$

Quadratic velocity and linear pressure interpolations are used within each six-node triangular element. Four-point integration is used to assemble the stiffness matrix and load vector. Deformation rates and vorticity are calculated at each integration point within the element, while velocities and pressure are calculated at nodes.

4.3 Stream Function Finite Element Formulation

A weighted residual approach is used to develop the stream function finite element equations. The following differential equation is to be solved

$$\nabla^2 \psi + \omega = 0 \qquad \text{in } V \tag{4.8}$$

which is subject to the following boundary conditions

$$\psi - \bar{\psi} = 0 \qquad \text{on } \Gamma_1 \tag{4.9}$$

$$v_s - \bar{v}_s = 0 \qquad \text{on } \Gamma_2 \tag{4.10}$$

where $v_s = \partial\psi/\partial n$ and $\bar{\psi}$ and $\bar{v}_s$ are prescribed values of stream function and tangential velocity, respectively.

Furthermore, an additional constraint is imposed on the system

$$v_n - \bar{v}_n = 0 \qquad \text{on } \Gamma_2 \tag{4.11}$$

where $\partial\psi/\partial s = v_n$. This additional constraint, which is generally not incorporated in field problems, has been found to improve results when compared to closed form solutions of test problems.

To reduce Equation 4.7 to the finite element equivalent, a set of weighting functions is selected such that

$$w = \beta_i w_i \tag{4.12}$$

where β_i are orthogonal weighting functions and w_i are weighting factors at nodal points. The approximate solution to the system is given by

$$\psi = N_i \psi_i \tag{4.13}$$

where N_i are the interpolation functions and ψ_i are the nodal values of stream function.

The weighted residual expression corresponding to this problem is obtained by equating the error on the boundary with error in the domain [1]

$$\int_V w(\nabla^2\psi + \omega)\,dV = \int_{\Gamma_2} w(v_s - \bar{v}_s)\,d\Gamma - \int_{\Gamma_1} (\psi - \bar{\psi})\,\frac{\partial w}{\partial n}\,d\Gamma$$

$$+ \int_{\Gamma_2} (v_n - \bar{v}_n)\left(\frac{\partial w}{\partial s}\right) d\Gamma\,. \tag{4.14}$$

The weighting function for the last term is $\partial w/\partial s$ to ensure a symmetric stiffness matrix component associated with the additional constraint given by equation 4.10.

Integrating the left-hand side of equation 4.13 by parts, and recognizing that

$$\int_{\Gamma_1} (\psi - \bar{\psi})\,\frac{\partial w}{\partial n}\,d\Gamma$$

is an essential boundary condition, yields

$$\int_V \frac{\partial w}{\partial x_i}\frac{\partial \psi}{\partial x_i}\,dV + \int_{\Gamma_2} v_n \frac{\partial w}{\partial s}\,d\Gamma =$$

$$\int_{\Gamma_2} w\,\bar{v}_s\,d\Gamma + \int_{\Gamma_2} \bar{v}_n \frac{\partial w}{\partial s}\,d\Gamma + \int_V w\omega\,dV \tag{4.15}$$

Substituting the values for the weighting function into Equation (4.14) gives

$$\int_V w_i \frac{\partial \beta_i}{\partial x_k}\frac{\partial \psi}{\partial x_k}\,dV + \int_{\Gamma_2} w_i \frac{\partial \beta_i}{\partial s}\frac{\partial \psi}{\partial s}\,d\Gamma$$

$$= \int_{\Gamma_2} w_i \beta_i \bar{v}_s\,d\Gamma + \int_{\Gamma_2} w_i \bar{v}_n \frac{\partial \beta_i}{\partial s}\,d\Gamma + \int_V \omega w_i \beta_i\,dV\ . \tag{4.16}$$

This must be true for all values of w_i, and choosing $\beta_i = N_i$ results in

$$\int_V \left(\frac{\partial N_i}{\partial x_k}\right)\left(\frac{\partial N_j}{\partial x_k}\right)dV\,\psi_j + \int_{\Gamma_2} \left(\frac{\partial N_i}{\partial s}\right)\left(\frac{\partial N_j}{\partial s}\right)d\Gamma\,\psi_j$$

$$= \int_{\Gamma_2} N_i \bar{v}_s\,d\Gamma + \int_{\Gamma_2} \frac{\partial N_i}{\partial s}\bar{v}_n\Gamma + \int_V \omega N_i\,dV \tag{4.17}$$

Equation (4.16) is the finite element equation to be solved. Upon discretization, in two dimensions, the stiffness matrix becomes

$$K_{ij} = t\int\int_A [N_{i,x}N_{j,x} + N_{i,y}N_{j,y}]\,dA$$

$$+ \frac{1}{\ell}\int_{\Gamma_2} N_{i,s}N_{j,s}\,d\Gamma \tag{4.18}$$

and the load vector becomes

$$f_i = t\int\int_A N_i\,\omega\,dA + \int_{\Gamma_2} N_i \bar{v}_s\,d\Gamma + \int_{\Gamma_2} N_{i,s}\bar{v}_n\,d\Gamma \tag{4.19}$$

or in matrix notation

$$[K]\{\psi\} = \{f\} \tag{4.20}$$

where the last two terms in Equation (4.18) are non-essential boundary conditions.

Originally, a three-noded triangular element, with linear interpolation of stream function was used, however, this element performed poorly and was replaced by a six-noded triangular element with quadratic interpolation of stream function within each element. As indicated previously, the addition of Equation 4.10 improved the finite element solution of test problems when compared to closed form solutions.

4.4 Tests of the Finite Element Model

The stream function finite element model was subjected to numerous tests to verify its performance. For test results of the primitive variable finite element model the reader is referred to Stolle [31]. Three simple flow regimes, for which closed form solutions exist, were modelled using the stream function model (Figure 4-1)

(i) laminar flow;

(ii) shear flow; and

(iii) Poiseuille flow.

The closed form solutions and finite element results are given in Tables 4-1,2, and 3. As indicated previously, stream function is interpolated quadratically by the stream function finite element model. For the case of laminar flow, stream function varies linearly and the finite element solution and the closed form solutions are identical. For the case of shear flow, stream function varies quadratically and the finite element and closed form solutions are identical. For the case of Poiseuille flow, stream function varies cubically, in this case the finite element solution is close to the closed form solution but is not identical to it due to the lower form of interpolation used in the finite element method.

4.5 Contour and Isochrone Plotting

To aid the interpretation of results from the stream function model, a computer program was developed to draw contours of stream function using the nodal values of stream function. These contours actually represent the paths that particles follow as the ice creeps. An option was included in the program to calculate the resident time of an ice particle along the particle path. Using the calculated times along the particle path, contours of equal time, referred to as isochrones, were drawn. Plots of particle paths for laminar flow in a rectangular domain is shown in Figure 4-2 . Use of these programs is made throughout this thesis to aid interpretation of results.

4.6 Study of the Double Slope Ice Mass

The finite element models were used to study an idealized ice mass, the double slope ice mass (Figure 4-3). Flow parameters obtained by Hooke [30] for the Barnes Ice Cap were used to simulate the creep of the double slope

$$\dot{\varepsilon}_e = 0.0327\, \sigma_e^{1.65} \tag{4.21}$$

where σ_e is measured in bars.

Two different finite element discretizations were used to simulate the flow behaviour of the ice mass; a 3 element grid and a 12 element grid (Figures 4-3 and 4-4). The boundary conditions for the creep simulations with the primitive variable formulation were a stress-free upper surface, a no-slip boundary along the bed, and vertical movement only along divide. The boundary conditions for the stream function simulations with the stream function formulation were $\psi = 0$ along the divide and bed, and velocities were specified along the upper surface of the ice mass. The results of the stream function simulations are shown in Figures 4-5 and 4-6, and isochrones for 10 and 50 years are shown in Figure 4-7. As can be seen, there is not much difference in the flow pattern between the two simulations. The

distribution of isochrones, however, is somewhat different. This is due to the fact that linear interpolation between flowlines is used to obtain the isochrone. In general it can be said that the more elements that there are, the better the representation of the actual flow field and the more flowlines used to obtain isochrones the more accurate the ages will be. Of course, one must keep in mind the limitations of the mathematical models.

4.7 Comparison of Finite Element Method to Budd's Method

To compare the results of the finite element model, Budd's method was applied to the double slope ice mass to obtain flow patterns

For the idealized ice mass the ablation rates were obtained from the normal velocities along the surface. A uniform depth, perpendicular to the plane of the ice mass, of 1.0 metres was used for calculations. Following Budd's method [2], the ice mass was divided into several columns along which the horizontal velocities are assumed to be constant. Using the ablation rates and geometry of the ice mass, the horizontal and vertical velocities were obtained from a consideration of continuity. From the velocity vectors obtained, the flow pattern was approximated.

Results from both Budd's method and the finite element model are shown in Figures 4-8 and 4-9. By neglecting the horizontal variation of velocity within each of the subdivided columns and variation of vertical strain-rate with depth, different flow patterns are obtained from Budd's method and the finite element model. For Budd's method the flowlines are depressed more towards the bed of the glacier. This depression results in longer particle paths and correspondingly higher resident times for ice particles.

LAMINAR FLOW $v = 10\ m/y\ ;\ \omega = 0$

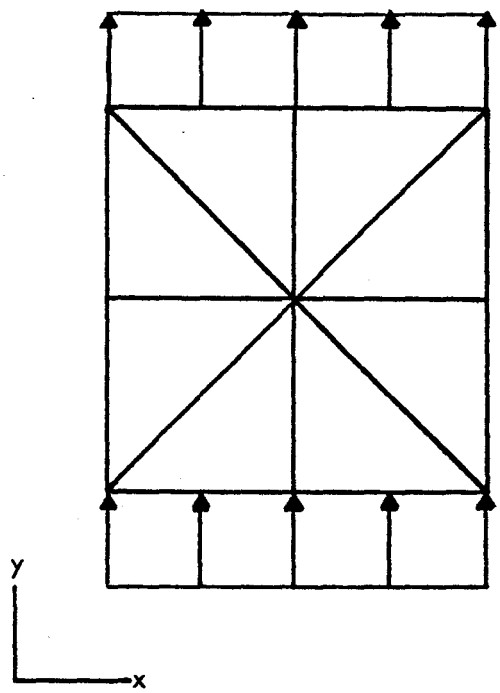

SHEAR FLOW $v = x\ ;\ \omega = 1$

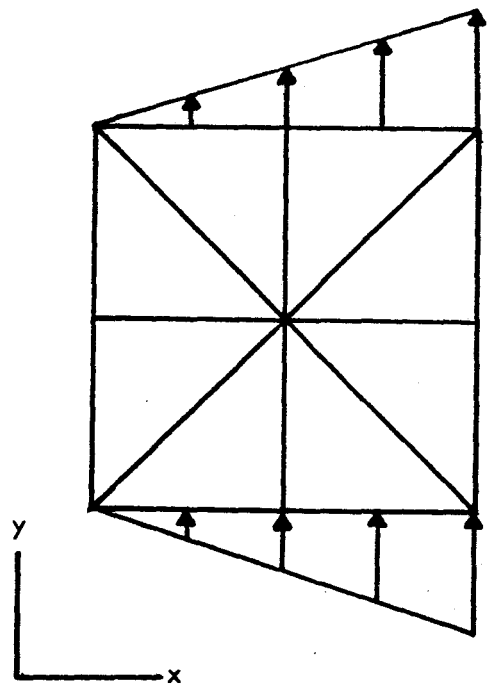

POISEUILLE FLOW $u = -0.015y^2 + 0.30y\ ;\ \omega = 0.015y - 0.015$

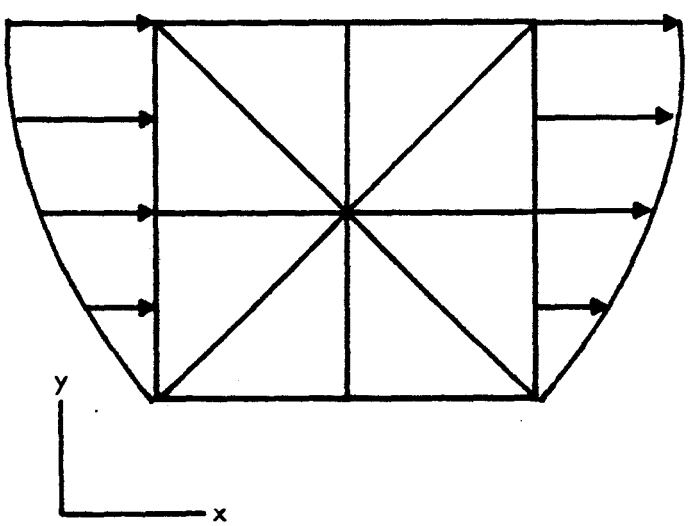

Figure 4-1 Test Flow Regimes for the Stream Function Model

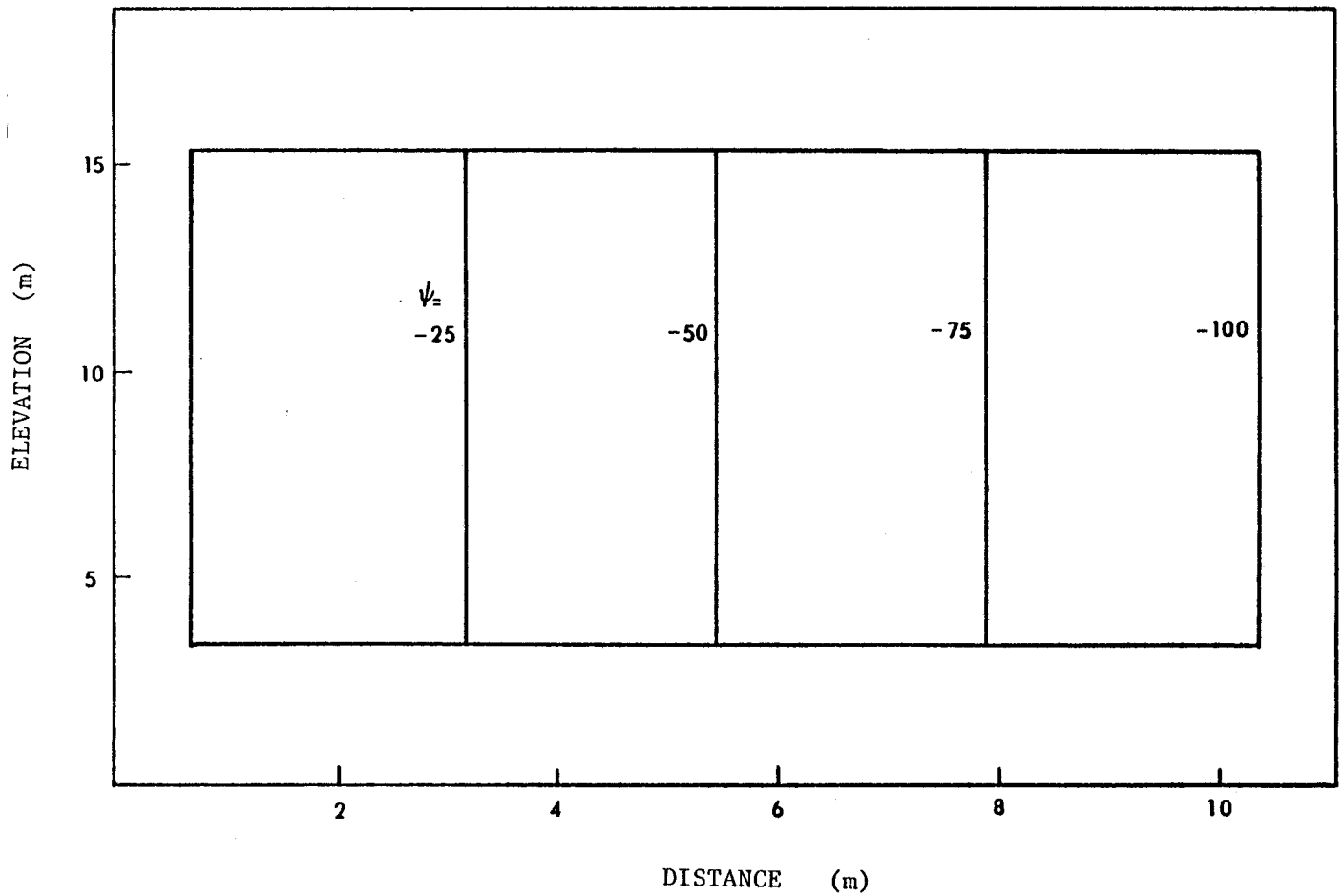

Figure 4-2 Particle Paths for Laminar Flow in a Rectangular Domain

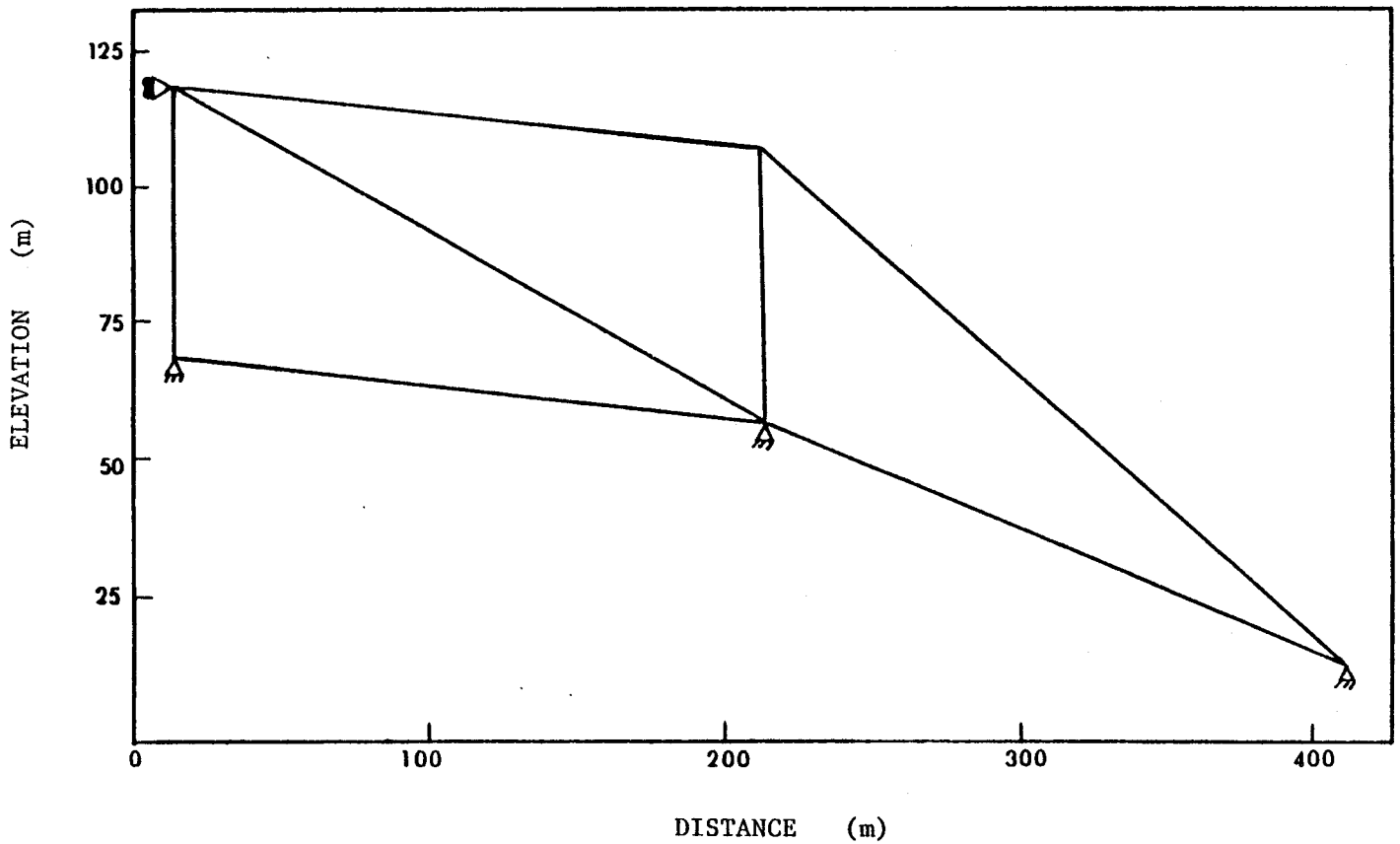

Figure 4-3 Double Slope Ice Mass - 3 Element Grid

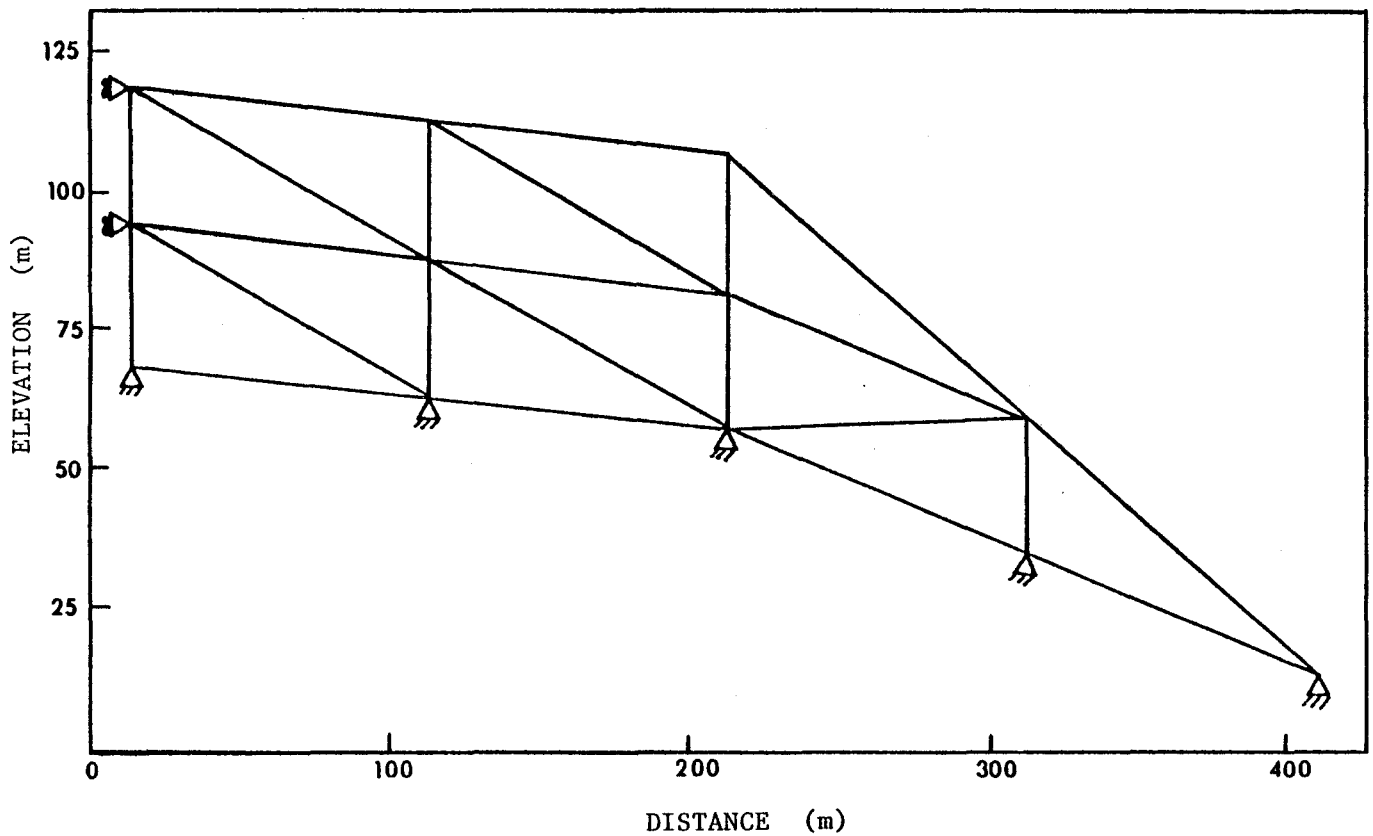

Figure 4-4 Double Slope Ice Mass - 12 Element Grid

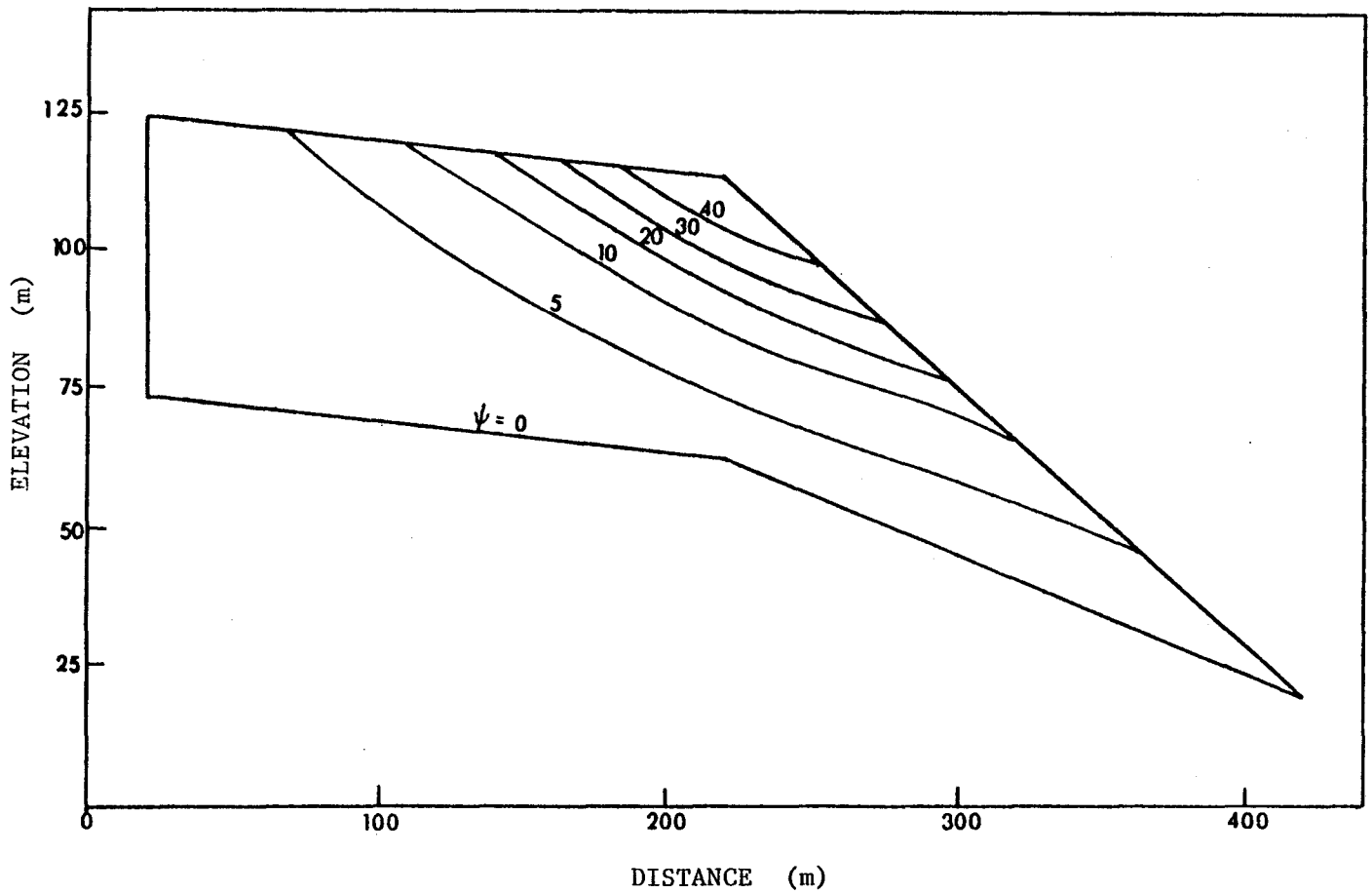

Figure 4-5 Particle Paths - 3 Element Grid

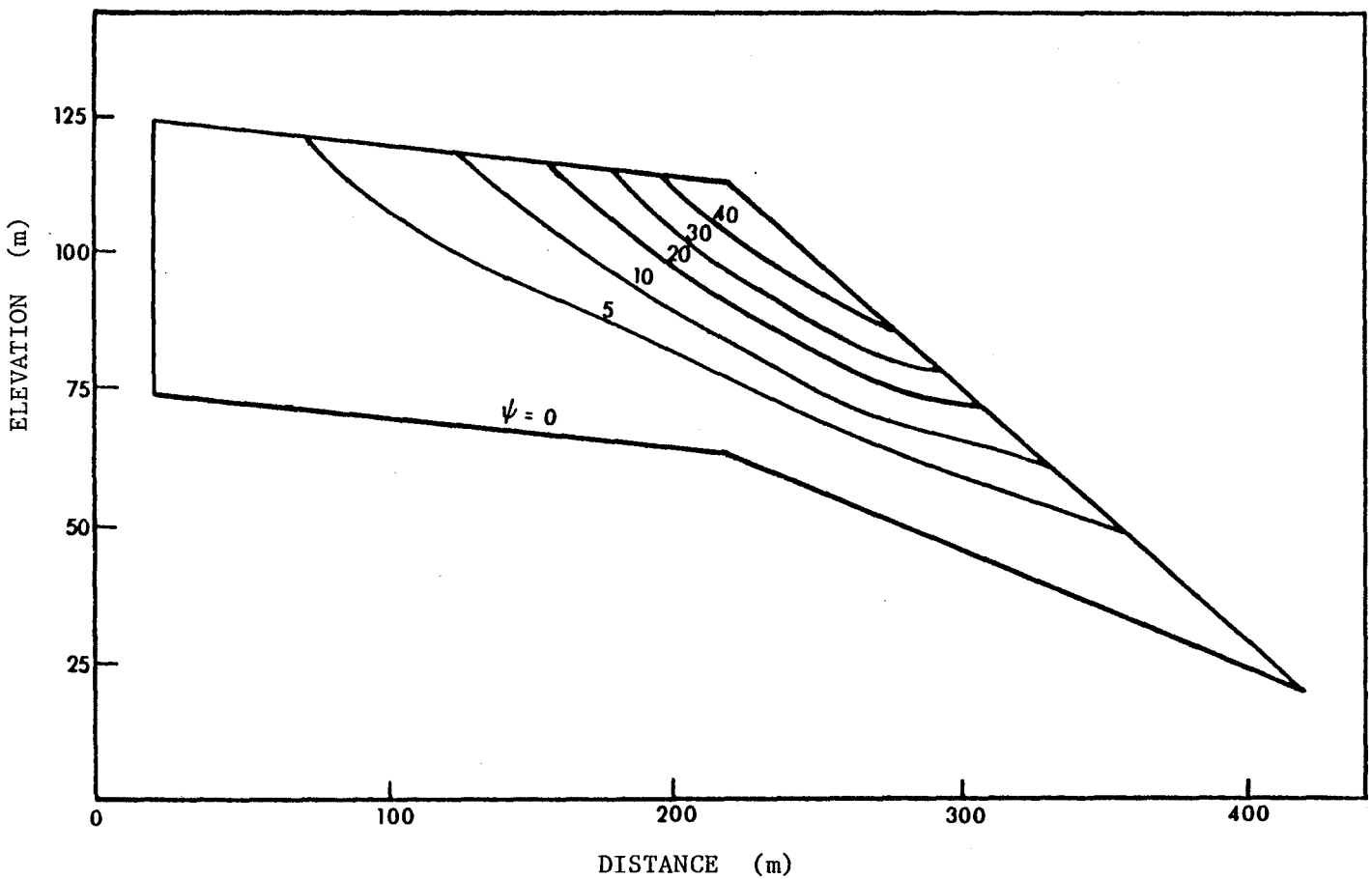

Figure 4-6 Particle Paths - 12 Element Grid

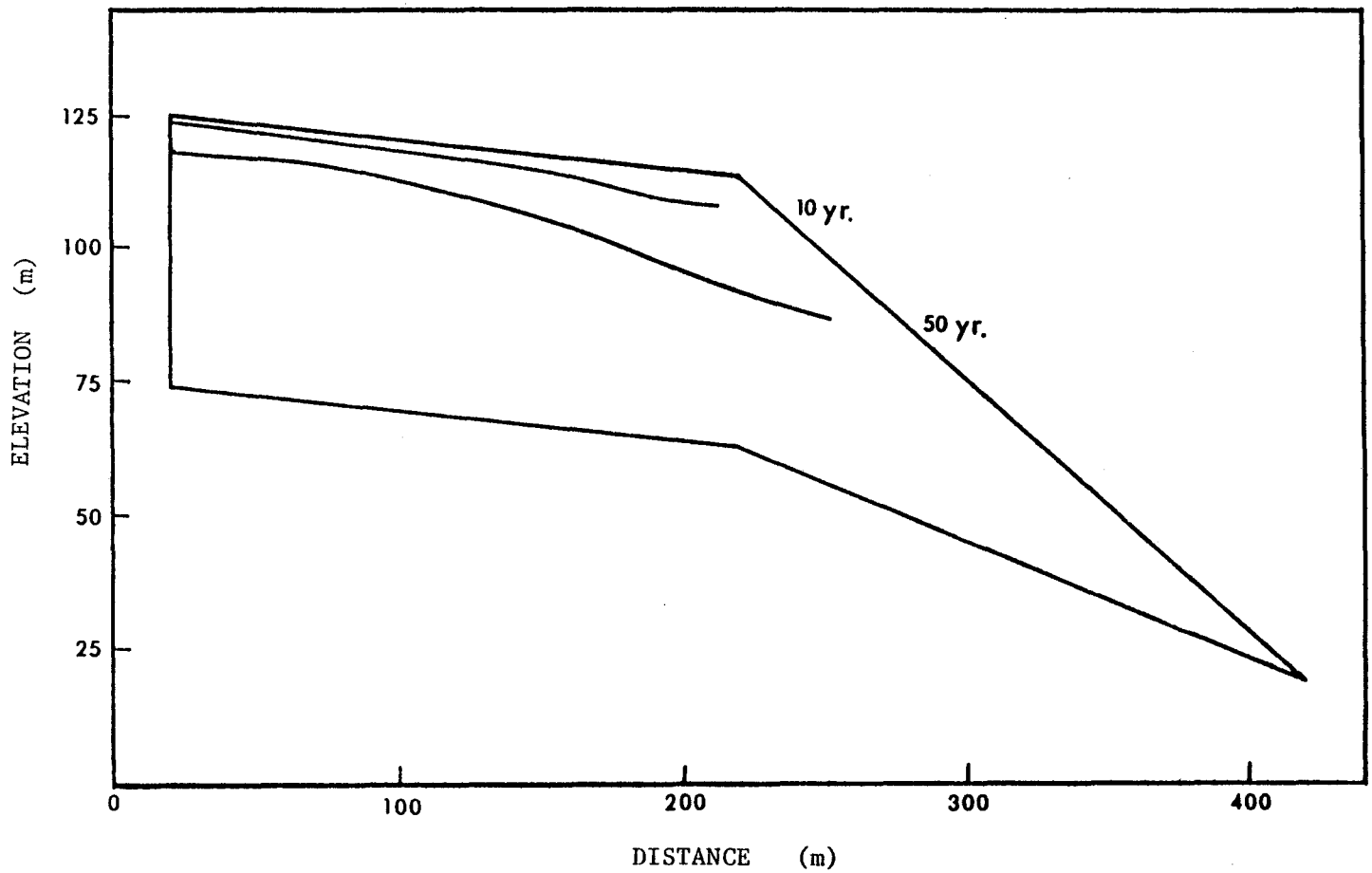

Figure 4-7 Isochrones - 12 Element Grid

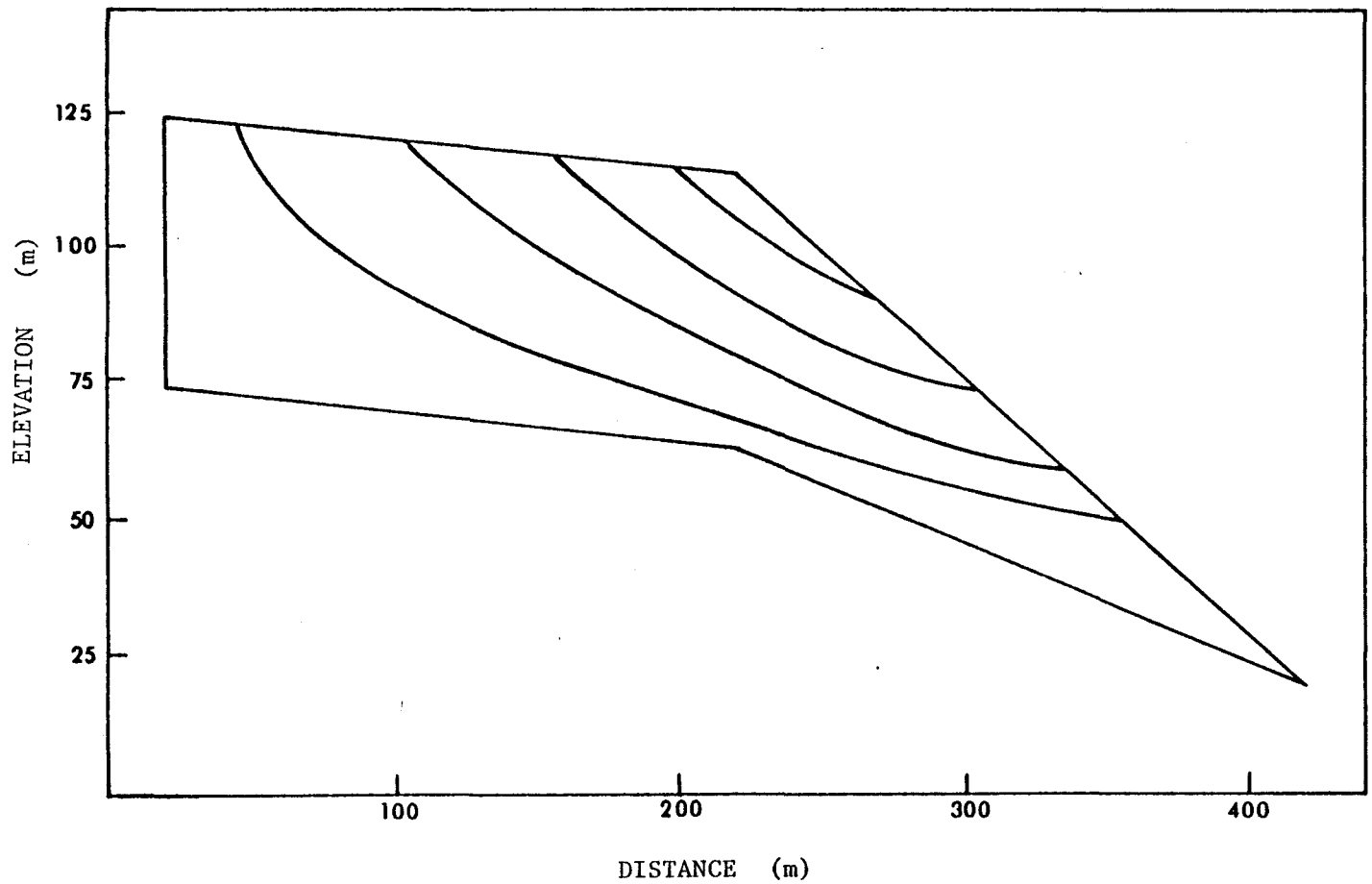

Figure 4-8 Particle Paths - Finite Element Method

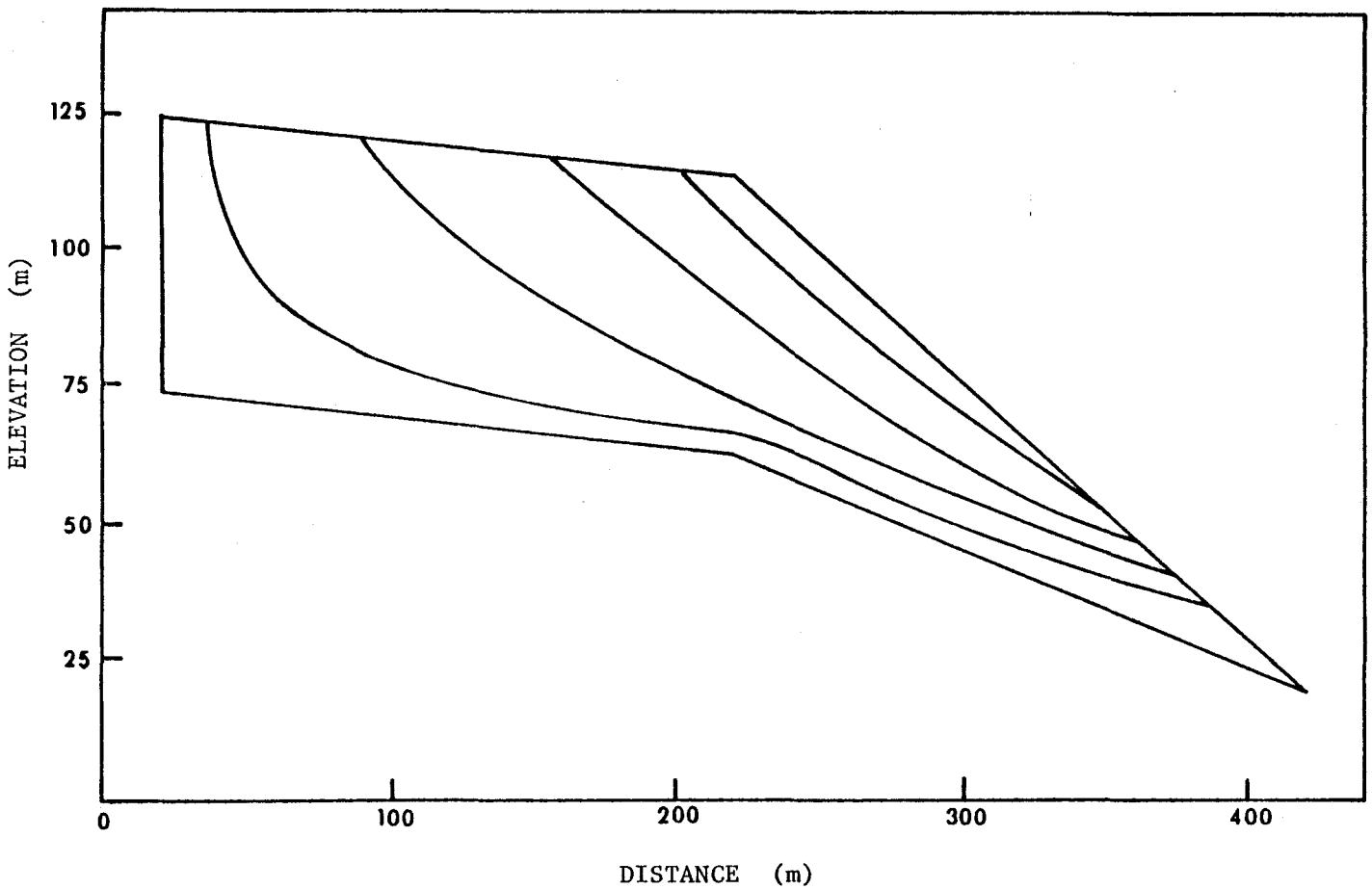

Figure 4-9 Particle Paths - Budd Method

TABLE 4-1 – LAMINAR FLOW

X-Coordinate	0	2.5	5.0	7.5	10.0
Calculated Values of ψ	0*	–25	–50	–75	–100
Theoretical Values of ψ	0*	–25	–50	–75	–100

* Fixed Values

TABLE 4-2 – SHEAR FLOW

X-Coordinate	0	2.5	5.0	7.5	10.0
Calculated Values of ψ	0*	-3.125	-12.500	-28.215	-50.000
Theoretical Values of ψ	0*	-3.125	-12.500	-28.215	-50.000

* Fixed Values

TABLE 4-3 - POISEUILLE FLOW

Y-Coordinate	0.0	2.5	5.0	7.5	10.0
Calculated Values of ψ	0.0*	0.8828	3.1250	6.3125	10.0310
Calculated Values of ψ with Extra Constraint	0.0*	.8755	3.1250	6.3160	10.0310
Theoretical Values of ψ	0.0*	0.8594	3.1250	6.3281	10.0000

* Fixed Values

TABLE 4-4 – MATERIAL PROPERTIES FOR THE DOUBLE SLOPE

A parameter	0.0327
n power	1.65
Unit weight	8.952 kN/m^3

CHAPTER 5

BARNES ICE CAP AND MOUNT LOGAN STUDIES

5.1 Introduction

The finite element models presented in the previous chapter were used to determine particle paths and to establish age of the glacier ice for two actual glaciers: the Barnes Ice Cap, Baffin Island, N.W.T., Canada; and Mount Logan, Yukon Territory, Canada. The geographic locations of these two glaciers are shown in Figures 5-1 (a) and (b), respectively.

The Barnes Ice Cap is a medium-sized, sub-polar ice cap, 6000 km^2 in surface area located in a highland area of North- Central Baffin Island [31]. The North-East slope of the Barnes Ice Cap is modelled along the Trilateration Net flowline [16]. Information on the bed and surface geometry was taken from Hooke and others [16].

Mount Logan is a small ice cap located in the Elias Range near the Alaskan-Yukon border. The North-West Col of Mount Logan was modelled; geometry of the glacier was taken from Holdsworth [12].

The purpose of these simulations was to determine the particle paths within actual glaciers, and then to use these particles paths to establish the age of the ice in the glaciers. Also, analyses of the flow regimes of both glaciers near the flow divides were studied; particular attention is paid to the position of the assumed flow divide with respect to the flow divide, and the variation in vertical velocity with depth at the divide.

To determine the age of the glacier ice using the stream function finite element formulation, the computed particle paths must correspond closely with actual particle paths in the glacier. To ensure this, the finite element velocity field must correspond closely with

the glacier velocity field. To approximate this condition the flow parameters used in the primitive variable method were adjusted so that the computed and measured surface velocity distributions were in good agreement. Owing to the fact that the horizontal velocity is generally much greater than the vertical velocity, it was decided to adjust only the horizontal velocities along the surface during optimization of flow parameters to arrive at a reasonable match between computed and measured velocities.

5.2 Barnes Ice Cap Simulations

The Barnes Ice Cap was modelled with 93 elements and 226 nodes, the grid is shown in Figure 5.2. A no-slip boundary along the bed, and a stress-free boundary along the surface were imposed; along the divide the horizontal velocity was fixed at zero.

Two distinct types of ice are found in the Barnes Ice Cap: blue ice and white ice. The white ice is concentrated in a band along the bottom of the glacier, and owes its colour to the presence of a high concentration of bubbles when compared to the surrounding blue ice. Owing to the higher concentration of bubbles the unit weight of the white is 8.535 kN/m^3, compared with 9.025 kN/m^3 for the blue ice [16]. The presence of these two types of ice is accounted for in the flow analyses. In these analyses both types of ice were considered to be incompressible and isothermal. Simulations for which the blue ice was considered to be slightly compressible did not significantly affect the horizontal surface velocity profile.

A constant n parameter (Equation 2.1) is used throughout the glacier, while the A flow parameter (Equation 2.1) was varied along the glacier from the margin to the divide. Computed horizontal velocities of simulations using Holdsworth's flow parameters of $n = 4.2$ and $A = 0.006$ [11], did not correlate well with the measured horizontal surface velocities. Simulations using Hooke's and others [16] flow parameters of $n = 2.59$ and variable A along the glacier, also yielded poor correlation with measured horizontal surface velocities. Based

on the results of these two simulations it was decided to simulate the glacier flow with $n=3.0$ and a varying A parameter, adjusted to correlate with the measured horizontal surface velocities. To accomplish this, the glacier was divided into 15 regions along its length, the measured velocity was compared to the finite element solution, the A parameter was adjusted based on the difference between the two velocities until the surface velocity over the section showed reasonable agreement with the measured values. The A parameter was treated as constant over the length of the section considered. The optimized variation of A with position along the glacier is shown in Figure 5-3.

The horizontal velocity profile is shown in Figure 5.4. The correlation between the measured and finite element solutions is generally quite good. The finite element solution tends to under-estimate the horizontal velocity near the margin. This may be due to the fewer number of elements used to model the margin as compared with portions of the glacier further upstream, where the velocity profiles correlate well.

The vertical velocity profile is shown in Figure 5-5. The measured and computed values of vertical surface velocity do not agree well. Owing to the small magnitude of the velocities, this can be attributed to small variations in longitudinal strain-rate caused by errors in modelling the geometry of the glacier surface and bed which result in significant changes in vertical velocity [16]; Hannafy notes that "the glacier bed topography and basal slope have a great effect on the horizontal and vertical displacements of the ice cap surface" [10].

Stream function finite element analyses were performed on the Barnes Ice Cap using the results of the primitive variable analysis. As there is no flow into the bedrock or across the divide, these boundaries must represent the limits of the flow field and as such they were fixed at a constant value of $\psi = 0$. Along the surface of the glacier the non-essential boundary condition is satisfied by prescribing velocities. The same grid was used for stream

function analysis as for the primitive variable analysis. Figure 5-6 shows the Barnes Ice Cap with particle paths. The general pattern of the particle paths agrees with those obtained by Hooke and Hudleston [17], shown in Figure 5-7. It should be noted that the particle paths obtained from the finite element analysis reflect changes in the bedrock topography, whereas the standard methods ignore the irregular bedrock geometry.

Isochrones are shown for 1000, 2500 years and 10000 years in Figure 5-8. The 10000 year isochrone is of particular interest because the white ice at the base of the Barnes Ice Cap is approximately 10000 years old. Based on O^{18} isotope studies, Hooke has confirmed that the top of the white ice is approximately 10000 years old [15]. The 10000 year isochrone calculated from the finite element analysis corresponds to the top of the layer of white ice, confirming that the ice here is approximately 10000 years old. The thickness of the white ice corresponds to the thickness calculated by Hooke.

To study the location of the flow divide several simulations were performed on a grid that contained part of the South-West slope of the Barnes Ice Cap. The grid for these simulations consisted of 100 elements and 241 nodes. Along the bed a no-slip boundary was imposed, and along line A-B (see Figure 5-9), the velocities were specified by using Nye's shear flow equation [24]. A simulation of the entire Barnes Ice Cap indicated that the ice was almost in a state of laminar shear flow along line A-B. The A flow parameter was adjusted to provide a smooth transition in velocities from the North-East slope to the South-West slope. The flow parameters are given in Figure 5-10. The horizontal surface velocity profile is shown in Figure 5-11. By using element shape functions the position of the flow divide was calculated to be offset 12 metres to the South-West of the assumed divide. This position differs from the position obtained by Hannafy [10]. However, it should be noted that Hanaffy [10] used Meier's flow law and accounted for some slippage. He also used a lower order of interpolation of velocity.

Another way of establishing the position of the flow divide is to determine the path of the streamline $\psi = 0$. The stream function was fixed at $\psi = 0$ along the bed of the glacier to satisfy the essential boundary condition of the problem. Physically this boundary condition is enforced to ensure that there is no flow into the bedrock. The flow divide is by definition the boundary that separates two flow regimes, that is, there can be no flow across the divide. Tracing the near vertical path of the streamline $\psi = 0$ should, therefore, within numerical limitations show the variation of the flow divide with depth in the glacier.

A stream function analysis of both the North-East and a portion of the South-West slopes was carried out, the results of which are shown in Figure 5-12. For this simulation the stream function was fixed at $\psi = 0$ along the bed of the glacier, a velocity boundary was imposed on the surface and along A-B (Figure 5-9). The divide was also shifted towards the South-West, however, it was shifted by 15 metres to the South-West. The difference in the predicted two positions of the divide is due to the fact that the two finite element models are not strictly compatible since velocity is interpolated quadratically in the primitive variable model and stream function is interpolated quadratically in the stream function model. From the definition of stream function given in Chapter 4, stream function would have to be interpolated cubically for the two models to be compatible.

Raymond [29] used the finite element method to study the deformation of ice near the flow divide of an idealized glacier. He found that at the divide the vertical velocity component, v_z, at a distance z above the bed is given by,

$$\frac{v}{v_s} = \left(\frac{z}{h}\right)^2 \tag{5.1}$$

where h is the ice thickness and v_s is the vertical velocity at the surface. One implication of this relationship is that the vertical strain-rate, $\dot{\varepsilon}_z$, decreases linearly from $2(v_s/h)$ to zero at the bed. Raymond's analysis shows that the surface value of vertical strain-rate is always

greater than the values assumed in simple flow models which have been used to establish the age of the ice.

Raymond's relationship for variation of vertical velocity at the divide was tested using the velocities obtained from the finite element model. The variation of vertical velocity with depth at the divide of Barnes Ice Cap is shown in Figure 5-13. It can be seen that Raymond's relationship fits quite well to the calculated finite element velocities. The slight scatter of data near the divide this is due to the fact that the relationship was developed for a glacier having a flat bed, whereas the bed at the divide of the Barnes Ice Cap is actually sloping.

5.3 Mount Logan Simulations

There were two parts to the Mount Logan simulations:

(i) a study of a major portion of the glacier; and

(ii) a study in the vicinity of the divide.

A much finer grid near the divide was used to better define the deformation patterns in the vicinity of the divide, and to establish the age of the ice of a core recently obtained from the divide region.

5.3.1 Mount Logan Study

Mount Logan was modelled with 100 elements and 243 nodes (Figure 5-14). Mount Logan is frozen to its bed, accordingly a no-slip boundary condition was used. Along lines A-B and C-D a velocity boundary condition was imposed by using the Nye shear flow equation [24].

Three distinct types of ice exist in the glacier:

(i) a firn layer;

(ii) a transitional layer; and

(iii) glacier ice.

Holdsworth [12] gives data on the variation of density with depth, reproduced in Figure 5-15. Each different layer was given an average unit weight based on this relationship. All the layers were modelled as being incompressible and isothermal. Initial simulations treating the firn as a slightly compressible material did not greatly affect the velocity distributions at the surface. The flow parameters were $n = 1.284$ and $A = 0.0086$ throughout the glacier.

The horizontal velocity profile is shown in Figure 5-16. The finite element solution and the measured horizontal surface velocities correlate. The surface velocities were not known over the entire length of the region modelled, therefore the finite element model was tuned to match only the known velocities over a restricted range of the glacier. The vertical surface velocity profile is shown in Figure 5-17. The measured vertical velocities and the finite element solutions do not correlate well at all. The finite element solution underestimates the vertical velocity. This has been attributed to the presence of some lateral strains not accounted for in this analysis. Furthermore, the assumption of incompressibility is not applicable to firn.

The stream function finite element analysis was performed on the glacier using the velocities and rotations obtained from the primitive variable analysis. The essential boundary condition of $\psi = 0$ along the bed, and a velocity boundary condition on the surface of the glacier, were imposed. Along lines A-B and C-D (Figure 5-14), a velocity boundary condition was also imposed. The resulting particle paths are shown in Figure 5-18. Again, as for the Barnes Ice Cap the particle paths in the vicinity of the bed tend to reflect changes in the bedrock topography.

Isochrones established with the particle paths are shown in Figure 5-19. Holdsworth [12] has established that the 21 year horizon of an ice core obtained from a

borehole 300 metres down the flowline from the NW Col lies at a depth of 18.3 metres. Figure 5-19 shows that the 21 year horizon based on the finite element model lies at 18.7 metres. In view of the comparison between measured and computed vertical velocities, this agreement is fortuitous.

5.3.2 Divide Study

To study the position of the divide region of Mount Logan a much finer finite element mesh was used. This grid consisted of 67 elements and 162 nodes. The same ice properties and flow parameters were used for these simulations as for the previous analysis of the glacier. For the primitive variable analysis a no-slip boundary along the bed, and a stress-free boundary along the surface were imposed. Along the right and left-hand sides of the grid a velocity boundary condition was imposed by using the velocities determined from the primitive variable model for the previous analysis (see Figure 5-20).

The horizontal and vertical surface velocity profiles agreed with those obtained from the primitive variable analysis of the previous analysis (Figures 5-21,5-22).

The stream function analysis was performed on the divide region by fixing $\psi = 0$ along the bed, and by imposing a velocity boundary condition along the surface, and the right-hand and left-hand sides of the model. The resulting particle paths are shown in Figure 5-23.

Holdsworth [13] has established that the 37 year and 68 year horizons for a core obtained from the NW Col, lie at depths of 25.0 metres and 44.0 metres, respectively. Isochrones drawn based on the finite element particle paths give the depths of these two horizons to be 22.0 metres and 35.3 metres, respectively (Figure 5-24). The discrepancy in depths is attributed to the differences between the actual vertical velocities and those obtained from the primitive variable model.

The positions of the flow divide and assumed flow divide are shown in Figure 5-25. The flow divide is offset 15 metres to the left of the assumed divide. It should be noted that the divide separating the flow regimes does not follow a straight line down to the bed, rather, it slopes down to the right until it intersects the bed. This fact severely limits the use of standard methods of dating the ice, near the bedrock, which assume that the ice flows straight down from the surface location of the divide.

Raymond's relationship, equation 5.1, was again verified for the flow divide, the plot of vertical velocity with depth is shown in Figure 5-26.

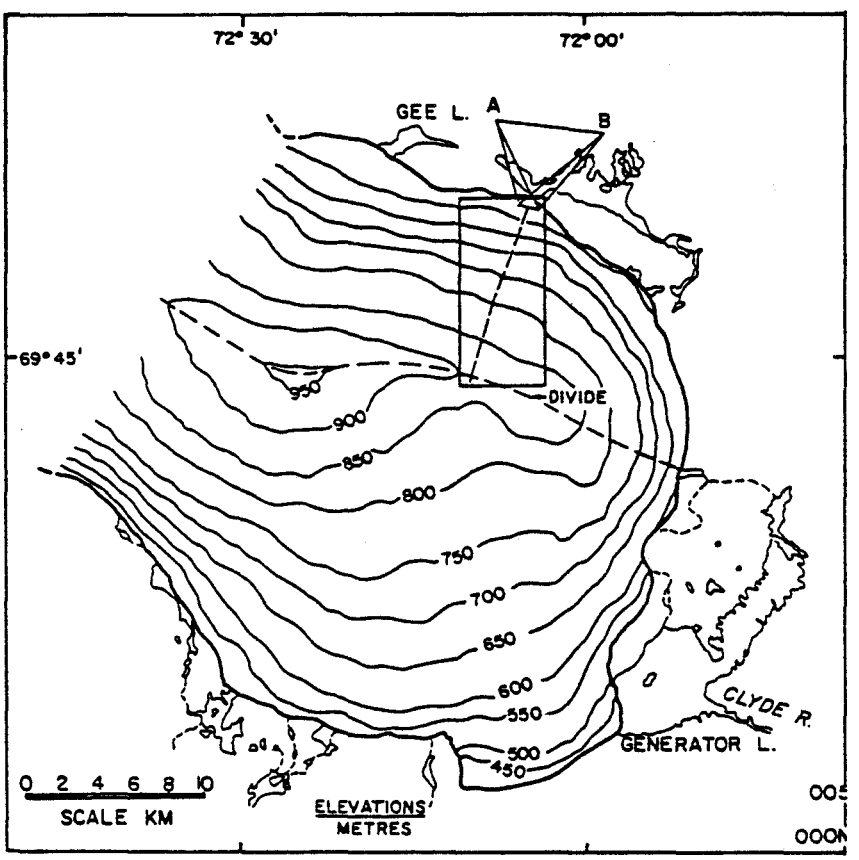

Figure 5-1 (a) Location of the Barnes Ice Cap [11]

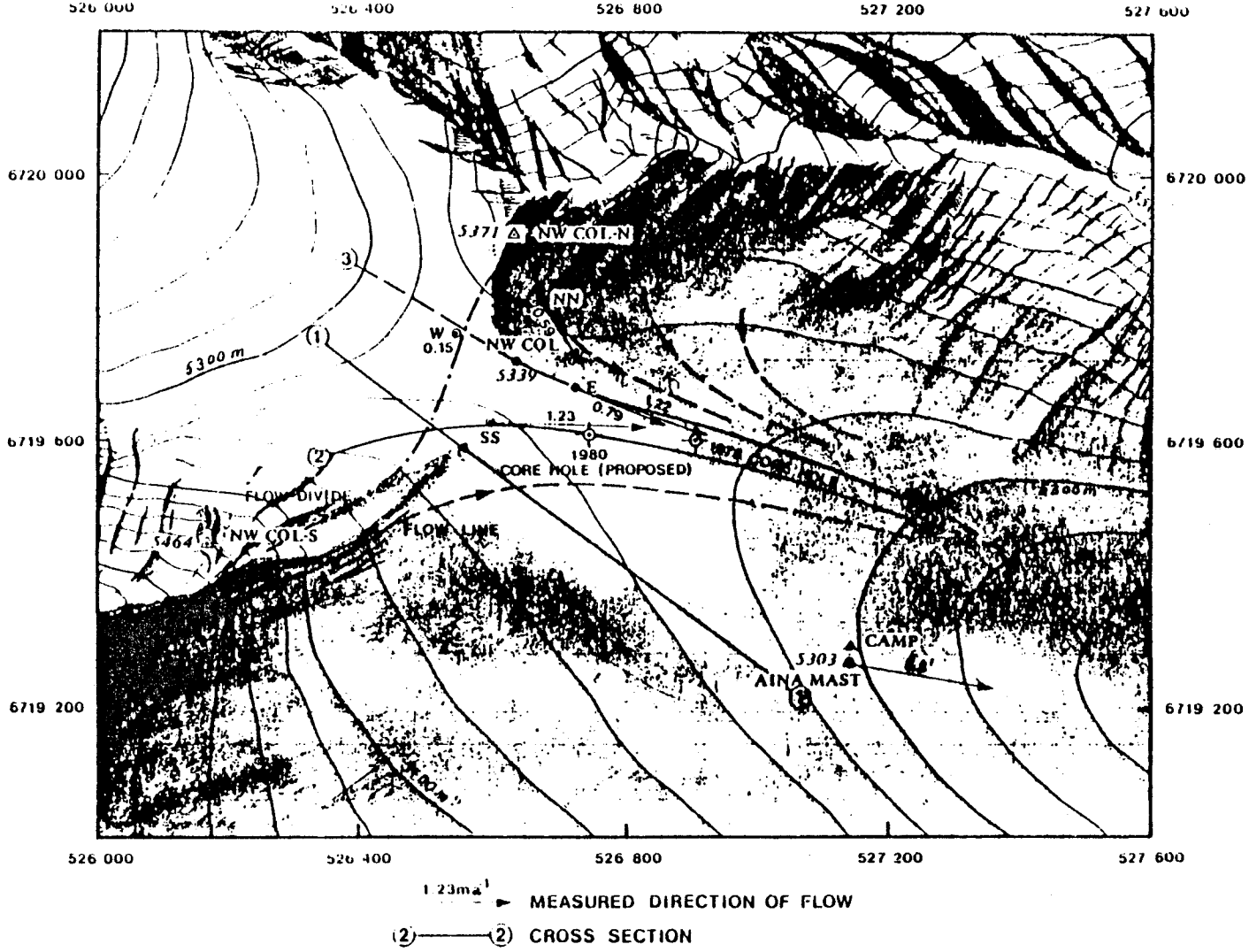

Figure 5-1 (b) Location of Mount Logan [12]

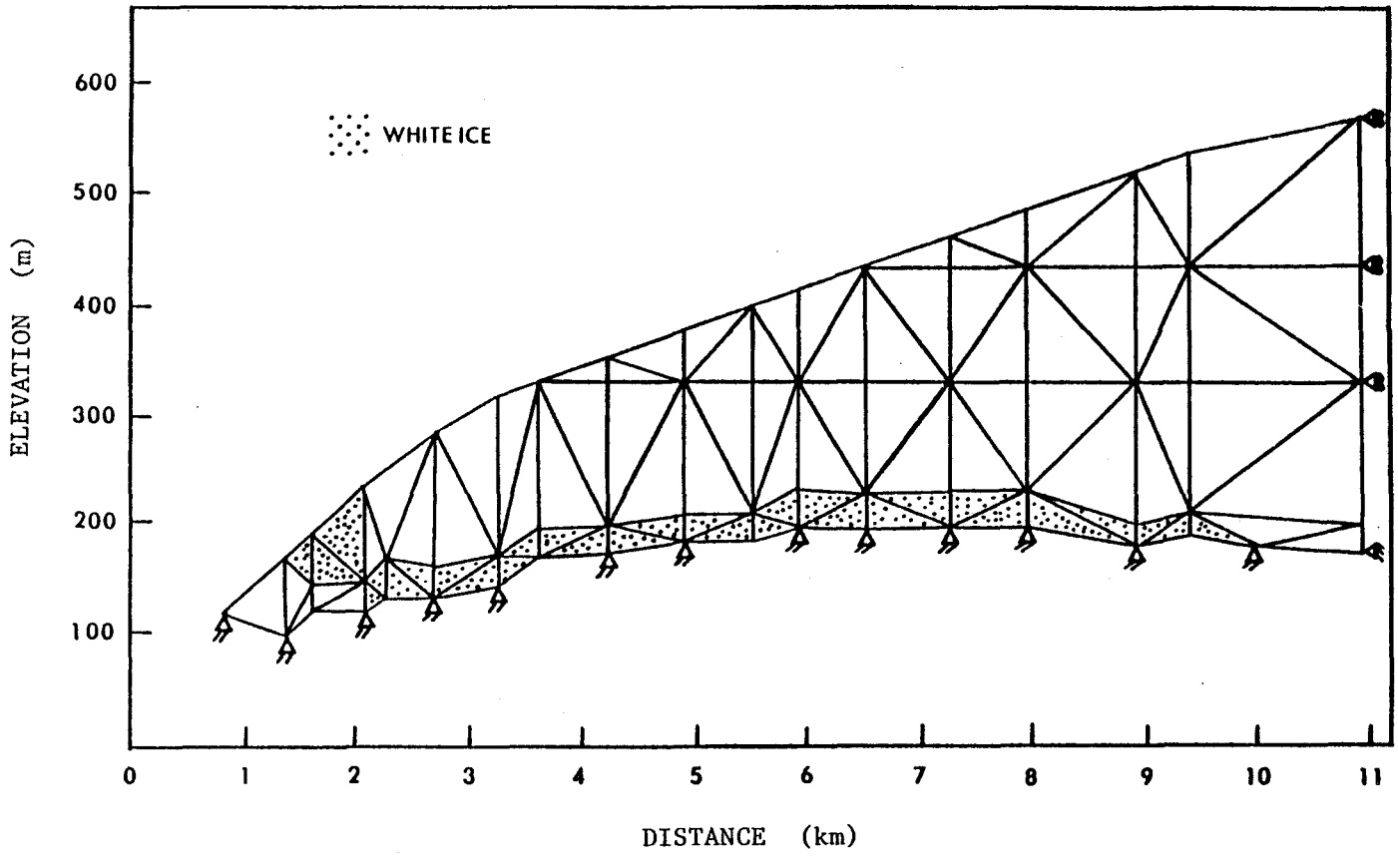

Figure 5-2 Barnes Ice Cap Grid

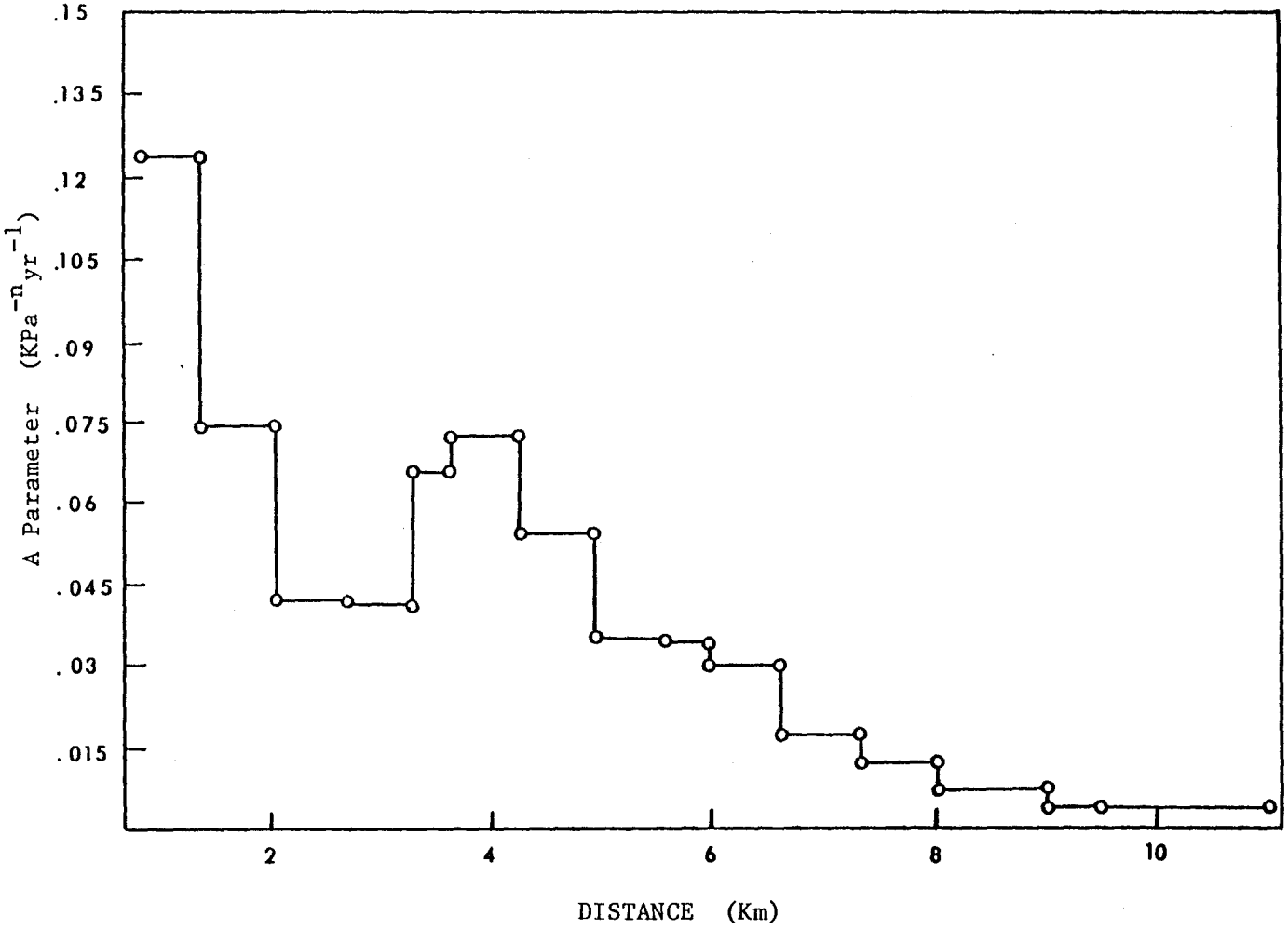

Figure 5-3 Variation of A Parameter - Barnes Ice Cap

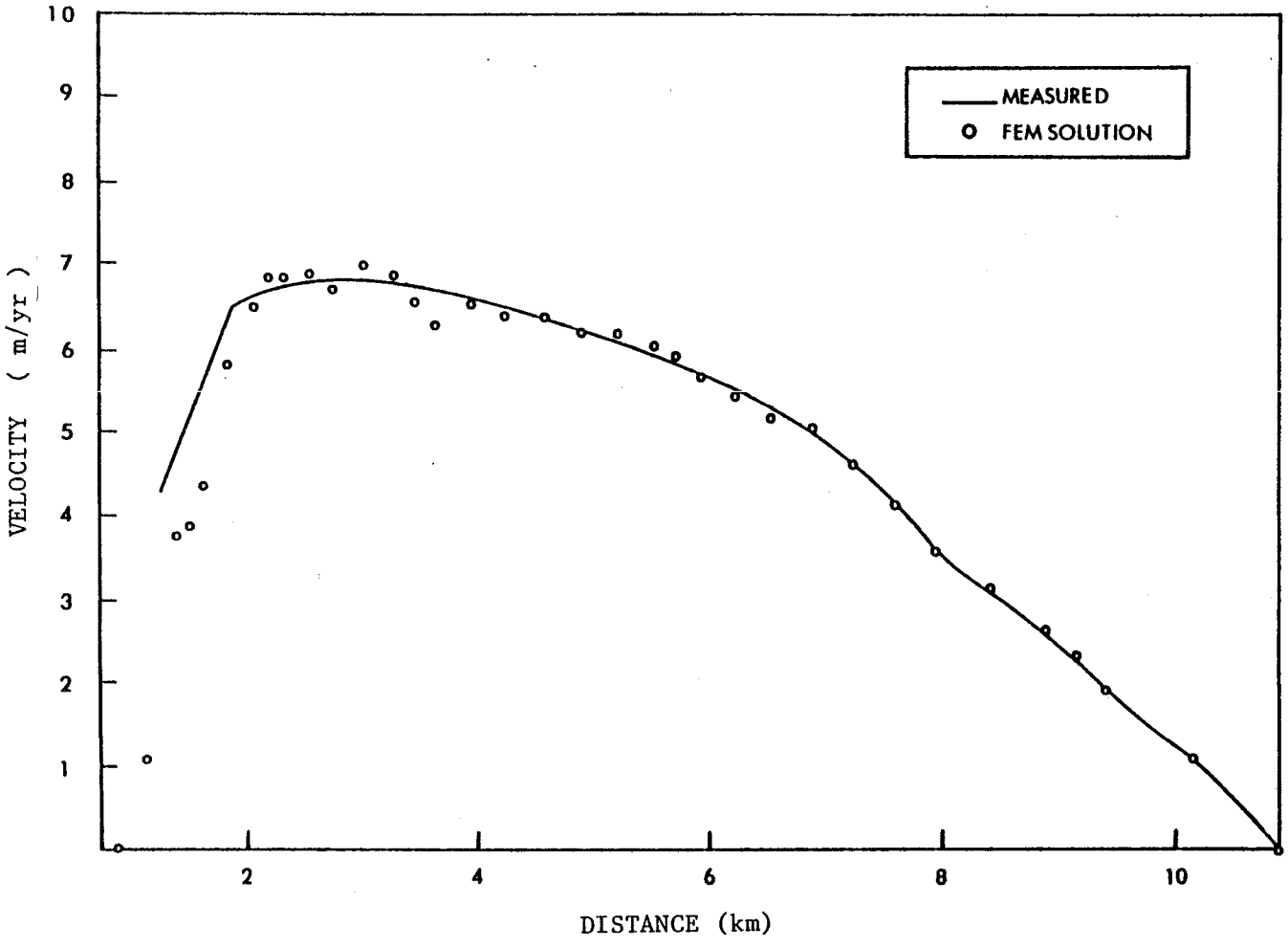

Figure 5-4 Horizontal Velocity Profile - Barnes Ice Cap

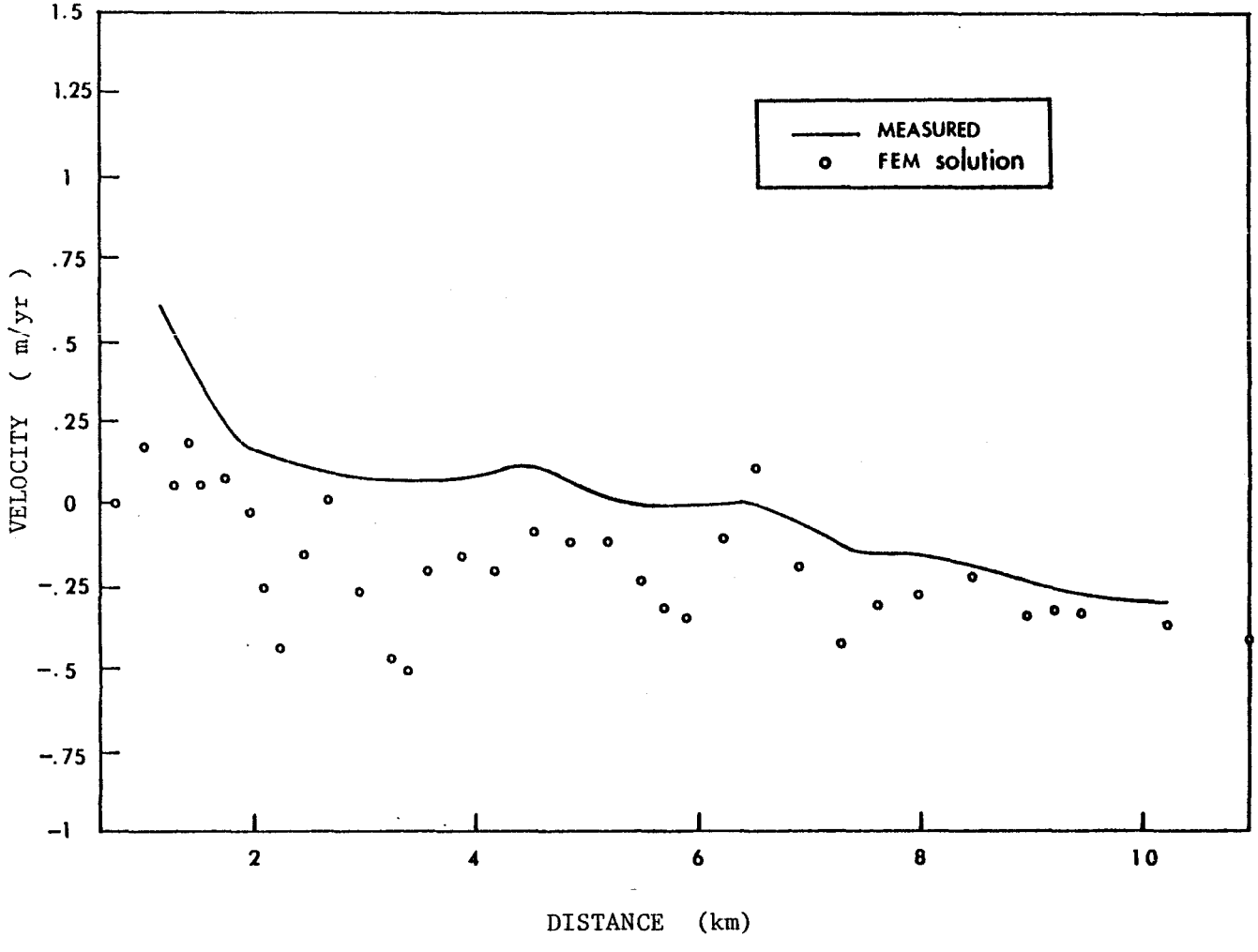

Figure 5-5 Vertical Velocity Profile - Barnes Ice Cap

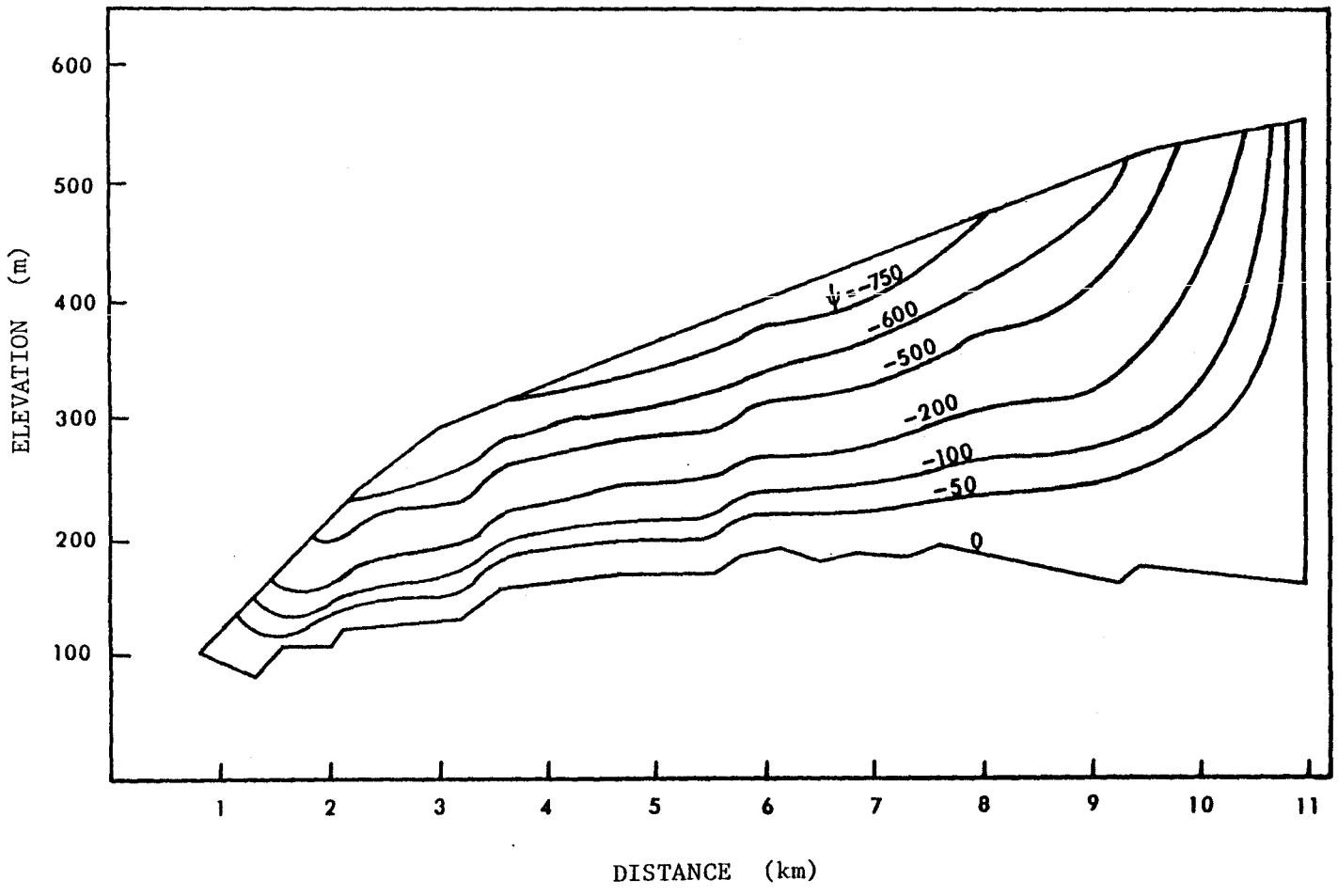

Figure 5-6 Particle Paths - Barnes Ice Cap

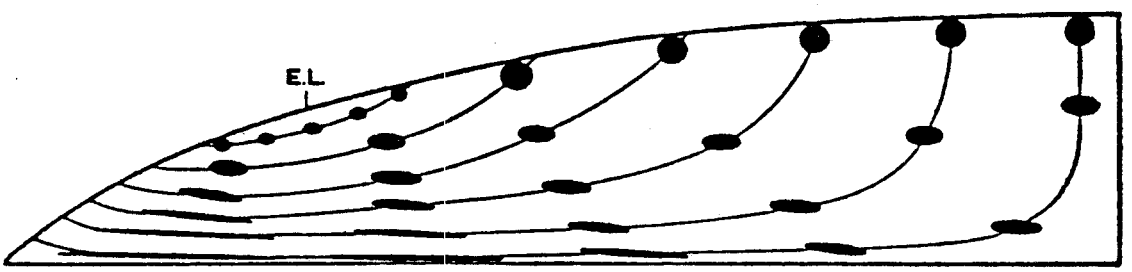

Figure 5-7 Idealized Particle Paths - Barnes Ice Cap [17]

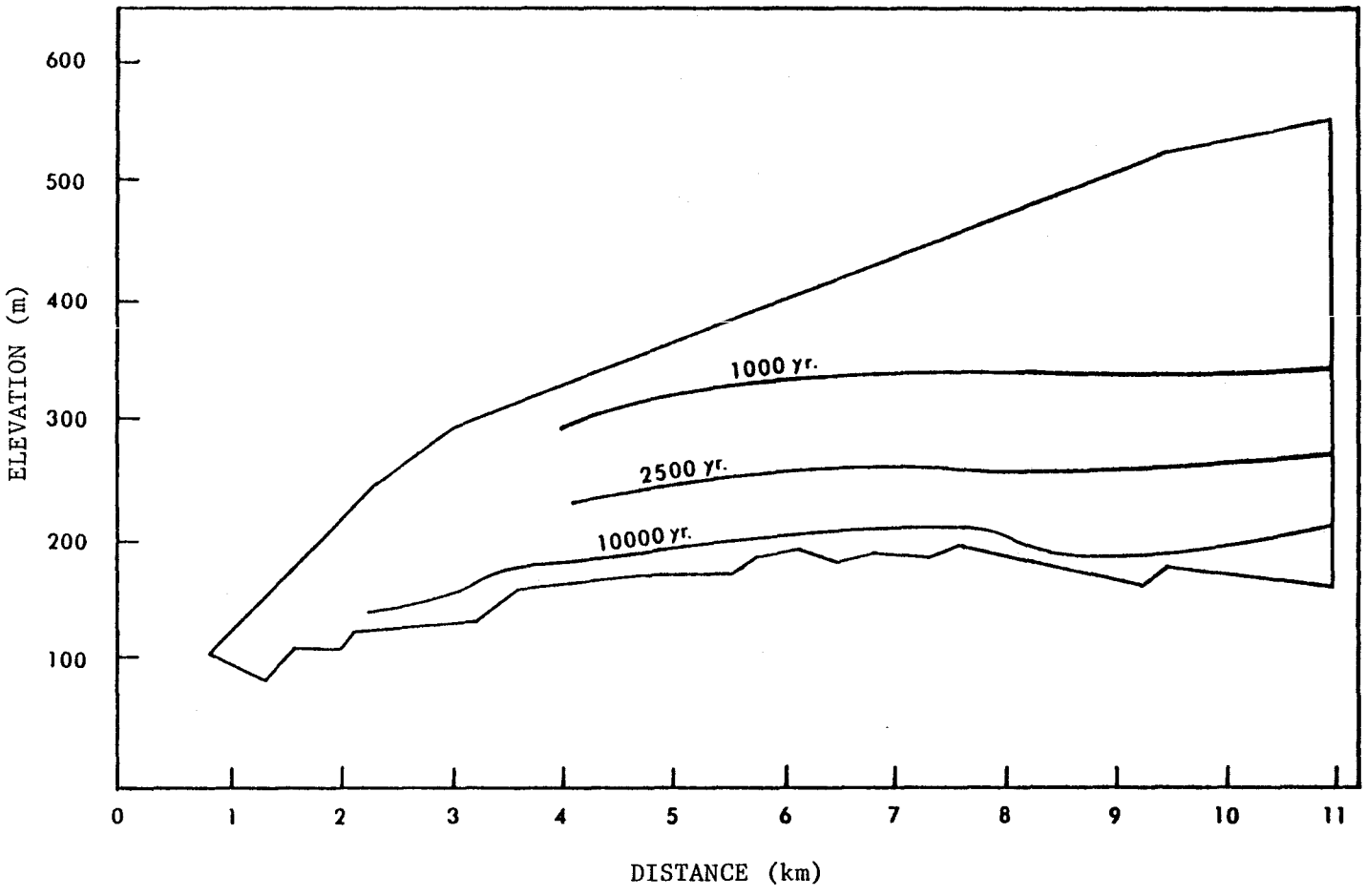

Figure 5-8 Isochrones - Barnes Ice Cap

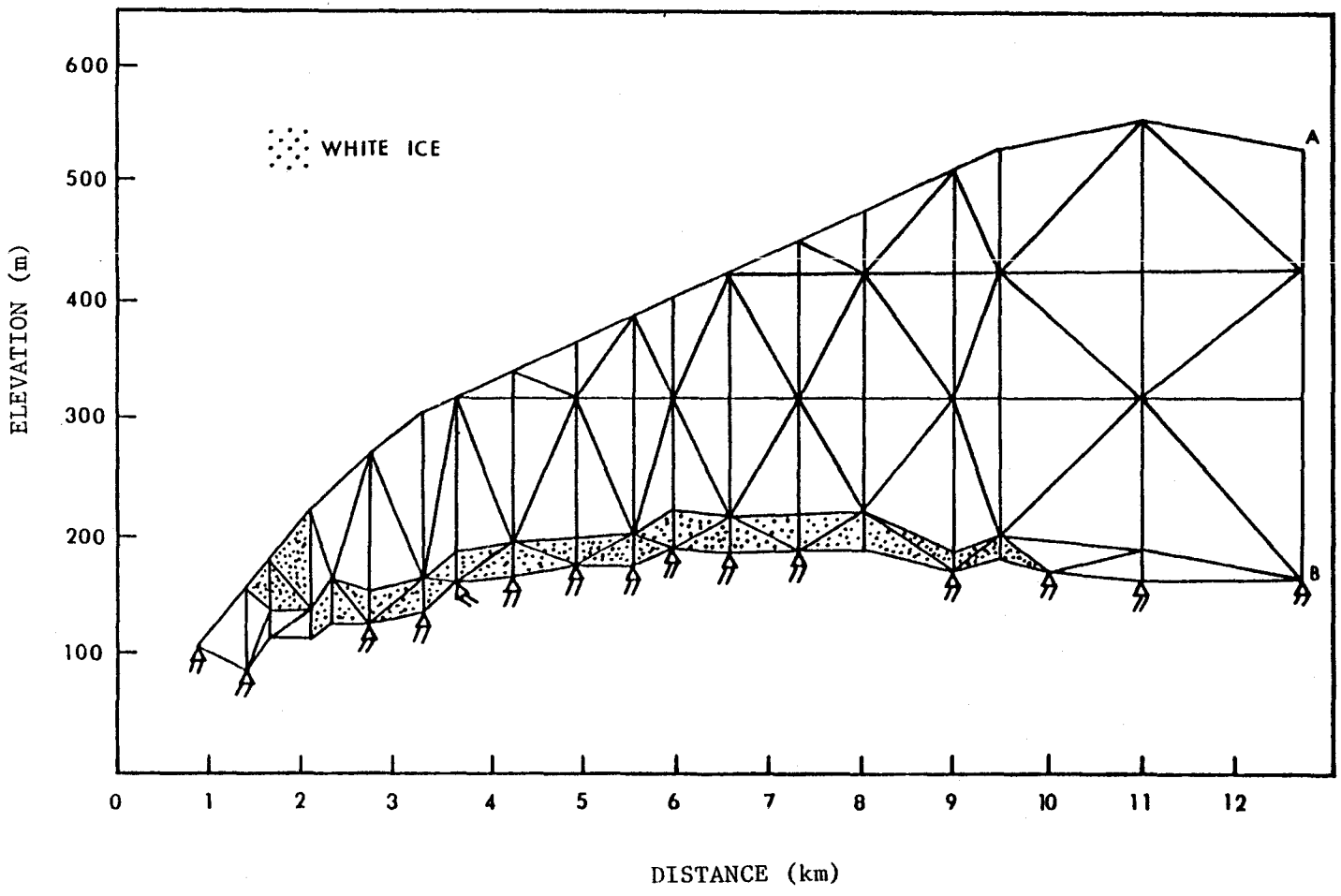

Figure 5-9 Barnes Ice Cap South-West Extension Grid

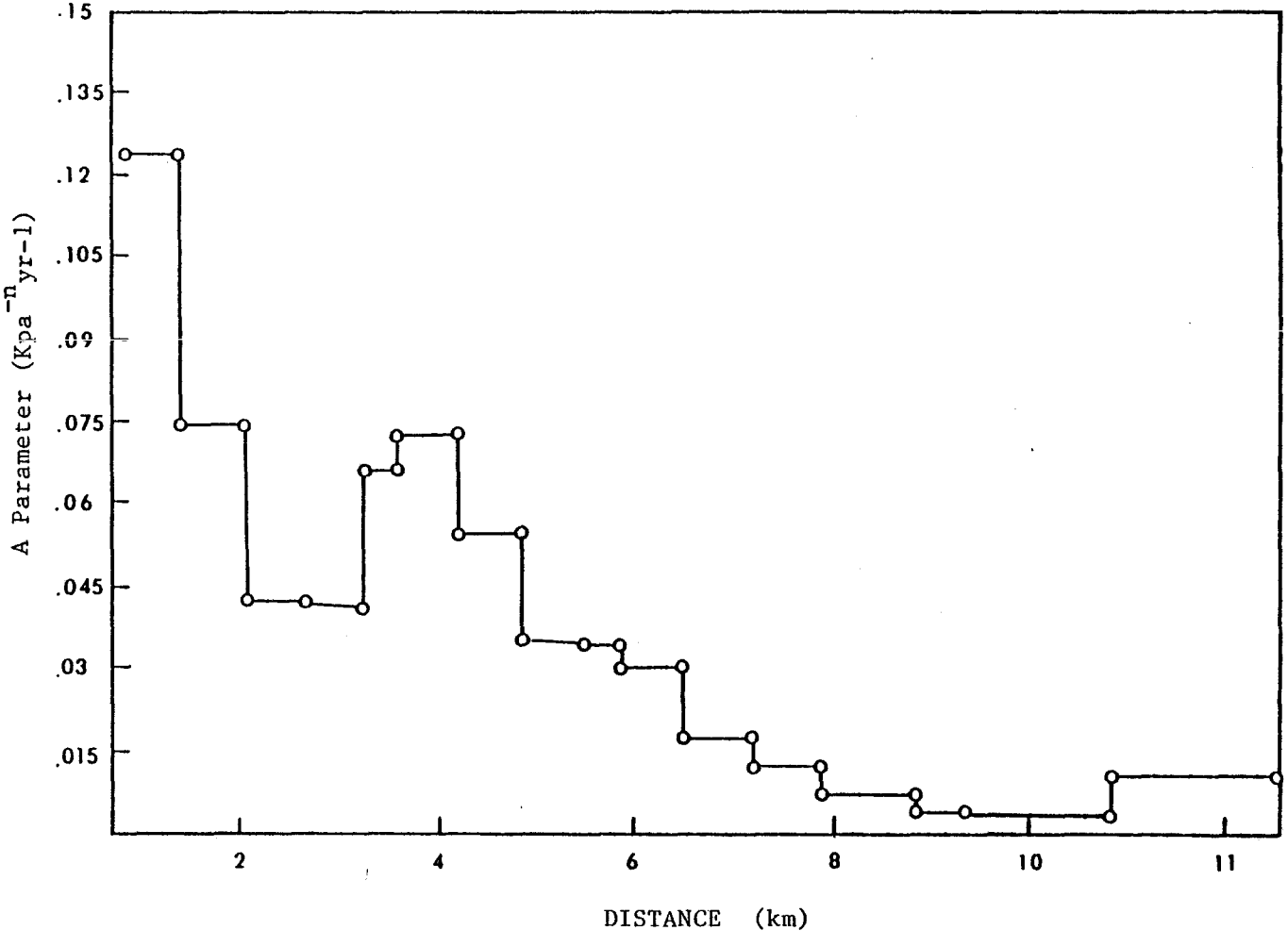

Figure 5-10 Variation of A Parameter - Barnes Ice Cap
South-West Extension Grid

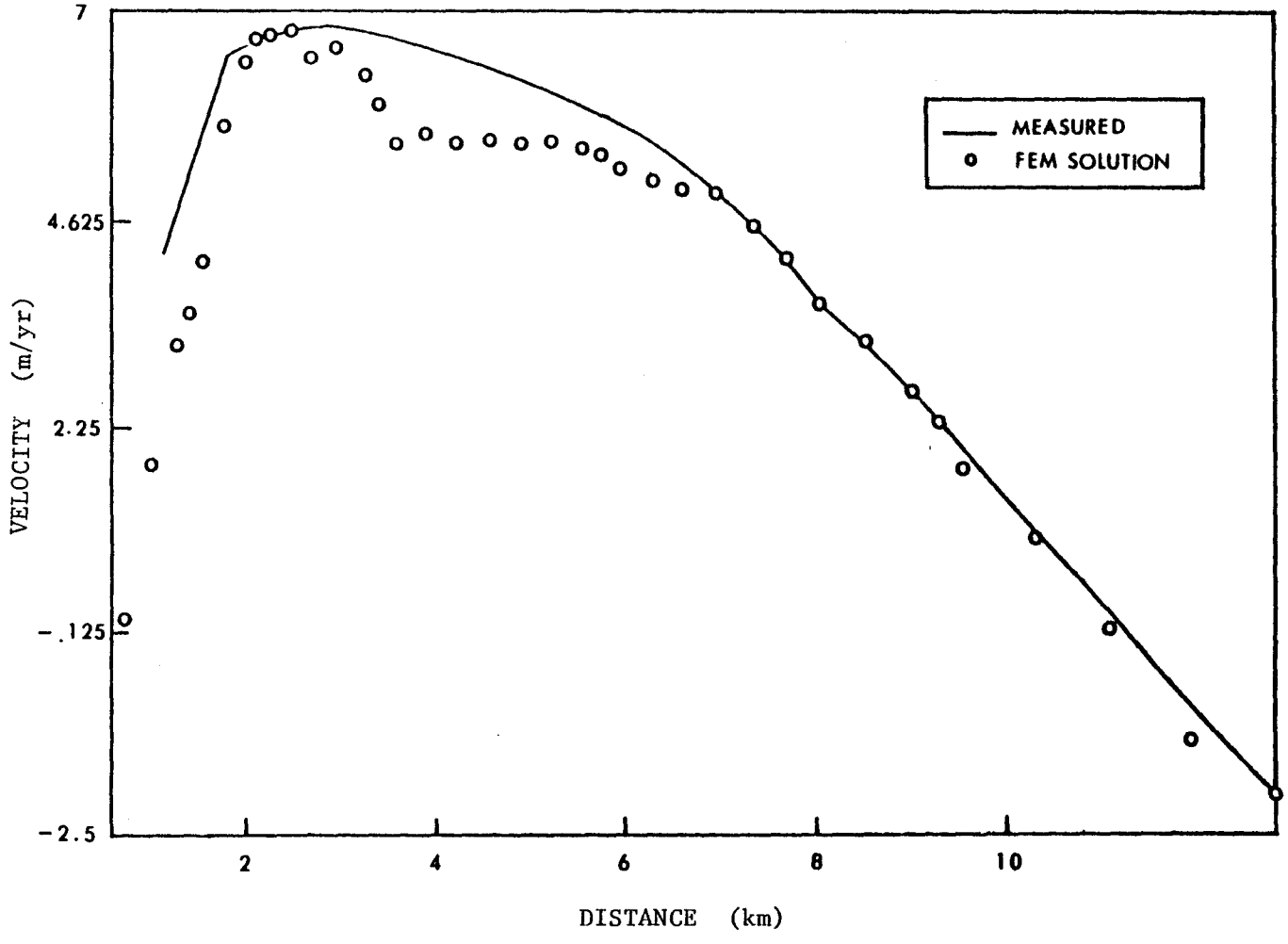

Figure 5-11 Horizontal Velocity Profile -
Barnes Ice Cap South-West Extension Grid

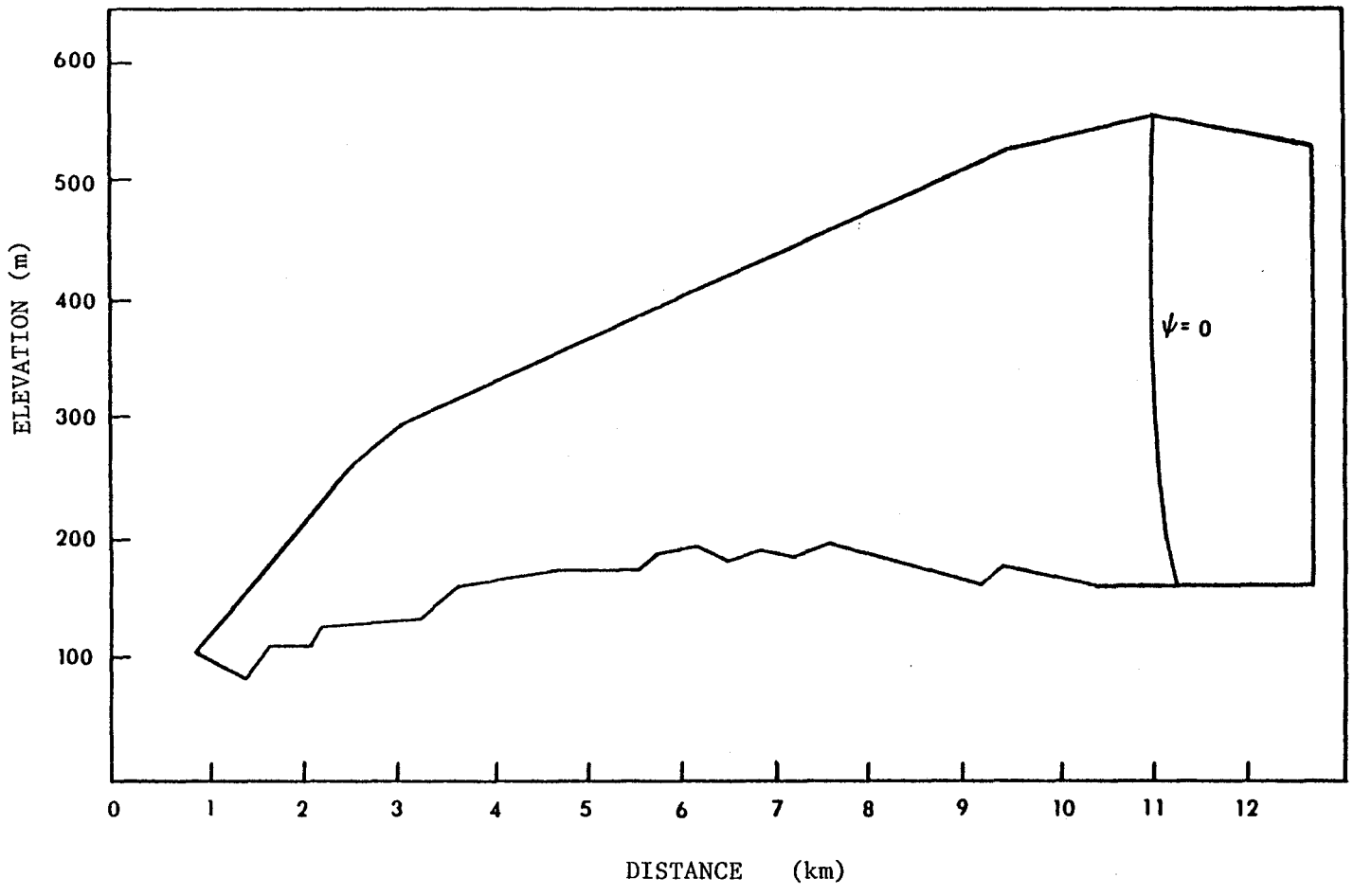

Figure 5-12 Particle Path for $\psi = 0$ - Barnes Ice Cap South-West Extension Grid

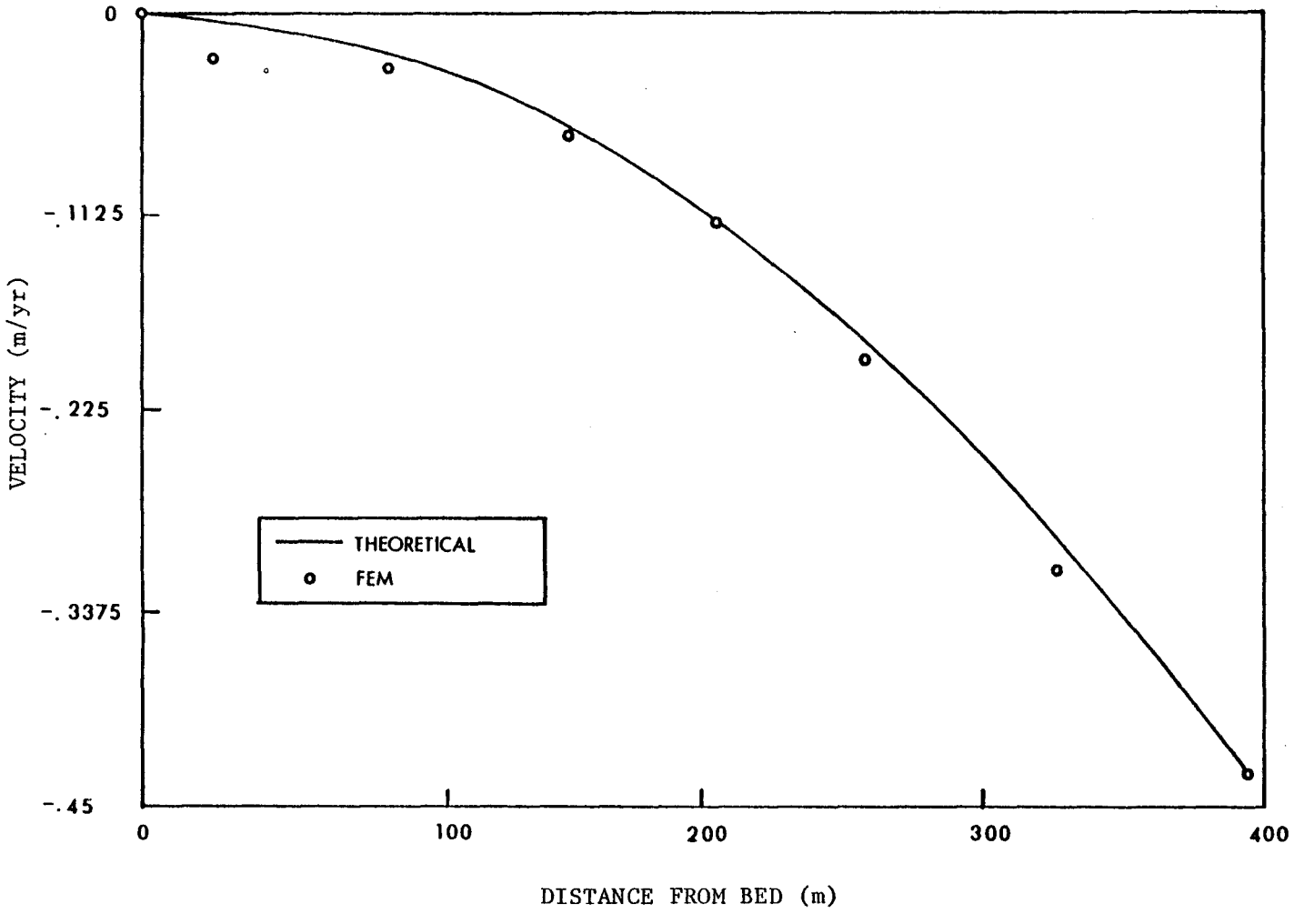

Figure 5-13 Raymond's Relation - Barnes Ice Cap

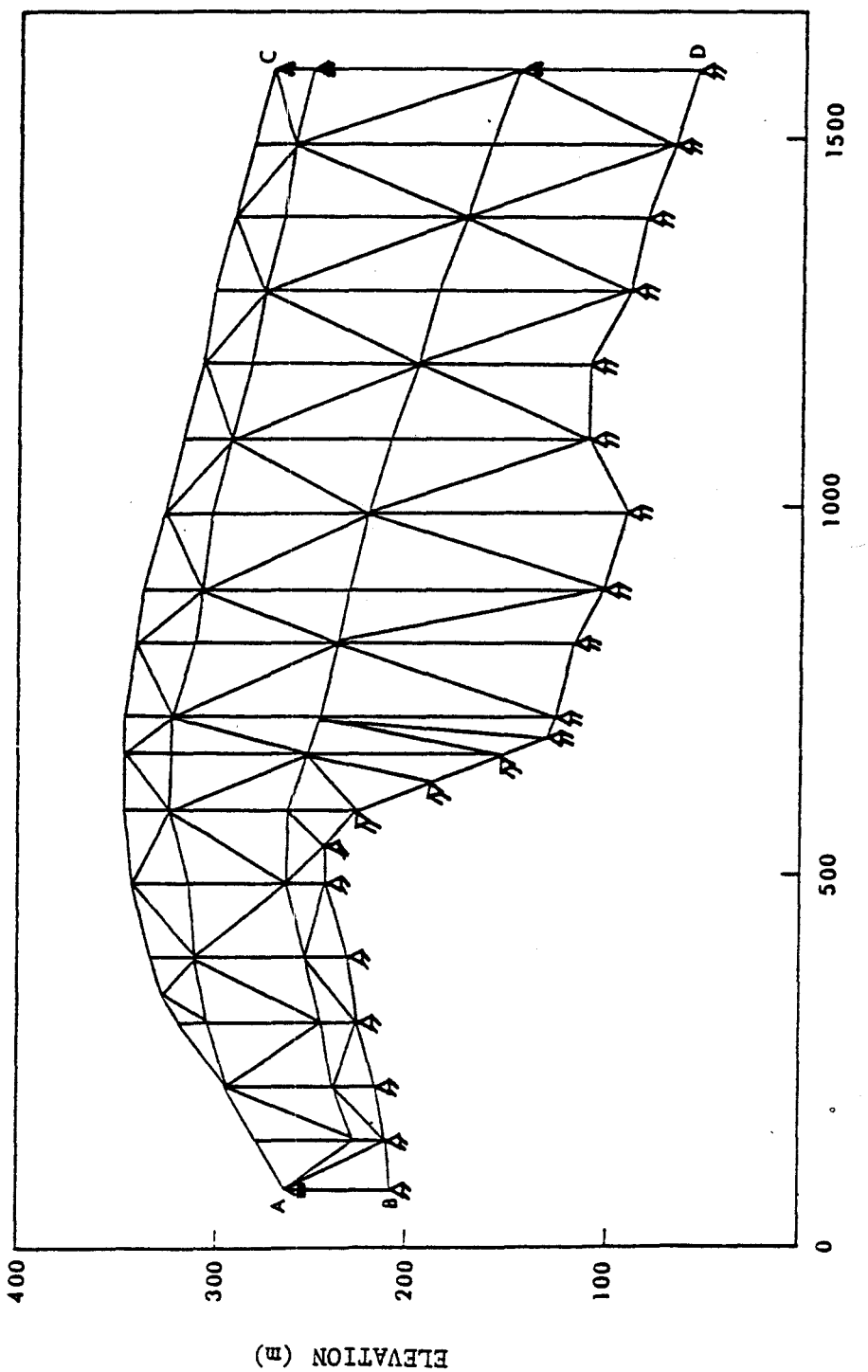

Figure 5-14 Mount Logan Grid

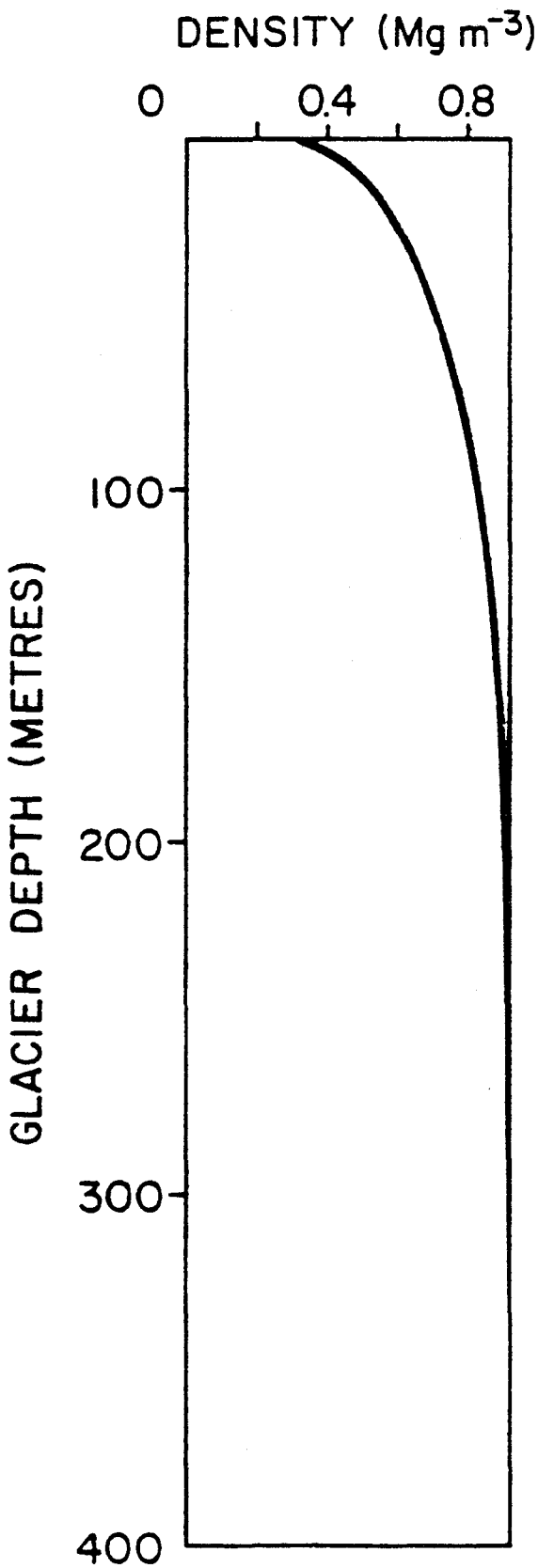

Figure 5-15 Variation in Density with Depth [12]

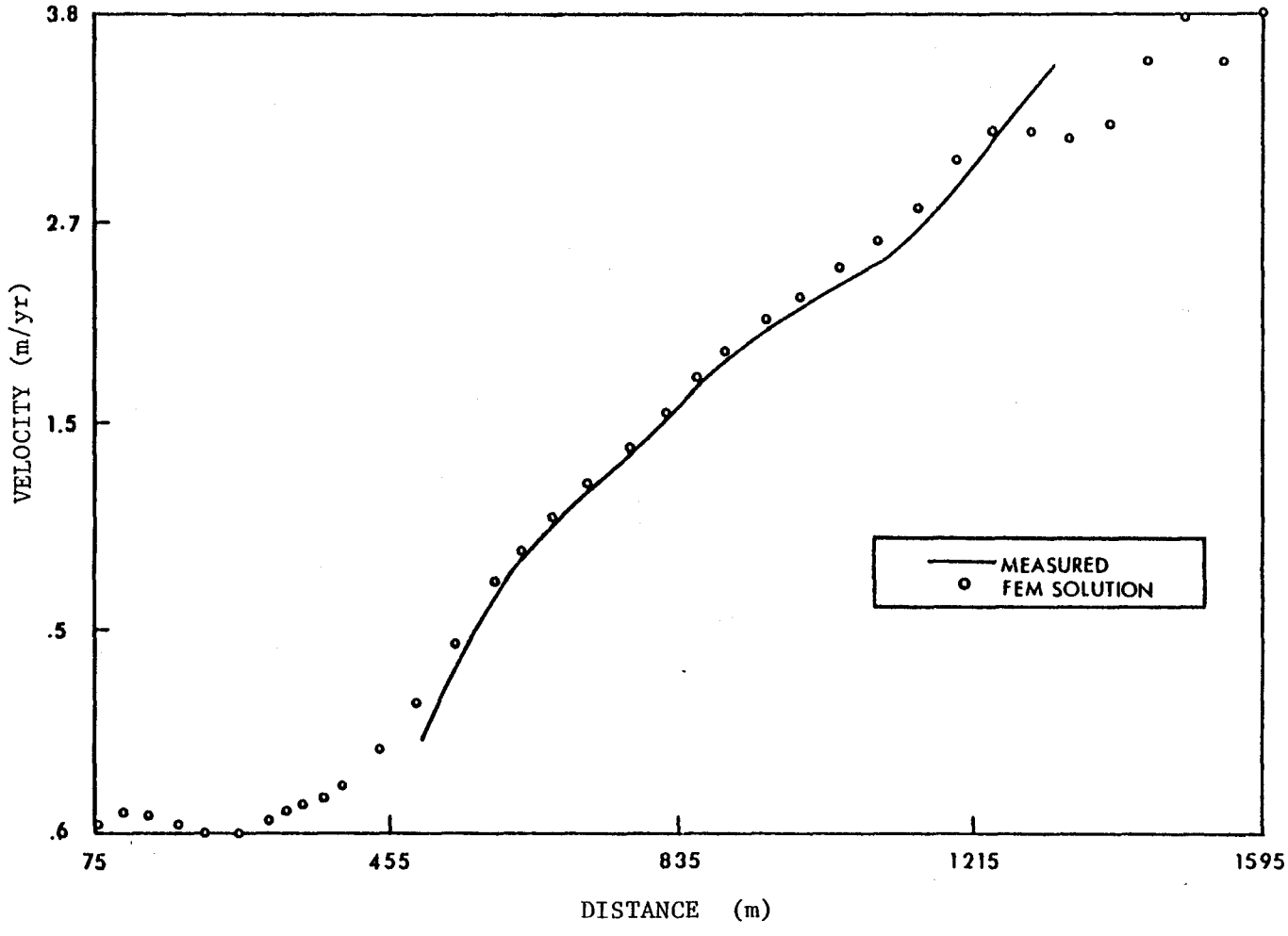

Figure 5-16 Horizontal Velocity Profile - Mount Logan

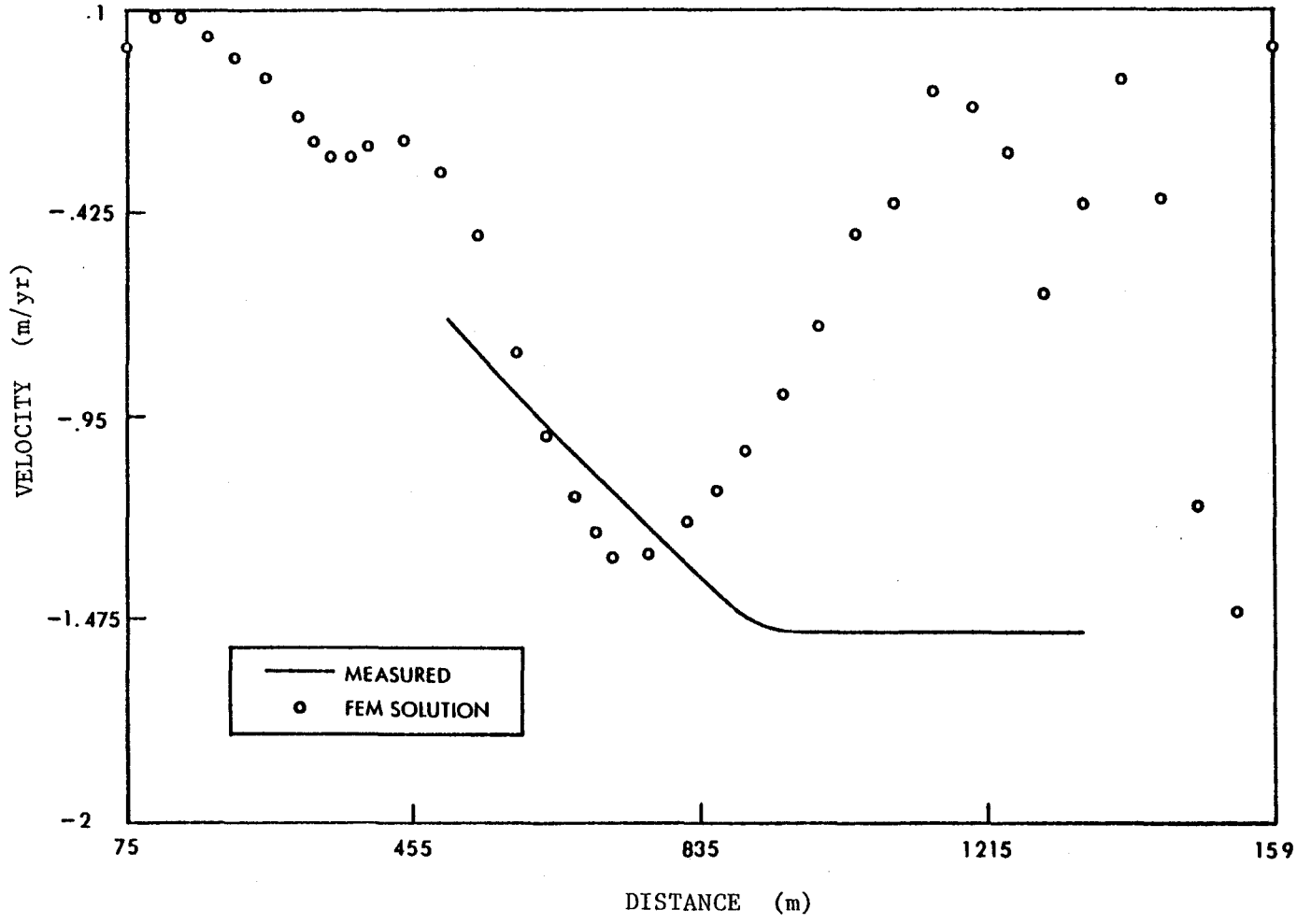

Figure 5-17 Vertical Velocity Profile - Mount Logan

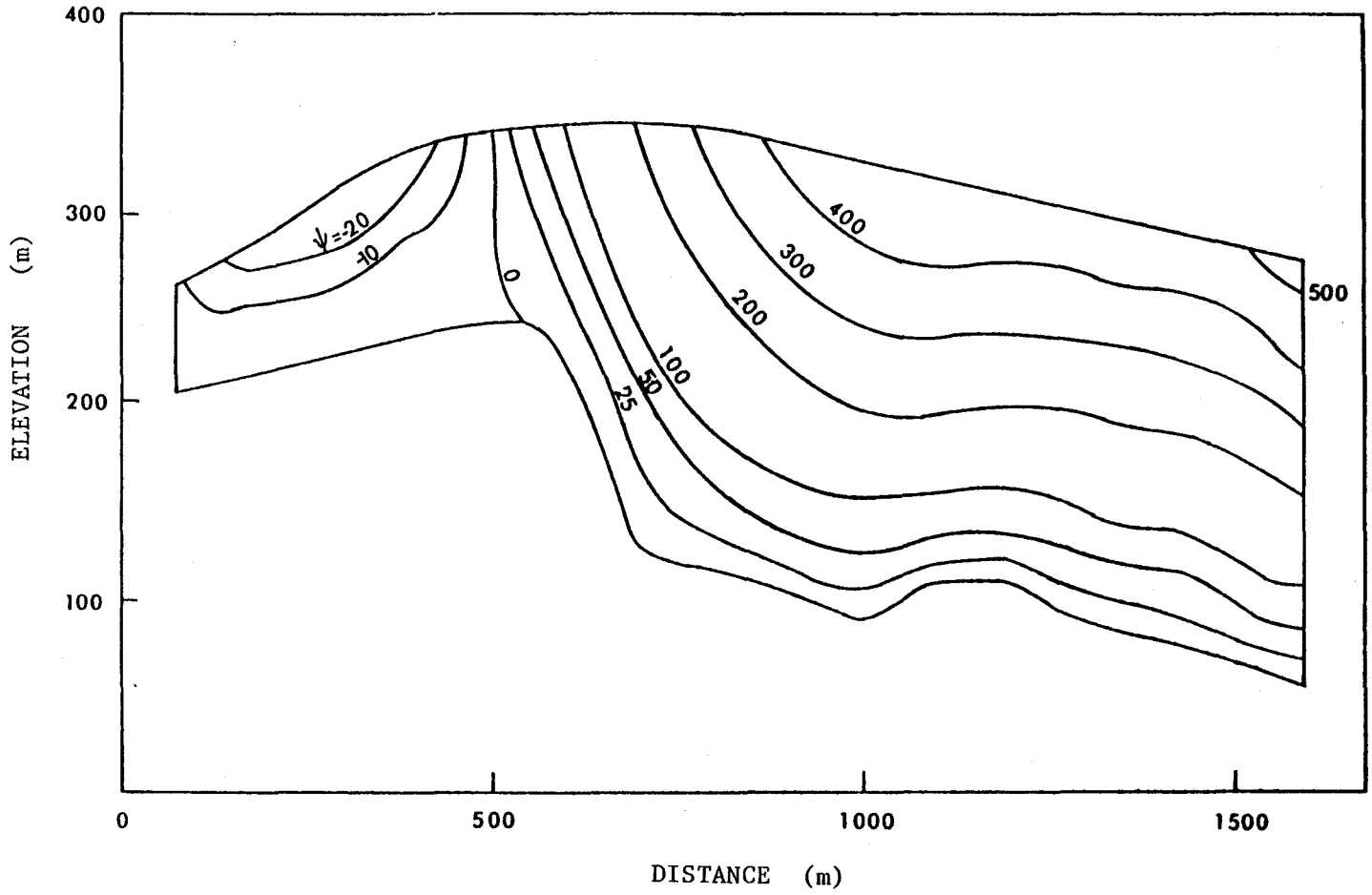

Figure 5-18 Particle Paths - Mount Logan

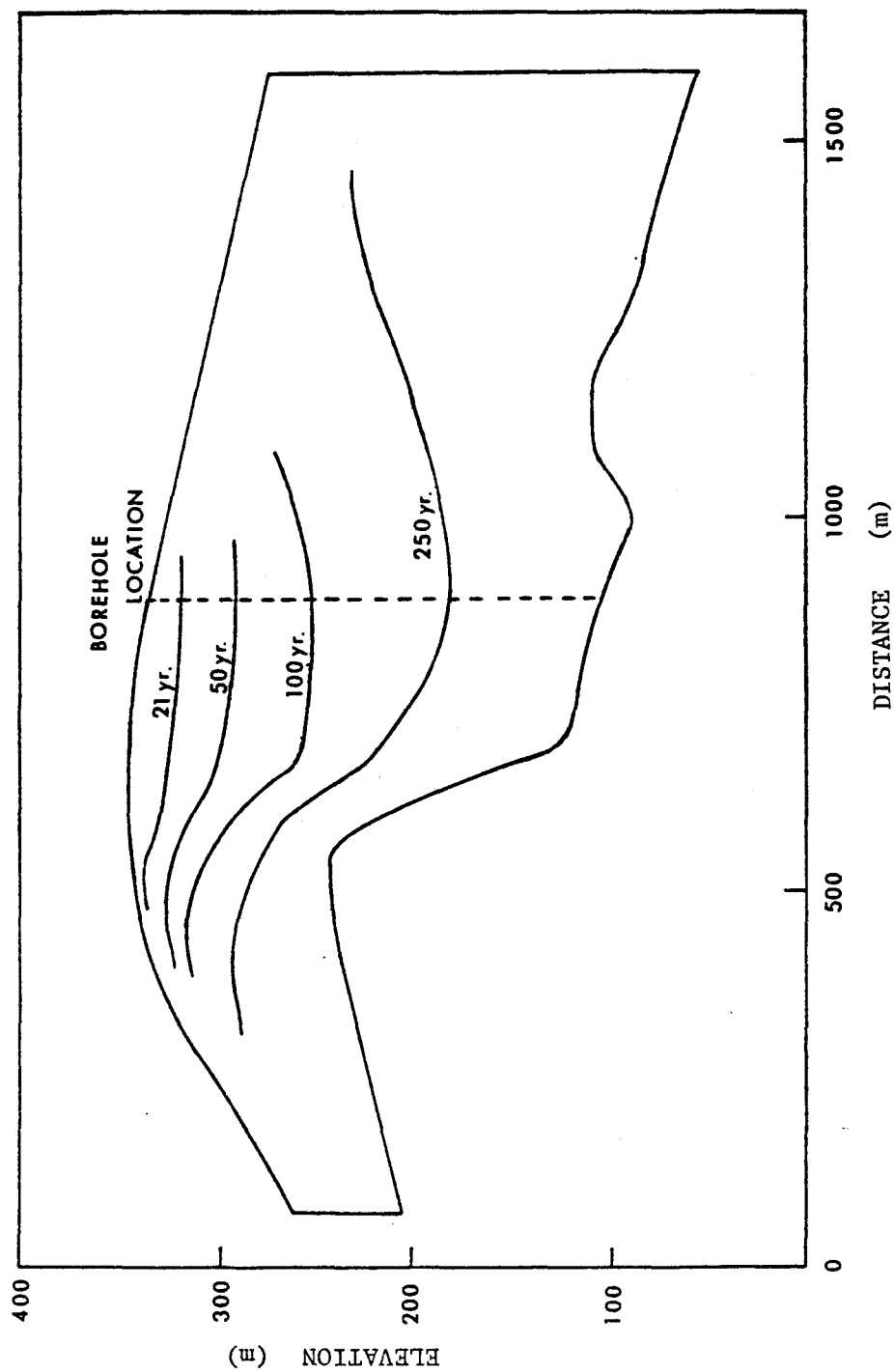

Figure 5-19 Isochrones - Mount Logan

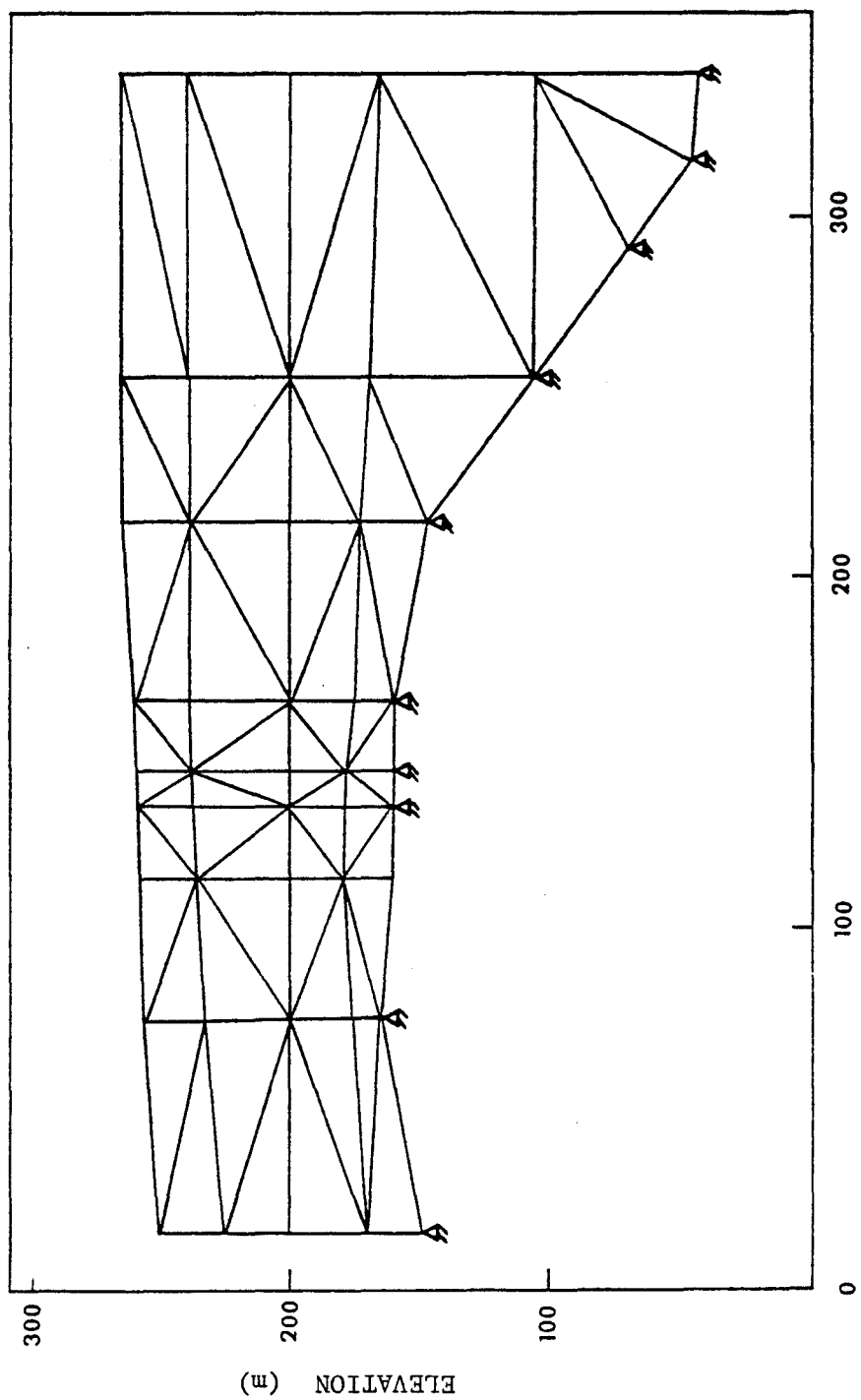

Figure 5-20 Mount Logan Divide Grid

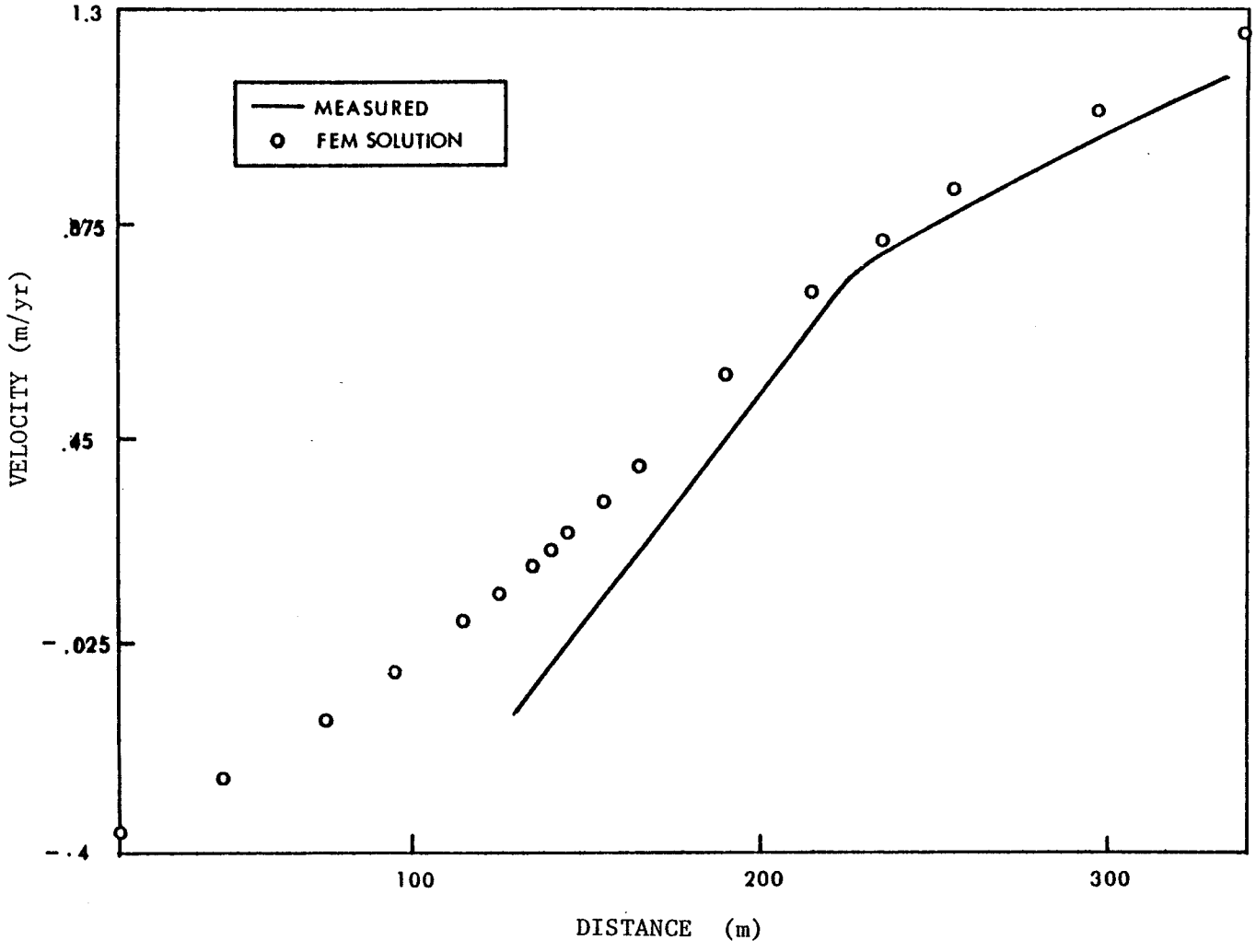

Figure 5-21 Horizontal Velocity Profile - Mount Logan Divide Grid

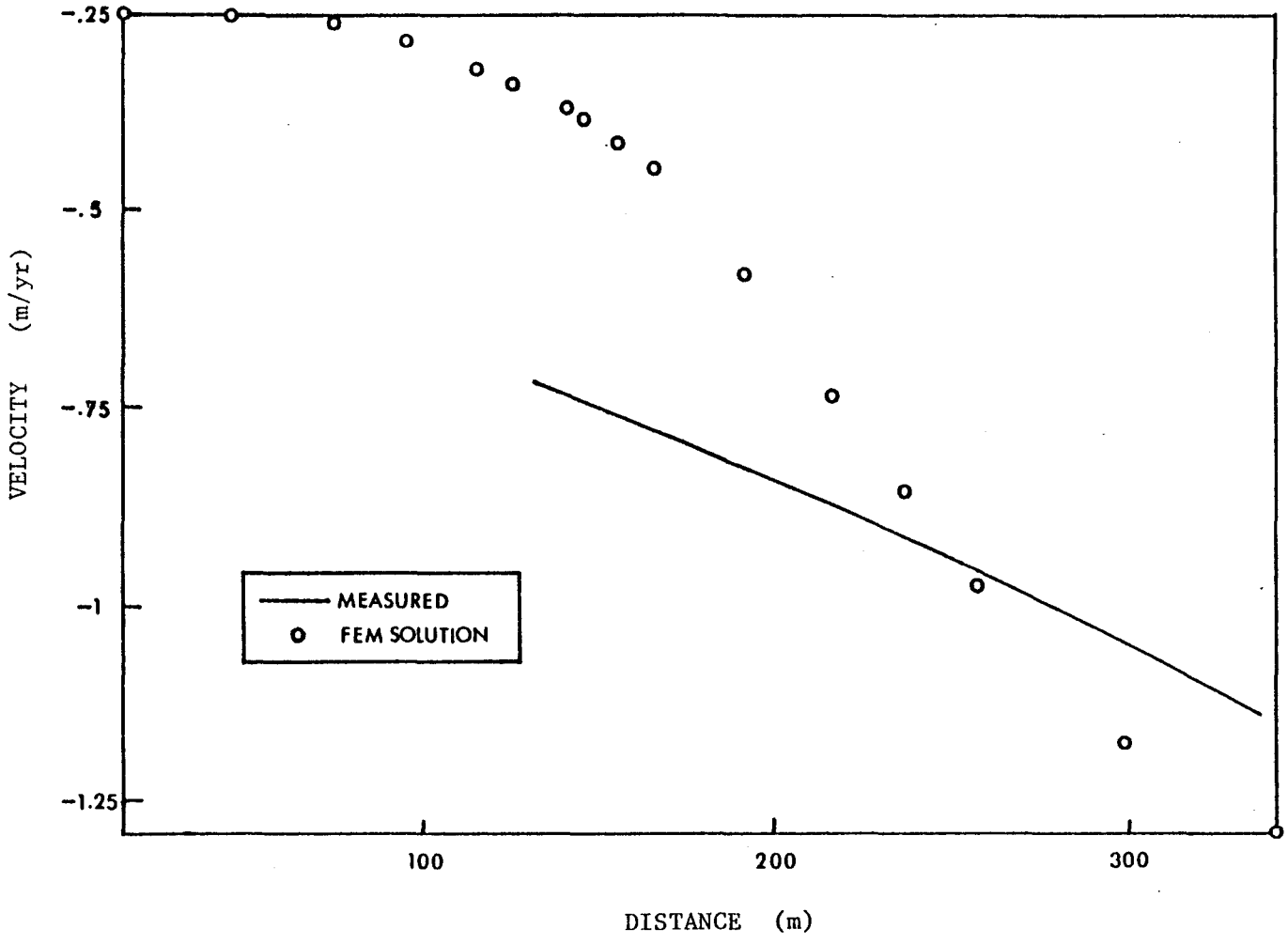

Figure 5-22 Vertical velocity Profile - Mount Logan Divide

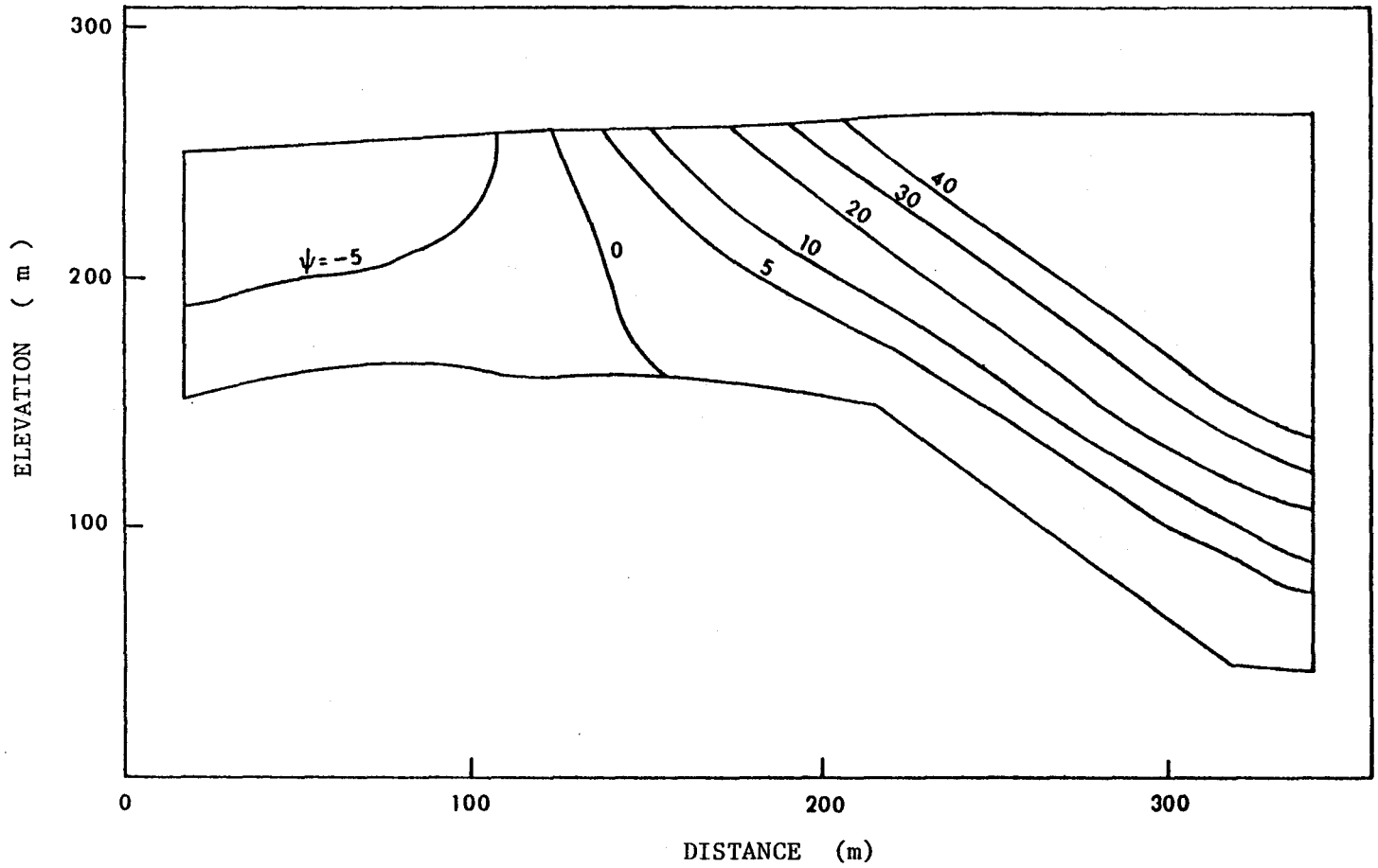

Figure 5-23 Particle Paths - Mount Logan Divide

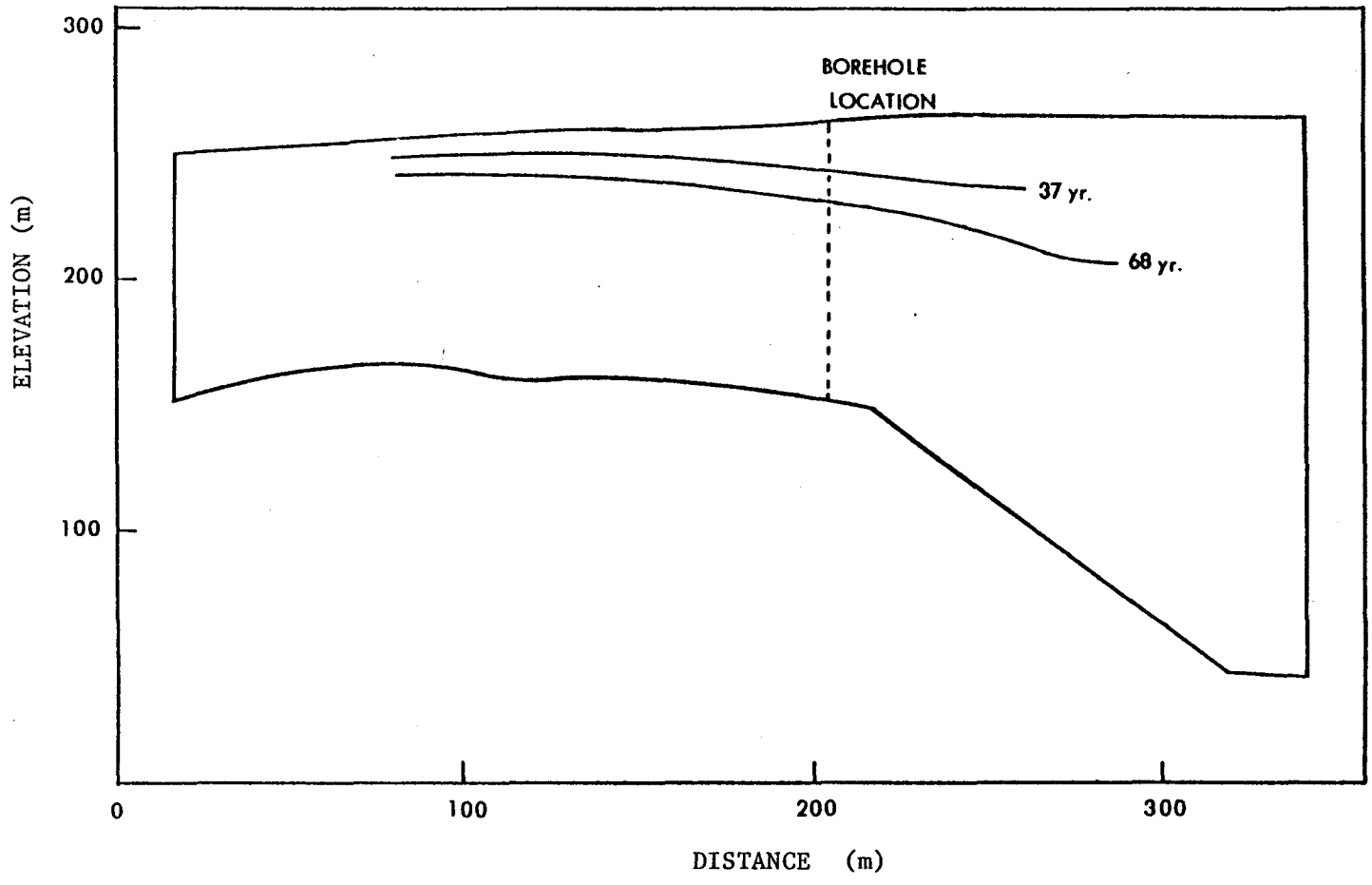

Figure 5-24 Isochrones - Mount Logan Divide

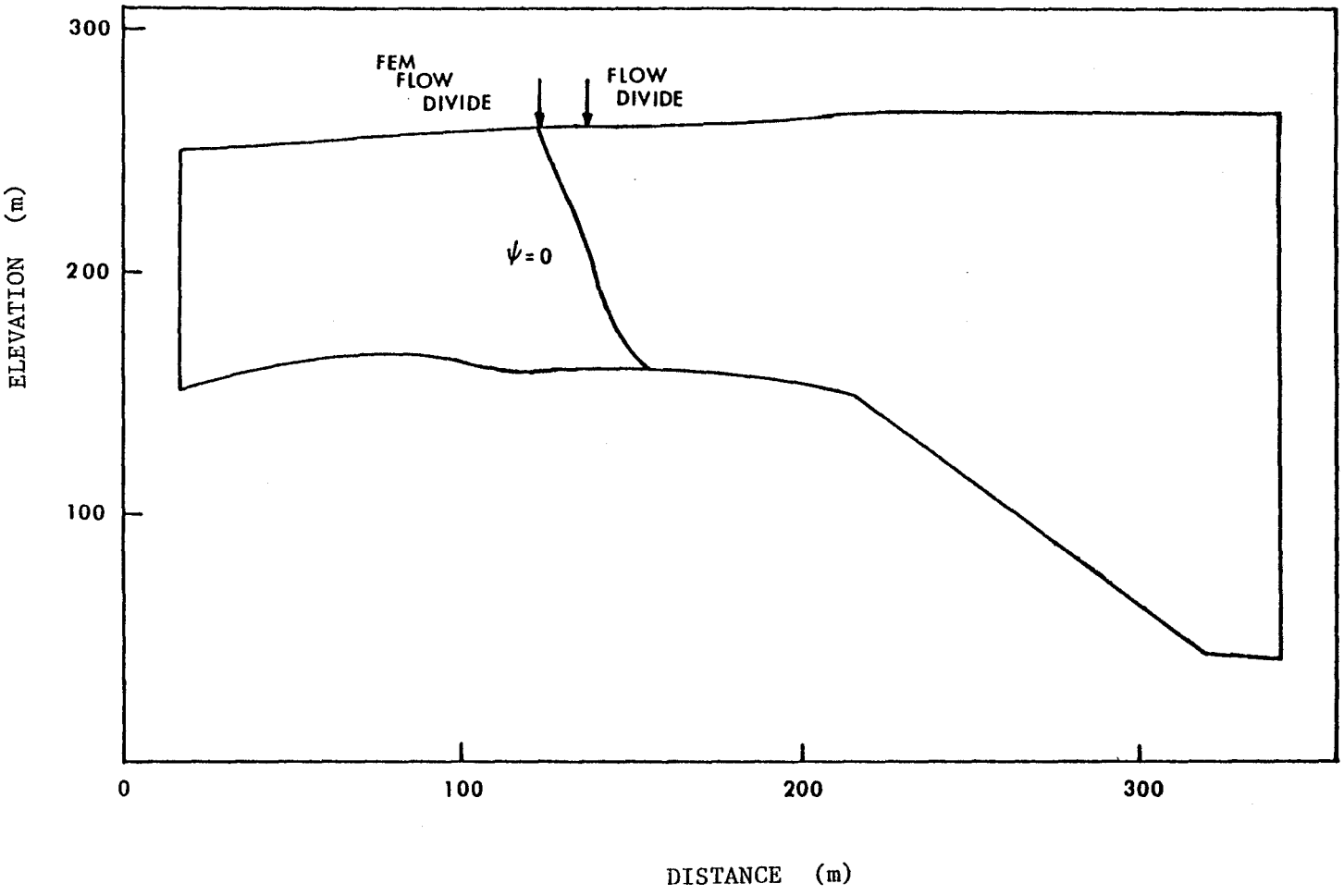

Figure 5-25 Location of the Divide for Mount Logan

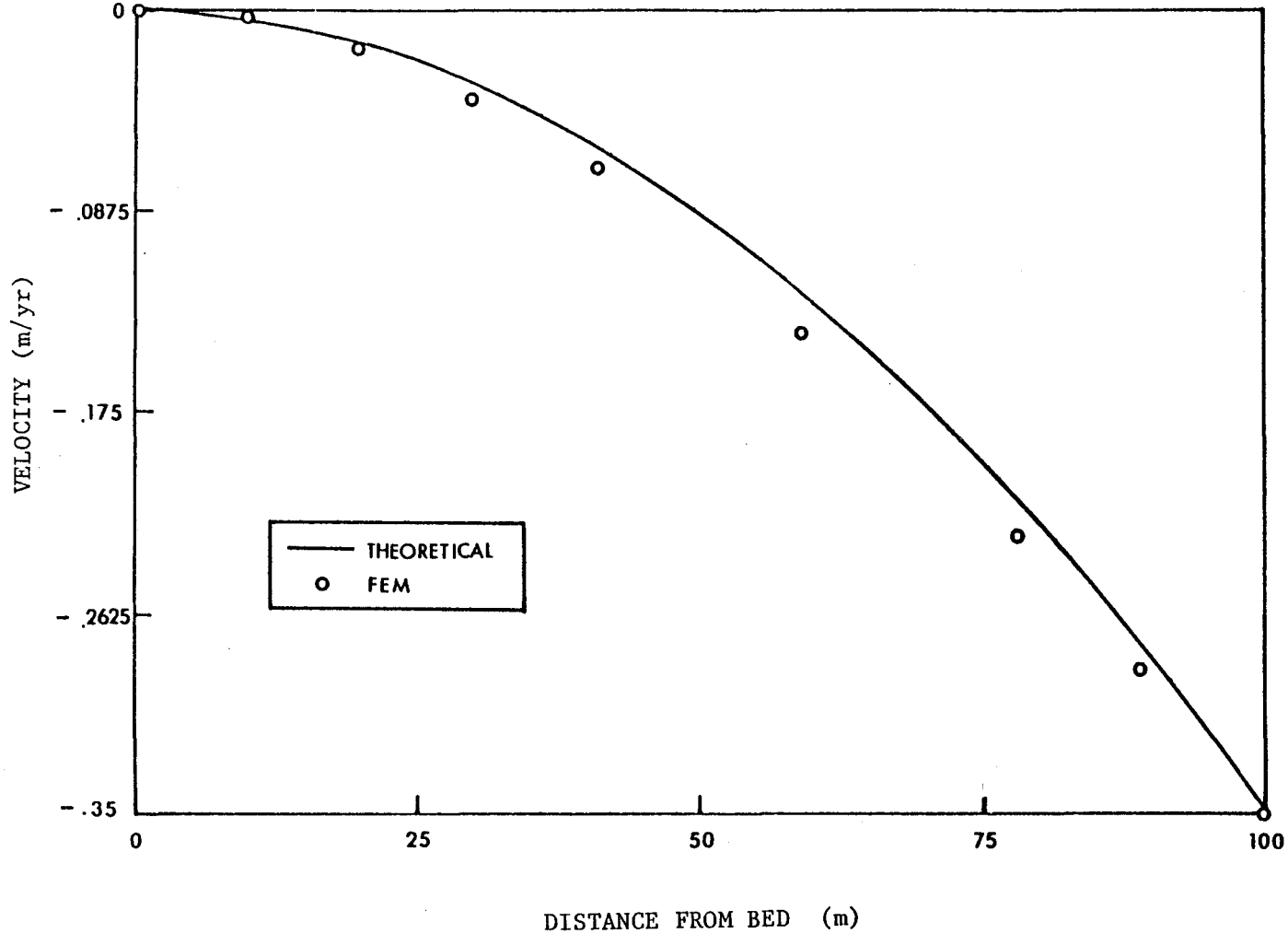

Figure 5-26 Raymond's Relationship - Mount Logan

TABLE 5-1 – MATERIAL PROPERTIES FOR THE BARNES ICE CAP

A parameter	see Figure 5-3
n power	3.0
Unit weight	8.535, 9.025 kN/m^3

TABLE 5-2 – MATERIAL PROPERTIES FOR MOUNT LOGAN

A parameter	0.0086
n power	1.284
Unit weight	4.0, 6.0, 8.952 kN/m^3

CHAPTER 6

CONCLUSIONS AND RECOMMENDATIONS

6.1 Conclusions

Based on the work in this thesis, several conclusions can be stated:

(i) Particles paths can be significantly affected by the bedrock geometry. Glaciologists usually ignore the affect of bedrock geometry on particle paths. Results of the Barnes Ice Cap and Mount Logan simulations show that the influence of bedrock geometry can be quite considerable.

(ii) The position of the predicted flow divide is offset from the flow divide established from field measurements. Also, the divide does not extend vertically downwards from the surface to the bedrock interface, rather it is displaced from the vertical; in the case of Mount Logan this displacement is rather significant because boreholes are drilled vertically downwards since it is assumed that horizontal velocity is negligible with depth. This is significant because most core drilling is done at geographic divides of the glaciers and it is assumed that the horizontal velocity is negligible. Results of the two ice masses studied indicates that both these assumptions are not applicable.

(iii) The vertical velocity at the divide of both ice masses studied varies quadratically with depth. Most flow models developed for the dating of ice cores assume that the vertical velocity varies linearly with depth, which results in the age of ice being over-estimated.

(vi) The stream function finite element method offers a new method of determining the particle paths, and establishing the age of glacier ice. A realistic approximation to

the velocity field must be computed for the stream function finite element model to yield correct results. The white ice at the base of the Barnes Ice Cap has been established at 10000 years which correlates with the age determined by Hooke [15].

6.2 Recommendations for Further Study

Based on the work in this thesis several recommendations for further study can be made:

(i) Ice is an anisotropic material. As ice deforms, a prefered fabric in the direction of the deformation develops. Incorporating anisotropy in finite element modelling would be a major advance in the study of glacier dynamics.

(ii) Though glacier ice is almost incompressible, firn exhibits considerable compressibility [25]. As indicated previously, the Mount Logan glacier is composed of a layer of firn near the surface, a transitional layer below the firn layer and below the transitional layer, glacier ice. To accurately compute the velocity field for Mount Logan the compressiblity exhibited by firn must be considered. A constitutive model incorporating firn compressibility would permit more accurate modelling of glaciers that contain significant amounts of firn.

APPENDIX A

TRANSIENT MODEL

A.1 Introduction

In order to verify the results of the primitive variable steady-state finite element model, and to demonstrate the insensitivity of glacier flow to the influence of elastic response, a transient non-linear visco-elastic finite element model was developed. The model developed herein incorporates the influence of material nonlinear effects, and uses an explicit time-marching scheme.

A.2 Finite Element Model

As is usual with most finite element analyses the matrix equations are developed from a virtual work equilibrium statement. If u_i is the displacement field, ε_{ij} are the strains and σ_{ij} are the stresses, for a virtual displacement δu_i and the corresponding change in strain $\delta\varepsilon_{ij}$, the total virtual work done on the system must be zero [35]

$$\int_V \delta\boldsymbol{\varepsilon}^T \boldsymbol{\sigma}\, dV - \int_V \delta\mathbf{u}^T \mathbf{b}\, dV - \int_\Gamma \delta\mathbf{u}^T \mathbf{T}\, d\Gamma = 0 \qquad (A.1)$$

where $\mathbf{b}$ denotes body forces and $\mathbf{T}$ denotes boundary tractions. Compatible strains and displacements are related by a linear differential operator, $\boldsymbol{\varepsilon} = \mathbf{L}\,\mathbf{u}$. The assumed trial expansion for $\mathbf{u}$ is $\mathbf{u} = \mathbf{N}\,\mathbf{a}$, where $\mathbf{a}$ is the solution of the system at nodal points.

Equation 6.1 reduces to

$$\int_V \mathbf{B}^T \boldsymbol{\sigma}\, dV - \mathbf{f} = 0 \qquad (A.2)$$

where $\mathbf{B} = \mathbf{L}\,\mathbf{N}$ and

$$\mathbf{f} = \int_V \mathbf{N}^T \mathbf{b}\, dV + \int_\Gamma \mathbf{N}^T \mathbf{T}\, d\Gamma$$

The constitutive relation used to relate strain increments to stress increments is

$$\Delta\boldsymbol{\sigma} = \mathbf{D}(\Delta\boldsymbol{\varepsilon} - \Delta\boldsymbol{\varepsilon}^c) \tag{A.3}$$

where **D** is the elastic constitutive matrix, $\Delta\boldsymbol{\varepsilon}^c$ are the creep strain increments.

The creep strain increments are calculated from the creep strain rates using a fully explicit (Euler) scheme over a time interval Δt_n [19]

$$\Delta\boldsymbol{\varepsilon}^c = \Delta t_n \, \dot{\boldsymbol{\varepsilon}}^c \tag{A.4}$$

Equation 6.2 is solved by using an incremental approach in which the effects of material non-linearity are incorporated into the load vector through initial strains.

Based on early work on creep problems it was observed that accuracy deteriorates as the time-step length is increased and with the explicit scheme, in fact, numerical instability is imminent. To avoid this deterioration in accuracy, a restriction is imposed on the length of the time-step [4]. The length of the initial time-step is determined by

$$\Delta t_1 = \frac{(0.05\,\Delta\varepsilon_e^E)}{\dot{\varepsilon}_e^c} \tag{A.5}$$

where ε_e^c is the equivalent creep strain-rate and $\Delta\varepsilon_e^E$ is the equivalent elastic strain increment. Subsequent time-steps are restricted by [35]

$$\Delta t_{n+1} \leq 1.2\,\Delta t_n \tag{A.6}$$

and,

$$\Delta t_{max} \leq \frac{4E(1+\nu)}{3n}\,\frac{\sigma_e}{\dot{\varepsilon}_e^c} \tag{A.7}$$

A.3 Results

The transient finite element model was subjected to several tests to check the results. The double slope ice mass discussed in section 4.6 was simulated with the finite element program. The transient model converges after 14992.93 minutes to approximately the same values as obtained when using the primitive variable formulation; the computed

velocity profiles from the steady-state and transient models are shown Figures A-1 and A-2. A plot of the horizontal velocity with time for node 25 (Figure A-3) is shown in Figure A-4. Figures A-5 and A-6 show plots of displacement with time and clearly demonstrate that the elastic response of a glacier is negligible.

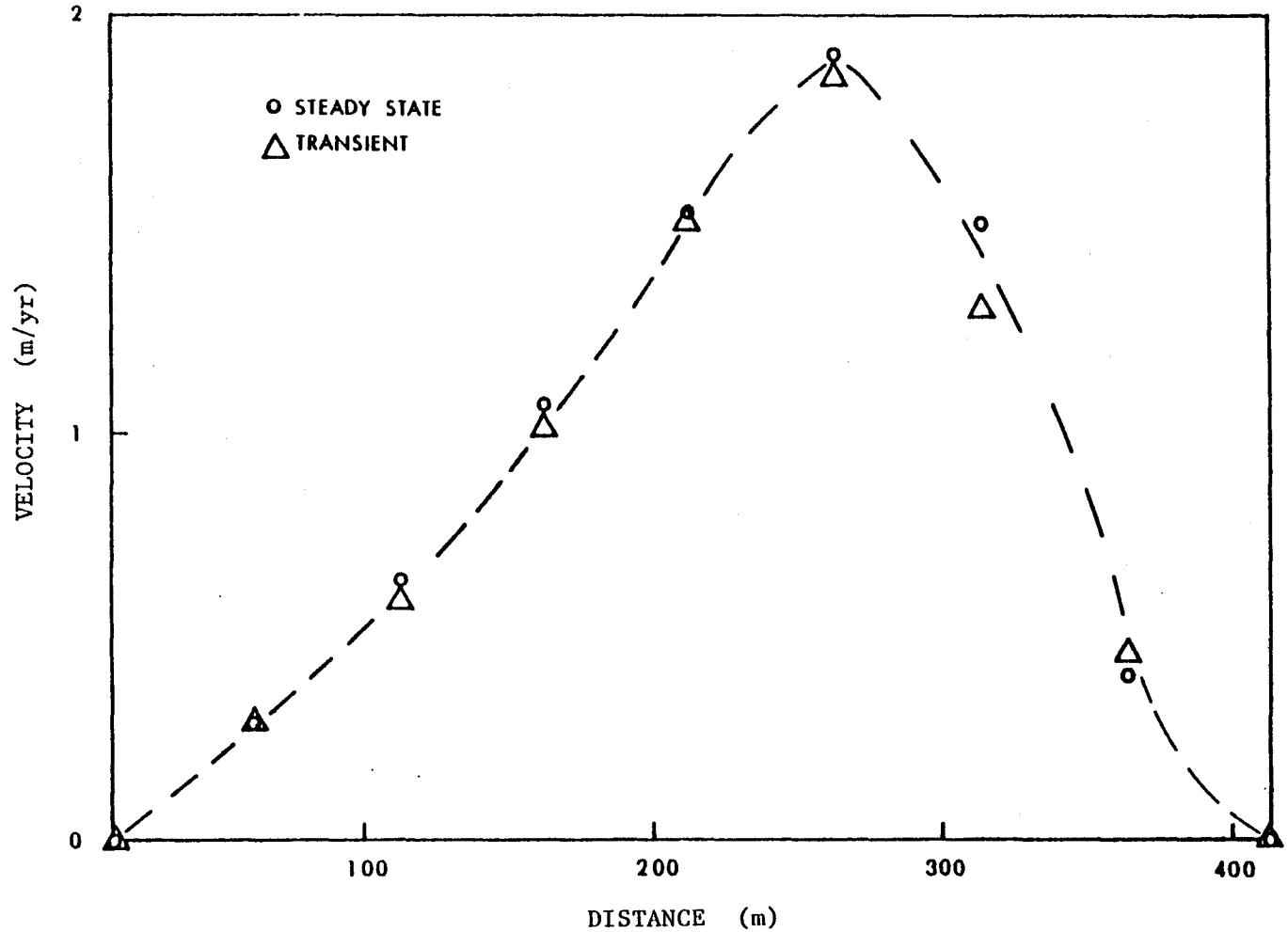

Figure A-1 Horizontal Velocity Profile -
Comparison of the Transient and Steady-state Models

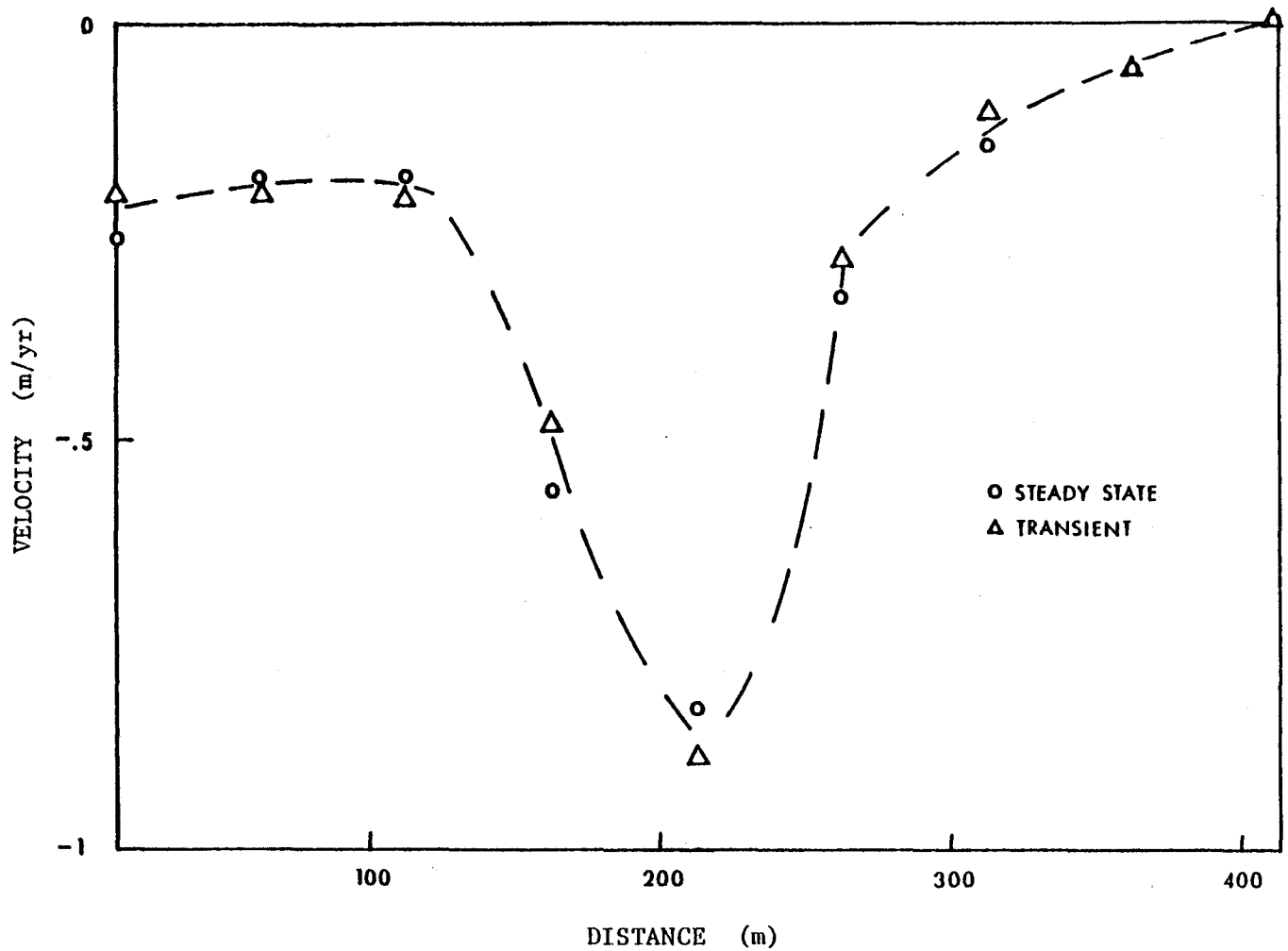

Figure A-2 Vertical Velocity Profiles -
Comparison of the Transient and Steady-state Models

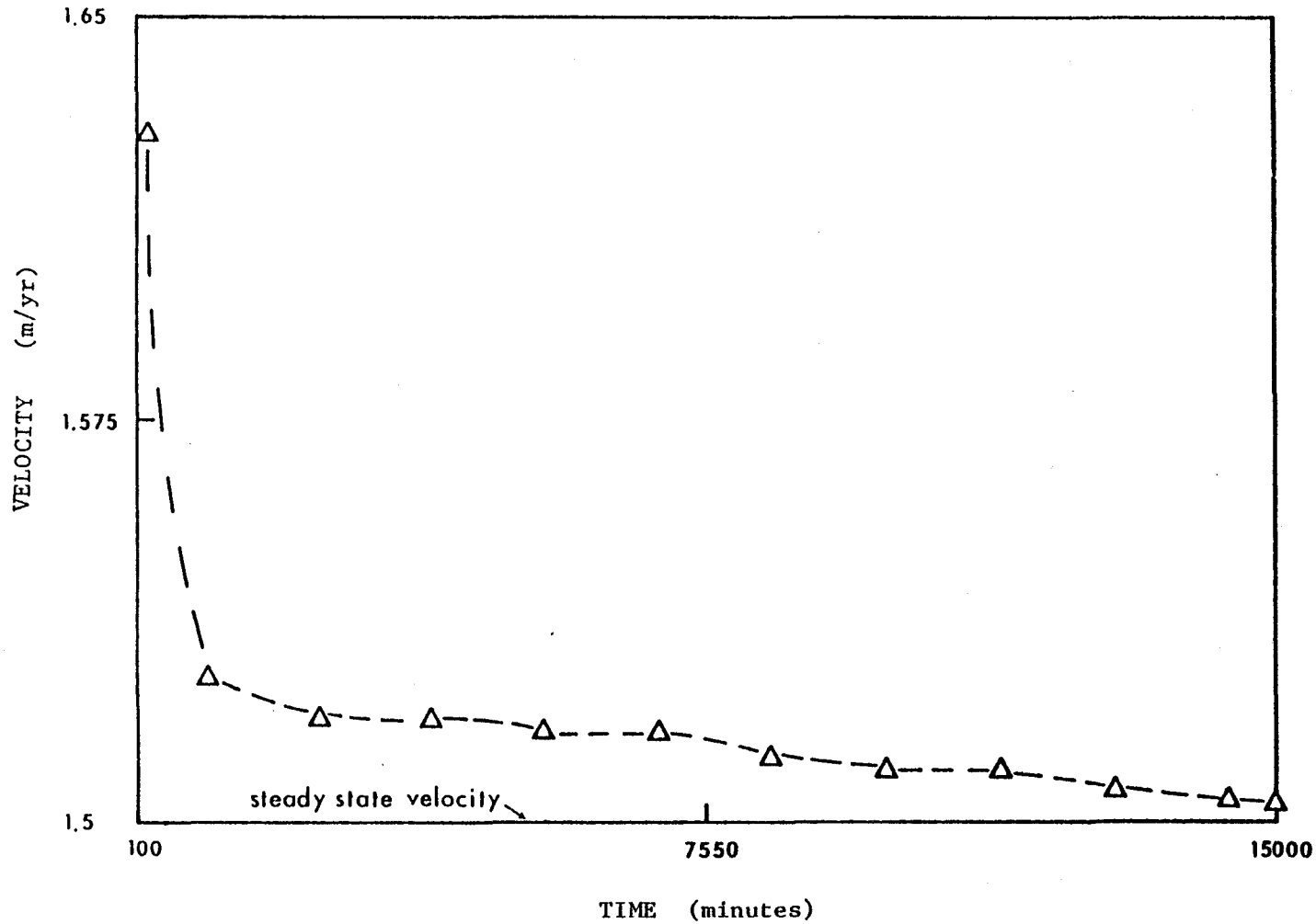

Figure A-3 Horizontal Velocity at Node 25

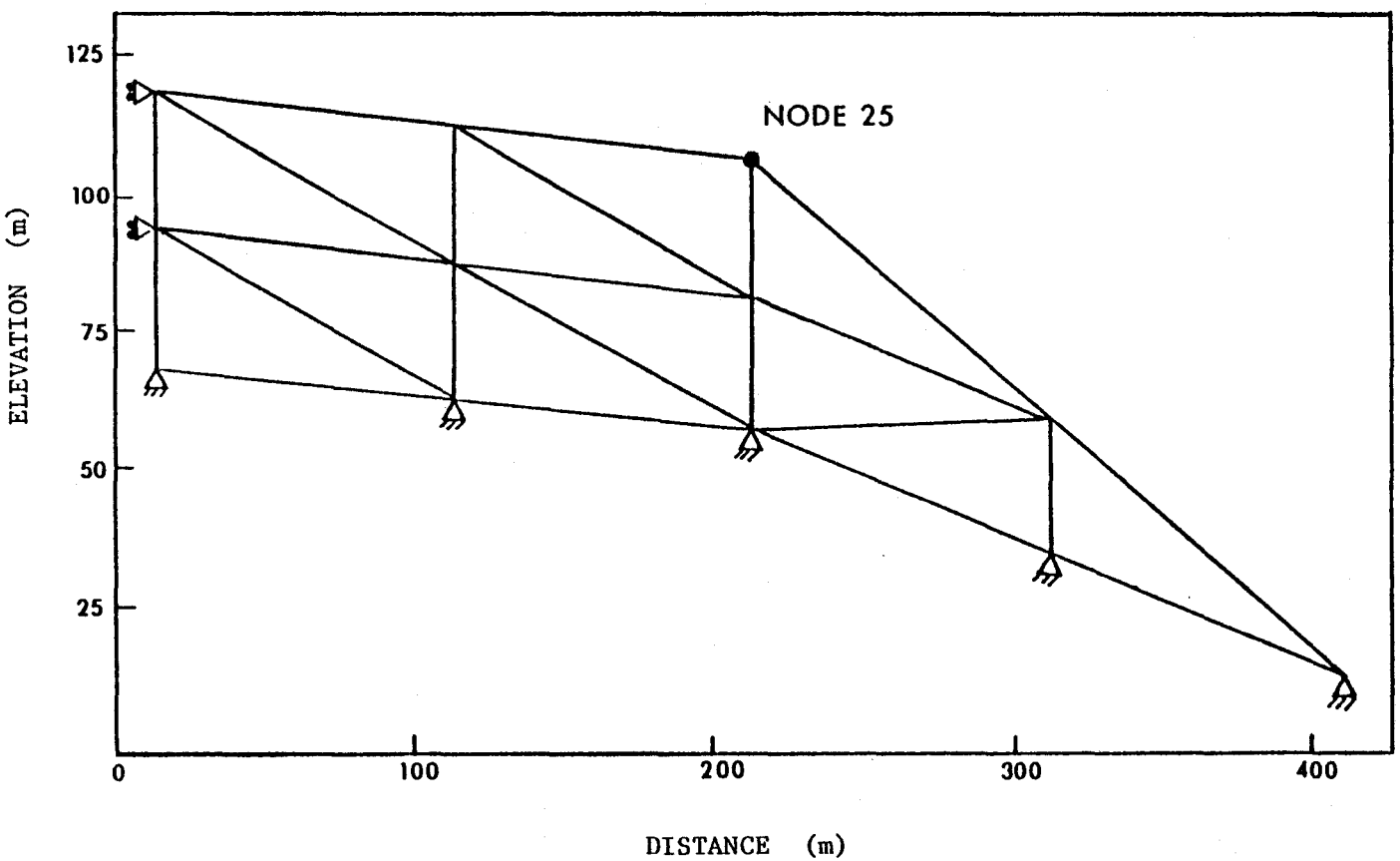

Figure A-4 Location of Node 25

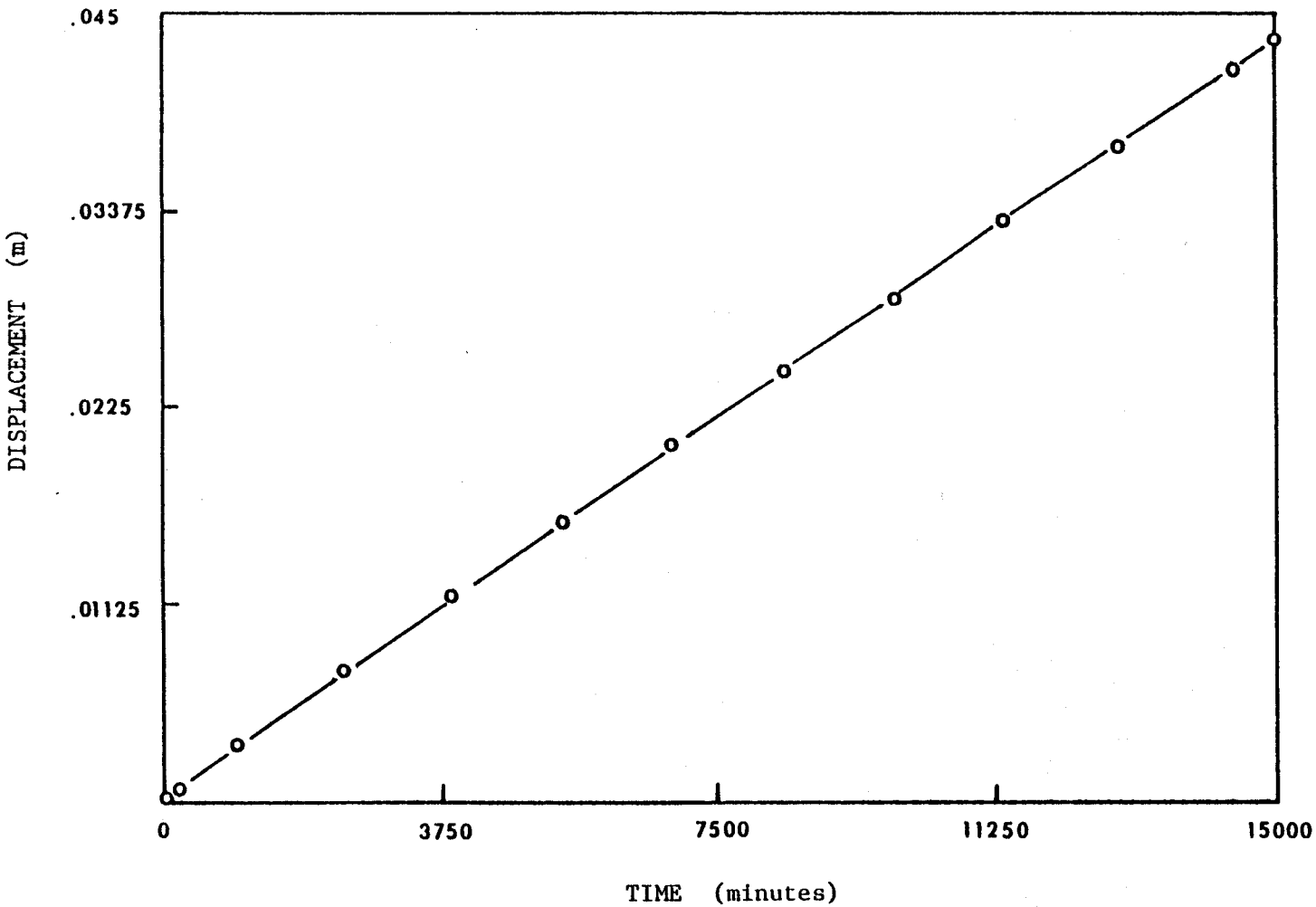

Figure A-5 Horizontal Displacement at Node 25

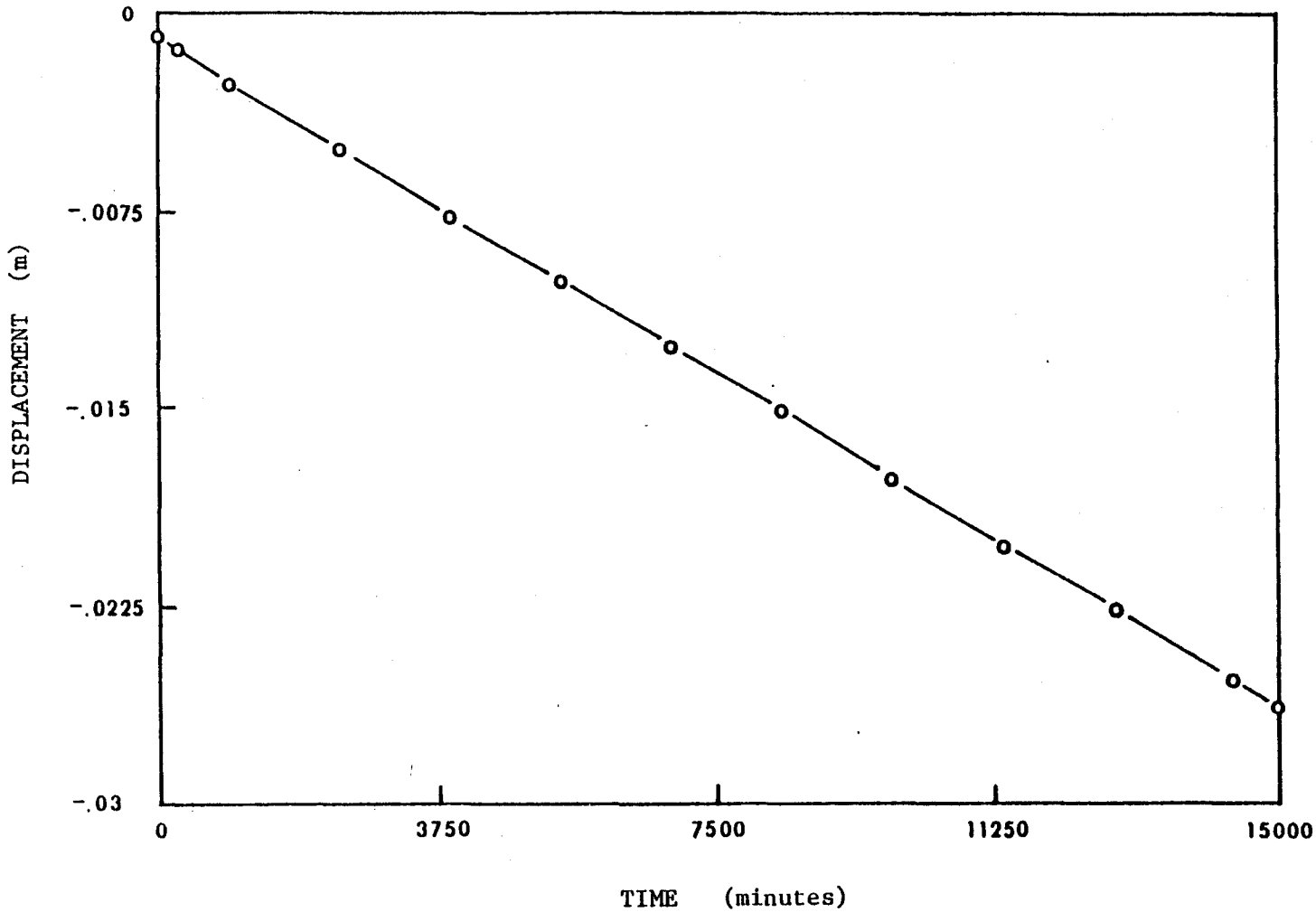

Figure A-6 Vertical Displacement at Node 25

TABLE A-1 – MATERIAL PROPERTIES FOR THE DOUBLE SLOPE

A parameter	0.0327
n power	1.65
Poisson's ratio	0.34
Elastic modulus	907500.0 KPa
Unit weight	8.952 kN/m^3

APPENDIX B

LIST OF SYMBOLS

A	- flow parameter for Glen's law
b_i	- body forces
E	- elastic modulus
h	- thickness of glacier
ℓ	- length along the boundary
N_i	- shape function
Q	- activation energy for creep
R	- universal gas constant
S_{ij}	- deviatoric stress tensor
T	- time
T_i	- surface traction
t	- thickness
V_i	- velocity in direction of i coordinate axis
V_s	- tangential velocity at the boundary
V_n	- normal velocity at the boundary
W	- weighting function
W_i	- weighting factor at node i
Z	- distance above the glacier bed
β_i	- orthogonal weighting functions
$\dot{\varepsilon}_e$	- equivalent strain-rate
$\dot{\varepsilon}_{ij}$	- strain-rate tensor

$\dot{\varepsilon}_z$ - vertical strain-rate

ψ - stream function

σ_e - equivalent stress

σ_m - mean normal stress

ω - vorticity

μ - viscosity

REFERENCES

[1] Brebbia, C.A., The Boundary Element Method for Engineers, John Wiley and Sons, New York, 1978.

[2] Budd, W.F., Jenssen, D. and Radok, U., Derived Physical Characteristics of the Antarctic Ice Sheet (Mark 1), University of Melbourne Meteorological Department Publication No. 18, Australia, 1971.

[3] Colbeck, S.C. and Evans, R.J., "A flow law for temperate glacier ice", Journal of Glaciology, vol. 12, 1973.

[4] Cormeau, I., "Numerical stability in quasi-static elasto-viscoplasticity", Int. Journal for Numerical Methods in Eng., vol. 9, 1975, pp. 109-127.

[5] Dansgaard, W. and Johnsen, S.J., "A flow model and a time scale for the ice core from Camp Century, Greenland", vol. 8, 1969, pp. 215-223.

[6] Dansgaard, W., Johnsen, S.J., Moller, J. and Langway, C.C., "One thousand centuries of climatic record from Camp Century on the Greenland ice sheet", Science, vol. 166, 1969, pp. 377-381.

[7] Emery, J.J., "Finite Element Analysis of Creep Problems in Soil Mechanics", Ph.D. Thesis, University of British Columbia, Vancouver, 1971.

[8] Haefeli, R., "Contribution to the movement and the form of ice sheets in the Arctic and Antarctic", Journal of Glaciology, vol. 3, 1961, pp. 1133-51.

[9] Hammer, C.U., Clauser, H.B., Dansgaard, W., Gundestrup, N., Johnsen, S.J. and Reeh, N., "Dating Greenland ice cores by flow models, isotopes, volcanic debris, and continental dust", Journal of Glaciology, vol. 20, 1978, pp. 3-26.

[10] Hanafy, E.A., "Ice Flow Studies", Directed Study Program Report, McMaster University, 1977.

[11] Holdsworth, G., "Deformation and flow of the Barnes Ice Cap, Baffin Island", Scientific Series No. 52, Department of the Environment, Ottawa, 1975.

[12] Holdsworth, G., "Mount Logan Field Report 1978", Glaciology Division, Department of the Environment, Ottawa, 1979.

[13] Holdsworth, G., Personal Communication, 1985.

[14] Hooke, R.L., "Structure and flow in the margin of the Barnes Ice Cap, Baffin Island, N.W.T., Canada", Journal of Glaciology, vol. 12, 1973, pp. 423-438.

[15] Hooke, R.L., "Pleistocone ice at the base of the Barnes Ice Cap, Baffin Island, N.W.T., Canada", Journal of Glaciology, Vol. 17, 1976, pp. 49-59.

[16] Hooke, R.L., Raymond, C.F., Hotchkiss, R.L. and Gustafson, R.I., "Calculations of the velocity and temperature in a polar glacier using the finite element method", Journal of Glaciology, vol. 24, 1979, p. 131-145.

[17] Hooke, R.L., Hudleston, P.J., "Origin of foliation in glaciers", Journal of Glaciology, vol. 20, 1978, pp. 285-298.

[18] Hughes, William, F., An Introduction to Viscous Flow, Hemisphere Publishing Corporation, Washington D.C., 1978.

[19] Kanchi, M.B., Zienkiewicz, O.C. and Owen, D.R.J., "The viscoplastic approach to problems of plasticity and creep involving geometric non-linear effects", Int. Journal for Numerical Methods in Eng., vol. 12, 1978, pp. 169-181.

[20] Meier, M., "Mode of flow of Saskatchewan Glaciers, Alberta, Canada", Geological Survey, Professional Paper 351, 1960.

[21] Mellor, M., "Mechanical properties of polycrystalline ice", International Union of Theoretical and Applied Mechanics Symposium on the Physics and Mechanics of Ice, Copenhagen, Denmark, 1979.

[22] Mitsoulis, E., "Finite Element Analysis of Two-Dimensional Polymer Melt Flows", Ph.D. Thesis, McMaster University, 1984.

[23] Nye, J.F., "Correction factor for accumulation measured by the thickness of the annual layers in an ice sheet", Journal of Glaciology, vol. 4, 1963, p. 785-788.

[24] Nye, J.F., "The mechanics of glacier flow", Journal of Glaciology, vol. 2, 1952, p. 82-93.

[25] Paterson, W.S.B., The Physics of Glaciers, 2nd Edition, Pergamon Press, Oxford, 1981.

[26] Paterson, W.S.B., "Ice sheets and ice shelves", in Dynamics of Snow and Ice, Ed. by S.C. Colbeck, Academic Press, London, 1980, pp. 1-78.

[27] Paterson, W.S.B., "Past precipitation rates derived from ice core measurements: methods and data analysis", Reviews of Geophysics and Space, vol. 22, 1984, pp. 123-130.

[28] Philberth, K. and Federer, B., "On the temperature profile and the age profile in the central part of cold ice sheets", Journal of Glaciology, vol. 10, 1971, pp. 3-15.

[29] Raymond, C.F., "Deformation in the vicinity of ice divides", Journal of Glaciology, vol. 29, 1983, pp. 357-373.

[30] Stolle, D.F.E., "Creep of Engineering Materials", Directed Study Program Report, McMaster University, Hamilton, 1979.

[31] Stolle, D.F.E., "Finite Element Modelling of Creep and Instability of Large Ice Masses", Ph.D. Thesis, McMaster University, 1982.

[32] Sugden, D.E. and John, B.S., Glaciers and Landscape, Edward Arnold Publishers Ltd., London, 1976.

[33] Van Egmond, J., "Simulation of Large Ice Mass Flow", M.Eng. Thesis, McMaster University, Hamilton, 1978.

[34] Weertmann, J., "Theory of steady state creep based on dislocation climb", Journal of Applied Physics, vol. 26, 1955.

[35] Zienkiewicz, O.C. and Cormeau, I.C., "Viscoplasticity - plasticity and creep in elastic solids - a unified numerical approach", Int. Journal for Numerical Methods in Eng., Vol. 8, 1974, pp. 821-845.

[36] Zienkiewicz, O.C. and Godbole, P.N., "Viscous, incompressible flow with special references to non-Newtonian (plastic) fluids", in Finite Elements in Fluids, vol. 1, Viscous Flow and Hydrodynamics, Ed. by Gallagher et al., J. Wiley and Sons, London, 1974.